Towards a One-Shot Printed Gripper for Part Extraction from Powder-Based 3D Printing Processes

Jordan Cormack

A thesis submitted in partial fulfilment of the requirements of the University of the West of England, Bristol for the degree of Doctor of Philosophy.

This research was carried out in collaboration with HP Inc UK Ltd.

Bristol Robotics Laboratory,
Department of Engineering, Design and Mathematics,
Faculty of Environment and Technology,
University of the West of England, Bristol.

July 2022

32787 Words

Abstract

As 3D printing moves from a tool used predominantly for creating one-off prototype parts to being a key part in high volume manufacturing, the need for increased automation becomes desirable to save time and cost in the process. For 3D printing processes which are already used for high volume manufacture, such as HP's Multi Jet Fusion, there is currently no automated method for removing printed objects from the powder based build volume individually, keeping them in a known pose. This thesis details the development of a compliant one-shot 3D printed gripper mechanism which is able to extract individual caked 3D printed objects from aged PA12 powder, in a known pose. The gripping mechanism was simulated using finite element analysis, and validated using a visual tracking tool. Through the use of strain gauges applied to the 3D printed gripper, it was found that the unfused powder does not easily flow from between the tips and the object, causing its perceived size to increase, and instability to occur during the grasp. A novel modified tip geometry and local vibration was shown to completely remove any increase in the perceived object size and slip during extraction from virgin PA12 powder using cleaned objects. Multiple caked objects were also extracted from within aged powder in a known pose, closely representing the actual MJF process, including a high variability of caked powder surrounding the objects. A new sensor comprised of an array of strain gauges was developed based on the toothed tip geometry of the gripper, which is able to provide more rich information about object grasp, such as force, torque, and slip detection. Elements of this work are also applicable more generally for grasping dirty objects, or ones buried in loose media. Future work to replace the commercial sensors and motors with fully 3D printed alternatives will allow the gripper to be manufactured even quicker, for less cost, and allow it to be fully tailored to the 3D printed objects which need extraction.

Contents

List of Figures

List of Tables

List of Related Publications

- Cormack, J., Fotouhi, M., Adams, G., Pipe, A. (2020) One-Shot 3D Printed Underactuated Gripper. In: Mohammad A., Dong X., Russo M. (eds) Towards Autonomous Robotic Systems. TAROS 2020. Lecture Notes in Computer Science, vol 12228. Springer, Cham. https://doi.org/10.1007/978-3-030-63486-5_41

- Cormack, J., Fotouhi, M., Adams, G., Pipe, T. (2021) Comparison of Concentrated and Distributed Compliant Elements in a 3D Printed Gripper. In: Fox C., Gao J., Ghalamzan Esfahani A., Saaj M., Hanheide M., Parsons S. (eds) Towards Autonomous Robotic Systems. TAROS 2021. Lecture Notes in Computer Science, vol 13054. Springer, Cham. https://doi.org/10.1007/978-3-030-89177-0_20

- Cormack, J., Fotouhi, M., Adams, G., and Pipe, T., (2021) Automated Extraction of 3D Printed Parts From Unfused PA12 Powder Using a One-Shot 3D Printed Compliant Gripper. *IEEE Robotics and Automation Letters*, vol. 6, no. 4, pp. 8655-8662, Oct. 2021, https://doi.org/10.1109/LRA.2021.3113383

Chapter 1

Introduction

HP's Multi Jet Fusion (MJF) 3D printing process finishes with printed parts which are surrounded in a volume of unfused powder. Currently, extracting individual parts from this powder is a manual process. Workers use their hands to reach into the powder to find parts, and use a vacuum hose to remove the majority of excess powder. This process can be seen in Figure 1.0.1. Printed parts can be separated from loose unfused powder using a combination of vibration, vacuum and air blasting, however this results in all of the parts being mixed up in an unknown pose. This bulk unpacking method is also not suitable for delicate parts, especially those printed with metal powder using the similar Metal Jet process.

Figure 1.0.1: Multi-Jet Fusion Manual Part Extraction (Hartzell and Moore, 2019). Image used with permission from SmileDirectClub.

Once the parts are extracted from the printer, they are post-processed. This involves cleaning to remove any remaining unfused powder and dyeing if a more desirable colour is needed for polymer parts, and sintering for metal parts. Being able to automatically extract printed parts in a known pose from the powder, without harsh vibrations and air blasting, could save time and cost in the MJF process, and prevent parts being damaged in the Metal Jet process. Removing humans from the process is also desirable from a safety perspective, as workers need to wear PPE to protect them from the small powder particles. Automation of the extraction step could also be beneficial as a starting point for automating subsequent steps such as post-processing, assembly or shipping.

One of the key complexities with manipulating 3D printed parts is the wide variety of shapes and sizes that are printed, unlike processes such as injection moulding which often create thousands or millions of identical parts. Another is the unfused powder or support material that can surround the parts. All current methods for automatic removal of parts from 3D printers result in either a mixture of parts in unknown locations and orientations, or parts in a known pose which are still fixed to a common build plate or support structure. This means that manual intervention is still needed to separate and sort parts before they can be used. Printing parts individually could solve this problem in some cases, but this is often not cost effective for smaller parts on powder based process such as MJF. Being able to extract parts individually from a build unit housing multiple parts would further enhance the automation of subsequent post-processing steps such as part finishing and assembly.

3D printing has already become a key process for manufacturing final use parts across all industries, with HP using many 3D printed parts in their own products (Davies, 2019). More complex geometries are possible with 3D printing compared to conventional subtractive manufacturing techniques, with multiple parts often being consolidated into a single 3D printable one. This is beneficial for a complex gripping application, as the grippers can be manufactured quickly and cheaply, and tailored to the specific items which need extracting. This means that costs saved in automated extraction would not just be passed on to assembling grippers, if they could be

printed in one-shot with no assembly required.

1.1 Aims / Research Questions

The main aim of this research is to develop a one-shot 3D printed gripper which is capable of extracting individual printed parts from a MJF build unit, in a known pose. To meet this aim, the following research questions must be answered.

- What gripping mechanisms are best suited for one-shot 3D printing using the MJF process?
- How is the gripping process affected by the unfused powder which surrounds parts after printing?
- What gripping techniques are best suited for extracting parts from a powder, in a known pose?
- What sensors are capable of being manufactured using the MJF process?
- What sensors are best suited for use in a gripping process involving parts embedded in powder?

1.2 Scope of the Thesis

This thesis will focus on developing a 3D printable gripper, suitable for extracting 3D printed parts from PA12 powder in a known pose. This will initially be limited to a single object, as shown in the dashed region of Figure 1.2.1. The size of the object will be between 10x10x10mm and 100x100x100mm as although larger objects can be printed using the MJF process, the majority of high-volume objects fall within this size range. The interaction between the gripper and printed part within unfused powder will be analysed by means of physical testing only, as computer

based simulations of this interaction are outside of the scope for this thesis and would still require physical verification and validation. The aim of this thesis is not to develop a universal gripper capable of extracting any 3D printable object, but to work towards a one-shot printable gripper which can extract an object (or series of objects) representative of those which are currently printed using MJF at high volume.

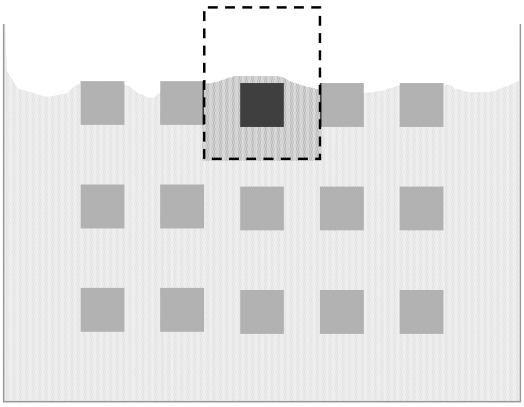

Figure 1.2.1: Scope of Initial Powder Testing

Although the project focuses on the MJF 3D printing process, some of the prototype grippers and supplementary 3D printed parts (e.g. mounts, actuator housings, control boxes) will be manufactured using the Fused Filament Fabrication (FFF) process, as the turnaround time for printing parts using FFF is a lot quicker on the University campus where this research was carried out than for MJF parts which need to be sourced externally.

1.3 Contributions and Novelty

The contributions and novel areas developed during this project are as follows:

- Gripping and interacting with a solid object surrounded by powder.
- Extracting solid objects from powder individually.
- Extracting solid objects from powder in a known pose.

- A novel one-shot 3D printed underactuated gripper.
- A novel one-shot 3D printed distributed compliance gripper.
- A standardised actuation method that allows many gripper types to be used, featuring a single input rod capable of actuating multiple degrees-of-freedom.
- A strain gauge array sensing system which allows grip, slip and instability to be detected.

1.4 Thesis Outline

In Chapter 2, common 3D printing processes are described as well as HP's Multi-Jet Fusion process, including current challenges and limitations in the automated extraction of individual printed parts. Existing relevant literature on interactions between solid objects and powder is shown, followed by a review of robot end effector and sensor types, focusing on those suitable for 3D printing.

Chapter 3 details the development of a gripping mechanism suited for one-shot 3D printing and operation within unfused powder, including comparisons between different types of compliant mechanisms when used as part of a gripper. Pneumatic and electromechanical actuators are trialed, along with a measurement of the possible grip force.

Chapter 4 presents a visual tracking system for validating the simulated gripper, showing that it is possible to use Finite Element Analysis (FEA) to accurately simulate the deformation of a real 3D printable compliant mechanism, including the interaction of a gripper and object.

Chapter 5 describes a sensing system based on strain gauges adhered to the 3D printed gripper, with initial testing showing how the output varies for a series of object widths. Simulated and experimental strain are compared, and other sensor types are also explored.

In Chapter 6, the gripper and sensing system are tested by attempting to extract cleaned printed parts surrounded by unfused powder. A test setup is defined, two different gripper mechanisms are trialed, and their performance at extracting objects from powder is explored.

Chapter 7 shows a series of adaptations to the gripping system, made in an attempt to improve the grip performance.

Chapter 8 shows the effect of using aged powder and printed parts still caked in powder, and how well the previously developed adaptations perform. A series of caked 3D printed objects are then extracted from PA12 powder individually one after the other automatically.

Chapter 9 details the development of a strain gauge array sensing system, based on the revised geometry from Chapter 7. Testing is conducted using a series of sensor arrays, showing the capability of the sensor for measuring gripping forces and object slip.

In Chapter 10, conclusions about the research and its contributions are made, followed by a discussion about its limitations and future work.

Appendix A shows a series of existing methods for the automated extraction of parts from 3D printers.

Chapter 2

Literature Review

2.1 3D Printing

3D printing is a term that covers many different processes which additively manufacture objects based on a 3D Computer Aided Design (CAD) model. This is in contrast to subtractive manufacturing methods (such as turning, milling and drilling) which remove material to create an object from a single larger piece of raw material. The vast majority of 3D printing processes are layer based, where the final solid object is made up of many smaller individual 2D layers (3D Hubs, 2020b). The three most common process types in 3D printing are:

Filament Based such as Fused Filament Fabrication (FFF)/Fused Deposition Modelling (FDM). A continuous thermoplastic filament is extruded through a heated print head and deposited onto the build plate or the previous layer (Scott Crump, 1992). This type of process is the most common as it is the cheapest and easiest to setup (Manufactur3D, 2018). Complex parts with overhanging regions require a support structure which is discarded after printing (Joris, 2008). Parts are highly anisotropic, with much weaker strength between the layers (Levenhagen and Dadmun (2018) and Uddin *et al.* (2017)).

Resin Based such as Stereolithography (SLA), Masked Stereolithography (MSLA) and Digital Light Processing (DLP). Photo-polymerisation is used to produce a solid part from a liquid, using a light source such as a laser or projector (Hull, 1986). This

process is more complex to setup and run than a filament based process, with parts often requiring curing, but higher detail is possible (Formlabs, 2020). A discarded support structure is still required for complex parts.

Powder Based such as Multi Jet Fusion (MJF), Selective Laser Sintering (SLS) and Selective Laser Melting (SLM). Thin layers of powder are selectively fused using a laser (Deckard *et al.*, 1989) or a combination of a fusing agent and heat. These processes are often the most costly to setup, but metals and polymer parts are printable, often with highly isotropic material properties. For polymers, the unfused powder supports the solid parts, removing the need for a support structure. This often means that more complex parts with better properties can be created. The majority of metal 3D printing processes are powder based, with many requiring the printed parts to be sintered after the printing step. Some metal processes also require a support structure for parts which is more complex to remove than for a polymer print.

Aside from simple FFF parts without support structure, all of these processes require some form of further processing after the part has finished printing. For filament processes this could involve the removal of support structure, resin based processes also require the parts to be UV-cured, and parts made using powder processes require excess un-fused powder to be removed. Depending on the end use, parts can also be finished with a painting or dyeing step.

As 3D printing becomes more popular, it is being used for not only rapid prototyping but also for final use parts. This has mostly been at low volumes, but recently companies are using 3D printing as a way to manufacture a high volume of unique parts, such as Smile Direct Club who produce up to 50,000 individual dental moulds per day using HP's MJF process (Hartzell and Moore, 2019). At this scale, manually extracting and handling individual parts from 3D printers one-by-one is not only costly, but monotonous and potentially hazardous for the workers if the recommended safety guidelines and personal protective equipment is not adhered to (HP Development Company L.P., 2019).

2.2 Multi-Jet Fusion

HP's MJF process is a combination of their history and experience of inkjet printers, along with multiple 3D printing technologies. The process starts by uniformly heating a build area before a thin layer of powdered material is spread. A print head then passes across the powder, controlling the temperature whilst selectively spraying a fusing agent and detailing agent using an inkjet array. The print head then applies just enough additional energy to cause the regions sprayed with a fusing agent to fuse together. The work area then lowers by a small amount and the process can be repeated with another layer of material. An illustration of this process is shown in Figure 2.2.1. At the end of the printing stage, the build unit is removed from the printer and placed into a post-processing station where it cools. A vacuum is then connected to the top of the build unit to remove some of the unfused powder at the top, before the lid is removed and printed parts are manually extracted from the remaining unfused powder. Figure 2.2.2 illustrates a cross-section of the printed parts suspended in the unfused powder after the initial vacuum but before manual part extraction.

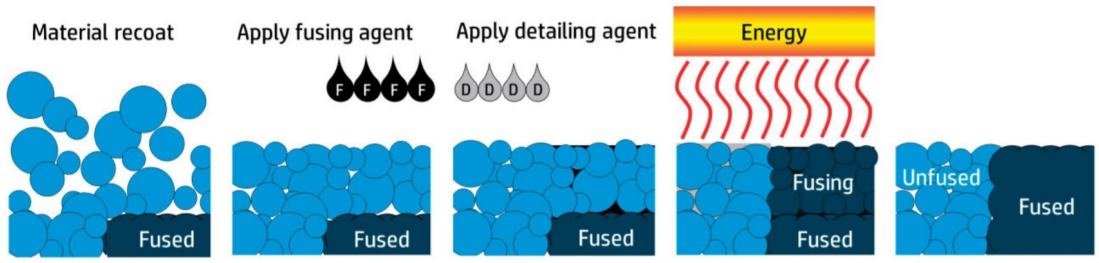

Figure 2.2.1: HP Multi Jet Fusion Print Process (HP Development Company L.P., 2019). Image used with permission from copyright holder.

Whilst the recent HP Automatic Unpacking Station does separate the printed parts from the majority of the loose powder which surrounds them, using a combination of vibration, air blasts, and vacuum, it still requires a person to manually sort through each printed part, as their pose is lost during the unpacking process. This means that although it does increase the efficiency of separating the parts from the powder, it does so in a manner which makes the subsequent automation of handling

individual parts more challenging. It is also not suitable for delicate parts, which could be damaged during the automated unpacking process.

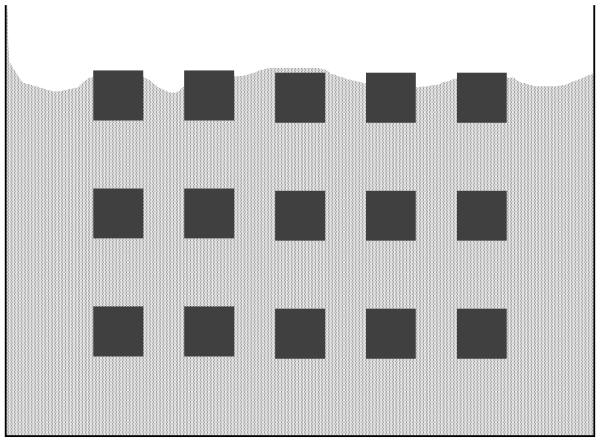

Figure 2.2.2: MJF Printed Parts Suspended in Unfused Powder

The unfused powder which surrounds the printed parts at the end of the MJF printing process is not completely homogeneous. Clumps of powder are formed throughout the unfused media, usually surrounding the printed parts, which is known as 'caking'. Although this clumped powder around the parts cannot be poured off, it is relatively friable and can be brushed or broken off by hand. Once the parts have been extracted from the build unit and the excess unfused powder has been removed, the parts are post-processed. This could involve more thorough cleaning or polishing to improve the surface finish, or dyeing if another colour is desired. Figure 2.2.3 shows three identical parts printed using MJF - the first is immediately after extraction from the build unit and still caked in powder, the second is after hand cleaning, and the third is after some post-processing (bead blasting in this case).

Unlike the majority of gripping applications where the air which surrounds the parts is of little importance, the unfused powder will restrict the design of not only the gripper, but also the sensor selection and the technique that is used to grasp and extract the objects. It is clear that the clumped powder surrounding the part causes it to be visually dissimilar to the final printed part, which would likely cause difficulties with a sensing or inspection system which relies on a vision technique.

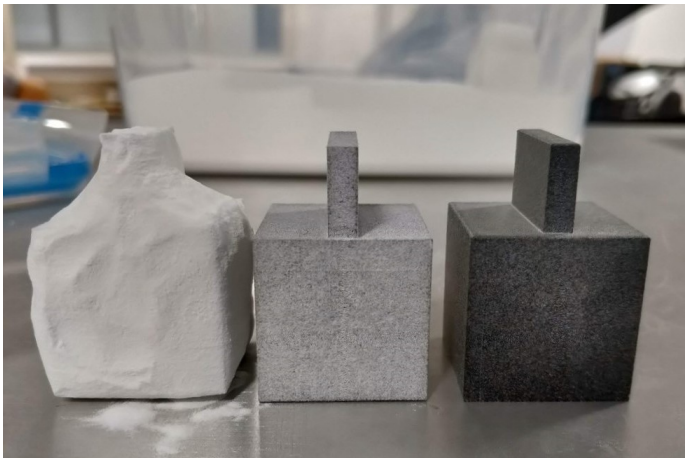

Figure 2.2.3: MJF Parts
Left: Raw
Middle: Hand Cleaned
Right: Post-Processed

What is not yet clear, is how the unfused powder and the caked powder affects the physical interaction between a gripper and the part, using a contact or tactile sensing approach.

2.3 Automated Extraction of 3D Printed Parts

Currently there are no methods for automatically extracting individual 3D printed parts from a powder-based 3D printer in a known pose. Existing automated extraction methods focus on removing a batch of parts attached to a common base, where each individual part then requires manual removal, or separating the printed parts from most of the unfused powder using vibration, vacuum, and air blasting, which results in a pile of printed parts in an unknown pose. Methods for individually extracting printed parts from filament and resin based 3D printers exist, but this is mostly due to the fact that these processes are often used for creating single parts at a time, unlike powder processes such as MJF where many parts are often printed at once. Almost all current automated extraction processes result in parts which are in an unknown pose, often with some form of support structure remaining. See Appendix A for more information on existing automated methods for extracting

printed parts from 3D printers.

An automated method capable of extracting 3D printed parts in a known pose would not only reduce the time and cost of the overall printing process, but also allow easier automation of subsequent part handling steps (such as post-processing and assembly).

2.4 Gripping and Force Transmission in Powder

When attempting to extract parts from the MJF build unit, any gripping system will first need to penetrate and move through some amount of loose unfused powder to reach the part location. It will then need to grasp the object, before lifting it from the build unit.

The majority of MJF parts are created from a polyamide powder material (PA12, PA11, or PA12 with glass beads), however other materials such as thermoplastic polyurethane (TPU) and polypropylene (PP) are also available. The powder has a mean particle size of 50-90 µm depending on the material, with a bulk density of around 0.5 g/cm^3.

Although physical interactions between powders and other granular materials is common in many natural and man-made processes (Askari and Kamrin, 2016), there are still many gaps in our understanding of the statics and dynamics of these interactions. Kang *et al.* (2018) states, "A canonical problem in the field is the modelling of the penetration dynamics of a large object within a granular material made of much smaller, but macroscopic particles". Since no existing literature has been found on using a gripper to extract objects from a powder, more low level research must be gathered on the individual steps in the gripping process.

The penetration process of a solid intruder into granular material, described by Kang *et al.* (2018), starts with an initially non-linear pressure-depth curve as the material ahead of the intruder is compressed. This forms a stagnant zone ahead

of the intruder and further penetration follows a linear pressure-depth relationship. The size of this non-linear stage and how it affects the penetration process varies depending on the granular material. It was also shown that the penetration reaches the steady state zone, the process is independent of the shape of the intruder, and only a function of the material. Albert *et al.* (2001) described a similar result when investigating granular drag on discrete objects at low velocities. Showing that as an object moves through a granular medium, there is jamming of grains in front of it. It was found that the drag has a quadratic dependence on the diameter of the object, but that there is a non-linearity to the dependence on depth which depends on the object shape (shown in Figure 2.4.1). Each object had the same circular cross section when viewed from the flow direction. This difference in drag force between different geometries was said to be an order of magnitude less than the differences for fluids. It is clear that the size of the gripper digits which penetrate the powder are of high importance, as large tips may cause resistance and a large stagnant zone could affect nearby objects, even if a physical collision does not occur. Katsuragi and Durian (2007) also showed that granular matter is very different from ordinary solids and liquids in terms of resistance to penetration. They demonstrated that the interaction between a solid object and granular material can be described as the sum of depth-dependent frictional forces plus velocity-dependant inertial drag. Keeping the majority of the gripper outside of the powder, and moving slowly would therefore be beneficial to reduce the drag force during the extraction process.

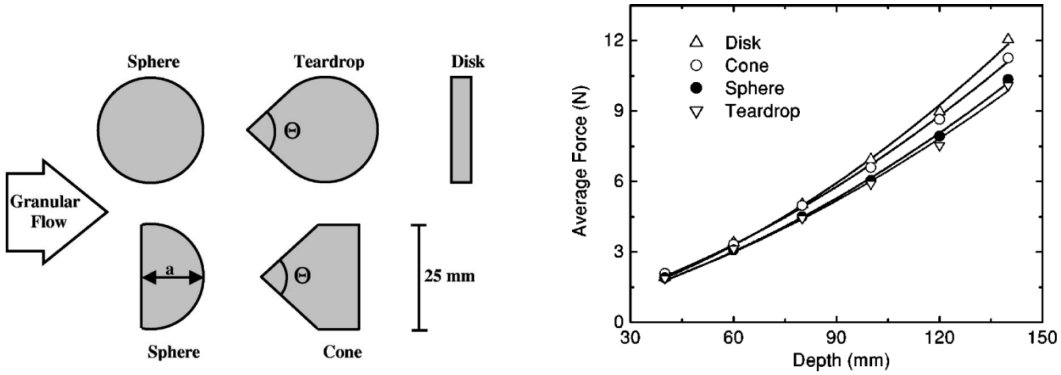

(a) Test Geometries

(b) Average Force vs Depth

Figure 2.4.1: Comparison of Depth Dependant Drag. Shown with permission from Albert *et al.* (2001). Copyright (2001) by the American Physical Society.

When a load is transmitted through granular media the stress is not applied uniformly, it is applied along heavily stressed chains of particles (Figure 2.4.2) (Mahmoodi (2012) and Peters *et al.* (2005)). As the loading direction changes, there is a rapid reselection of this relatively sparse network of contact forces, which can result in instability (Thornton, 1997). This is not ideal for a gripping application, as any changes in the direction or speed of movement, or the applied gripping force, could cause a grip on the part to become unstable.

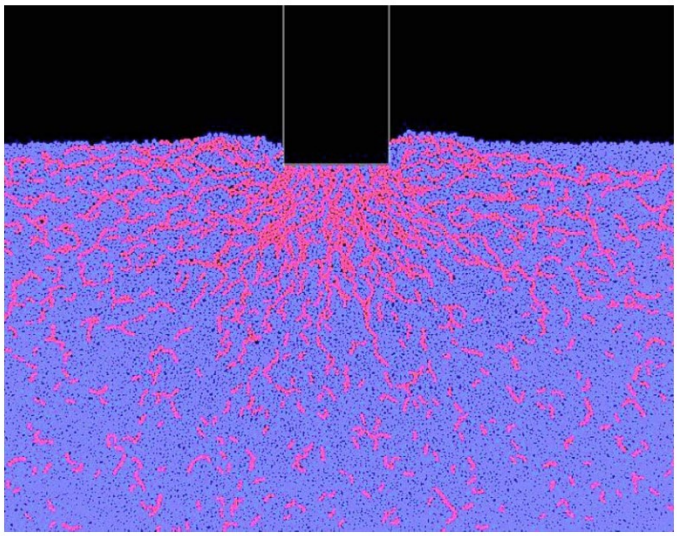

Figure 2.4.2: Force Chains Under Flat Intruder (light colours are part of the force chain, darker ones are not). Shown with permission from Peters *et al.* (2005). Copyright (2001) by the American Physical Society.

Although this existing literature sheds light on the interaction between a solid object and powder media, the effects and descriptions are often given on the microscopic scale. It is clear that there is a gap in the existing research for studies that focus on the applied macroscopic effects for processes such as grasping buried objects.

2.5 Robot End-Effectors

An end-effector is the part of a robotic system that interacts with the work environment, e.g. a grasping device for manipulation, a camera for inspection or a welding tool for fabrication. In the context of this project, the end-effector would extract the object from the MJF build unit and pass it on to the next step in the post-printing process. This could be manual finishing or packaging, but in some cases it may be further automated post-processing or assembly. This type of end-effector which interacts with a single object is known as an 'active pair'. Monkman *et al.* (2007) gives four general categories for active pair robotic end-effectors:

- **Impactive** - Physical grasping of the object with direct contact (e.g. jaws or claws).
- **Ingressive** - Penetrative methods such as hooks or pins.
- **Astrivtive** - Attractive forces such as magnets or a vacuum.
- **Contigutive** - Adhesive methods requiring direct contact such as glue.

As the unfused powder surrounding the finished parts in the MJF process is recycled for further printing, contigutive methods such as glue could contaminate this unfused powder, reducing its re-usability. Astrictive methods such as magnetic grippers are not viable with the current non-magnetic parts, but a vacuum based gripper may be useful as a vaccum hose is already used to manually remove loose unfused powder from the MJF build unit. Due to the wide variability in part geometry and some clumping of powder against the parts, a vacuum is likely a good option to *aid* in the

extraction process, but it is probably not the best option for lifting parts, or handling them for subsequent post-processing steps. This is because vacuum gripping devices often need a relatively flat and clean surface to build up enough suction force to lift an object (Bajd *et al.*, 2010), which may not be possible depending on the geometry of the 3D printed part which is to be extracted.

Ingressive methods are usually used on soft or flexible materials like fabrics where pins or hooks can penetrate the object Fantoni *et al.* (2014a). Although the printed parts themselves are solid, this type of method could be used to pass through the clumped powder which surrounds the printed parts, being used as a sub-method to an impactive type gripper.

Impactive grippers are often chosen as the main method for physically gripping and manipulating objects, especially those with some variance in geometry (Gupta *et al.*, 2017). This is due to the movement of the gripping digits allowing different sized objects to be grasped. Figure 2.5.1 shows a series of impactive gripping/grasping methods. The first two types show a one-finger gripper, which often requires either unobstructed access around the part, or a large rigid element to grasp against. Both of these may be less than ideal for an object embedded in powder. The next set is a two-finger type which ranges from simple flat parallel digits, to ones which are designed to perfectly encompass an object. These the most widely used, as they can grasp a wide range of objects and are relatively simple to control, often with a single joint (or degree-of-freedom). More complex two-finger grippers may have multiple independently controllable joints to help encompass an object more securely, or with more control. Multi-finger grippers are the most complex to manufacture and control, being used for gripping tasks where there is a large object variety. To keep costs low, and to reduce or eliminate the need for assembly, a two-finger gripper with low degrees-of-freedom will likely be the most suitable option.

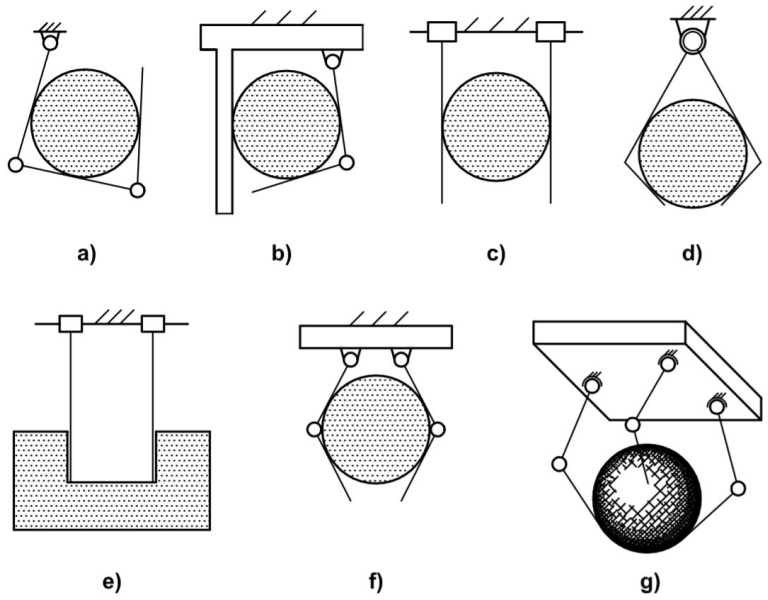

Figure 2.5.1: Typical Grasp-Type Grippers (The British Standards Institution, 2002)

a,b: one-finger type gripper

c,d,e,f: two-finger type gripper

g: multi-finger type gripper

Image used with permission from The British Standards Institution

Some of the most common industrial gripping mechanisms are based on a pincer type motion (Edwards, 1996). Figures 2.5.2a and 2.5.2b show two gripping mechanisms that translate a linear input motion into a pincer-like gripping motion. One uses a series of revolute joints and the other uses a rack and pinion gear set. Mechanisms such as these would be connected to an actuator such as an electric linear servo or a hydraulic/pneumatic piston.

Figure 2.5.3 shows a gripper which houses the actuator within the gripper itself. Although this could reduce the size of the overall gripper and actuator system, the complexity of the gripper itself is increased, often at the expense of power as well, as the actuator size is more constrained.

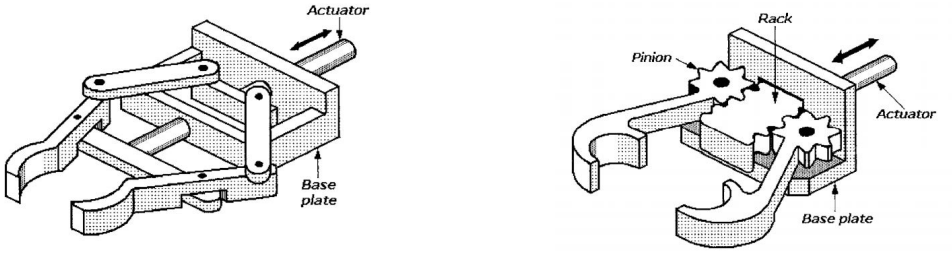

(a) Revolute Joint Mechanism (b) Geared Mechanism

Figure 2.5.2: Linearly Actuated Gripping Mechanisms (Edwards, 1996). Used with permission from Elsevier.

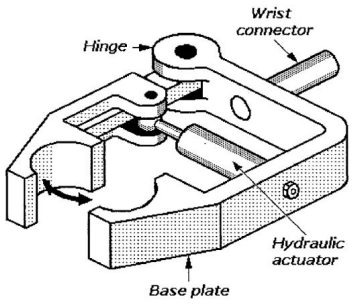

Figure 2.5.3: Embedded Actuator Gripping Mechanism (Edwards, 1996). Used with permission from Elsevier.

2.5.1 Industrial Grippers

Figure 2.5.4 shows two industrial grippers. Figure 2.5.4a is a Festo pneumatically actuated gripper, and Figure 2.5.4b is a Schunk electrically actuated gripper. Both move in a similar manner with the tips opening and closing parallel to each other, and both feature digits which allow many different shapes and sizes of tips to be mounted. The majority of industrial grippers allow custom tips or digits to be mounted, which are tailored to the object which is to be grasped. A rough cost for this type of industrial gripper is around £700.

(a) Festo Pneumatic Parallel Gripper DHPS ©Festo SE & Co. KG, all rights reserved

(b) Schunk Electrical Gripper ©SCHUNK GmbH & Co. KG

Figure 2.5.4: Industrial Grippers

These parallel grippers have a single degree of freedom, allowing the tips to move in only one axis. Sometimes this is sufficient, but depending on the task, a more complex grip may be required. Figure 2.5.5 shows a Robotiq gripper which is capable of multiple gripping modes including an encompassing grip, a parallel grip, and an internal grip. This allows a much wider range of objects to be gripped, but at the expense of complexity. Before each grip takes place, the user or control system must determine what mode is most appropriate. Increasing the degrees of freedom usually adds manufacturing complexity too, which can be seen by the increased number of visible joints and components.

Figure 2.5.5: Robotiq 2F-85 Gripper. Image used with permission from Robotiq.

2.5.2 Anthropomorphic Grippers

Anthropomorphic robot grippers are designed to more closely mimic the human hand, with many separately controllable degrees of freedom. The main goal is to create a gripping device that is much more flexible in the range of objects it can grasp and how it can manipulate them. This increases the complexity of the gripper in not only its design and manufacture, but also in the software control system. This added complexity results in an increased cost for this type of gripper.

Figure 2.5.6 shows a commercially available anthropomorphic gripper manufactured by SCHUNK GmBh (2020). It features 20 individual axes controlled by 9 DC motors, all of which are contained within the gripper. The main structure of the gripper is metal, with rubber tips for added grip. Due to the high complexity and precision manufacture of grippers such as these, the cost is inaccessible to all but the most demanding applications.

Figure 2.5.6: Schunk SVH Gripper (SCHUNK GmBh, 2020) ©SCHUNK GmbH & Co. KG

In an effort to gain some of the benefits of an anthropomorphic hand, but at a lower cost, 3D printing is commonly used for not only prototyping, but final end-use grippers. Open Bionics (2019) create prosthetic hands which feature fully 3D printed mechanical parts. This brings considerable cost savings (costing under $1,200, compared to $35,000-$120,000 (Ultimaker, 2017)), allowing the grippers to be more

accessible. The main structural parts are 3D printed from a rigid material such as PLA (polylactic acid), with the flexible joints being printed using TPU (thermoplastic polyurethane). Like many anthropomorphic grippers, the digits are actuated using tendon lines, which are fixed to the end of each digit, and run through each joint to an actuator embedded inside the hand or arm. These grippers allow a range of complex grasps to be carried out, but each gripper needs careful, time consuming assembly with many separate parts, fasteners, and materials.

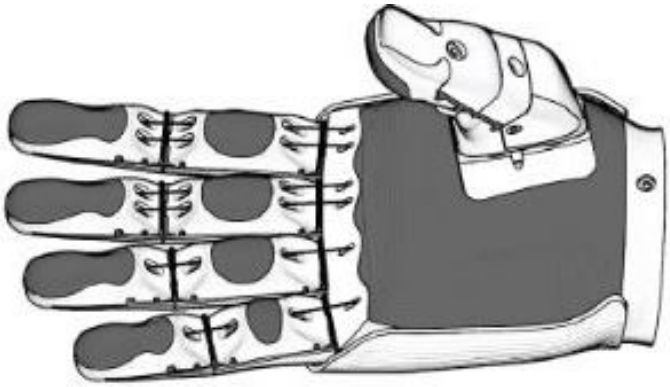

Figure 2.5.7: 3D Printed Prosthetic Hand (Open Bionics, 2019). Image used with permission from OpenBionics

2.5.3 3D Printed Mechanisms and Grippers

In an attempt to reduce the part count and manufacturing complexity, 3D printing can be used to not only produce many individual parts, but to consolidate multiple parts into a single one that does not need assembly. 3D printing the types of mechanisms used in conventional grippers in one-shot without the need for assembly is possible, but successful joint performance can easily be affected depending on the surface finish or excess material (such as un-fused powder) still present after printing. Cuellar *et al.* (2018) details a series of joints for non-assembly 3D print fabrication, but highlighted the loose unfused powder as having the potential to increase friction and lead to poor joint performance. Calì *et al.* (2012) found that creating non-assembly joints using 3D printing required many careful design decisions such as creating holes or sockets in joints to allow excess material to be removed, with many

calibration models needing to be printed for each joint size. As almost every 3D printing process manufactures parts in parallel layers, curved surfaces in the CAD model are approximated by individual steps. This results in a 'staircase effect' on any surface which is not exactly parallel or perpendicular to the layers (Figure 2.5.8), which can have a negative effect on the performance of joints and faces which require tight tolerances (Singamneni *et al.* (2010) and Wenbin *et al.* (2005)). Many 3D printing guides and services recommend a gap of around 0.5mm for interlocking or print-in-place parts. A gap of this size on every joint of a conventional gripping mechanism could lead to large errors and backlash at the tips. The rated backlash of many industrial grippers is an order of magnitude smaller than this, gap at around 0.05mm (Festo AG & Co. KG, 2020).

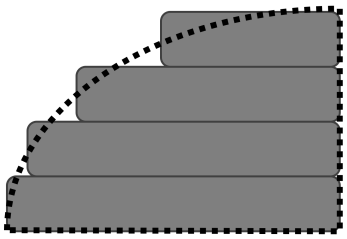

Figure 2.5.8: 3D Printing Staircase Effect

One of the benefits to 3D printing gripping devices, is the ability to produce complex geometries which would be difficult to create using more conventional manufacturing methods. Figure 2.5.9 (Blanes *et al.*, 2014) shows a single piece gripping mechanism which features two coils that flex to allow rotation of the digits. The mechanism is actuated using a double effect pneumatic cylinder. This means a simple linear input motion is transferred into an opposing gripping motion, using a single 3D printed part with no separate joints or assembly, apart from the connection to the actuator. The paper focuses on grippers for food handling applications, and notes that the surface finish and excess material remaining in and around parts, due to the powder based printing process, was not ideal. This gives an insight to some of the issues that could be faced when developing grippers using the MJF process, especially if they are to be used without going through post-processing steps such as cleaning and polishing.

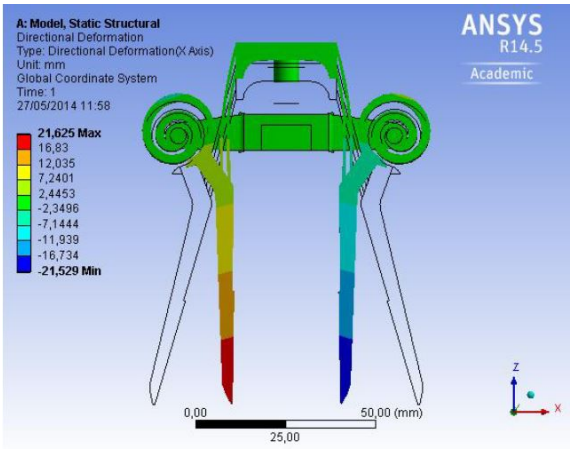

Figure 2.5.9: Angular Gripper Mechanism (Blanes *et al.*, 2014) (MDPI open access)

One of the issues with single piece mechanisms, such as the one shown in Figure 2.5.9, is that the elements which are designed to allow the digits to move, also allow movement in other axes which might be undesirable. This, coupled with large digits, can cause errors to build up in the alignment of the tips in contact with the object (Monkman *et al.*, 2007).

These types of single piece flexing joints are often called compliant mechanisms. These can be classified into two sub-divisions, where the first and most common type is concentrated (or lumped) compliance (Chen and Wang, 2007), which is where a mostly rigid part has small regions where deformation is concentrated as a hinge. The second type is where the compliant region is spread over a much larger area, distributing the stress concentration and compliance. Figure 2.5.10 shows two objects with a compliant element. It can be seen that the concentrated compliance object features a mostly rigid design with a high stress hinge section. The distributed compliance object spreads this region over a much larger area.

Figure 2.5.10: Concentrated vs Distributed Compliance

Schotborgh *et al.* (2005) details a comparison between three types of compliant flexure elements: a circular hinge, a beam hinge, and a cross hinge (Figure 2.5.11). It was found that the best performance would be to use a hybrid geometry, with two perpendicular beams crossing each other, however this geometry is not as easy to manufacture or use as part of a mechanism when compared with a simple beam hinge.

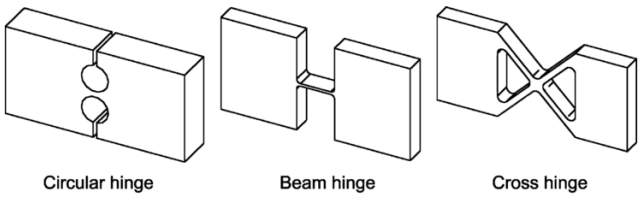

Figure 2.5.11: Compliant Flexure Elements. Image from Schotborgh *et al.* (2005), used with permission from Elsevier.

3D printing is also used to consolidate not only separate joint elements, but multiple components into a single piece. An example of this is the integration of 3D printed pneumatic actuators within a gripping device. This usually takes the form of a bellow type structure, which expands when pressurised, and contracts when evacuated or depressurised. Figure 2.5.12 (Grzesiak *et al.*, 2011) shows a gripper with an integrated bellow actuator. As the inside of the bellow is pressurised it expands, causing a rotation of the gripper digits around two pivot points. The image shows the gripper during an FEA simulation, used to determine what stresses and deformation would be experienced by the gripper in real use. The image is given without a scale or description of colour contours, but it can be assumed that the blue areas are in a low stress state, with the green areas around the bellow and pivot points being of a higher stress. This gripper was designed to be printed using the SLS powder based 3D printing process. This means enough space must be left to remove the unfused powder from inside the bellow after the print has finished.

Figure 2.5.12: Integrated bellow gripper (Grzesiak *et al.*, 2011)

Figure 2.5.13 shows another gripper design which uses a triple and single bellow actuator, 3D printed using SLA (Berger, 2012). The author states that a typical SLA gripper can have a performance index similar to most commercially-available grippers, with a weight of 100g and a force of 25N. It is not clear if these SLA pneumatic grippers have been printed in one-shot, as the black elements on either side of the bellows indicate that some assembly may be required post-printing.

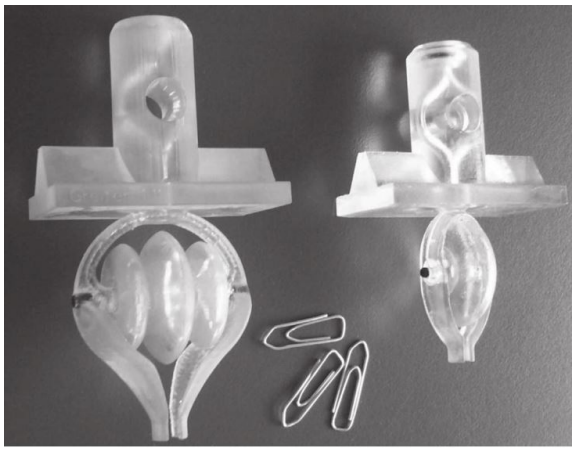

Figure 2.5.13: SLA Pneumatic Grippers (Berger, 2012).

Bourdon tubes, which are often used inside pressure gauges, can also be used to create a torsional actuator (Monkman *et al.*, 2007). These tubes typically take the form of a 'C', a spiral, or a helix, with an elliptical or oval cross section (Conway, 1995). With one end capped, pressure can be applied through the open end, causing the cross section to become more circular and the coil to straighten. This principle is

shown in Figure 2.5.14 with the red dotted lines indicating the expanded geometry during pressurisation.

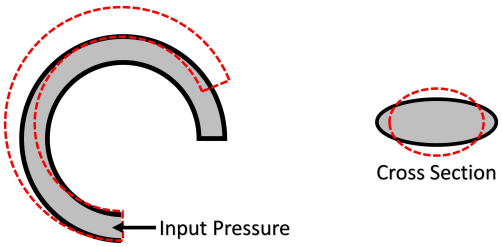

Figure 2.5.14: Bourdon Tube

Figure 2.5.15 shows a gripper manufactured using MJF which features this actuation principle. The gripper was designed to be capable of over one million actuation cycles, and the left gripper features an additional structure to help keep movements symmetrical (HP, 2018), and to reduce the undesired motion in the other axes. Technical details such as input pressures or how/if the unfused powder within the gripper is removed is unknown.

Figure 2.5.15: MJF Pneumatic Gripper (IAM 3D Hub, 2018). Image used with permission from IAM3DHub-Leitat.

2.5.4 Gripper Digits and Tips

The majority of impactive industrial gripping devices feature rigid digits. This is because it is usually desirable for the input motion to be rigidly transferred to the

tip location, where the digit is in contact with the object to be gripped. However in some cases, the digits themselves form part of the gripper mechanism and are required to flex as part of the gripper design.

Figure 2.5.16 shows a digit which flexes based on the Fin Ray® effect. Similar to the fin of a fish, as the digit is loaded from the side, it deforms around the object in the direction of the load. This means the digit is able to passively match the shape of the object being grasped. Some gripping devices such as those used in the agricultural industry, where objects to be grasped can vary widely in shape and size, have started to use this effect to increase gripping performance.

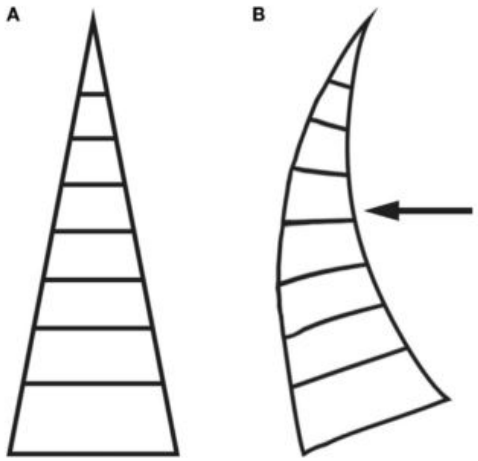

Figure 2.5.16: Fin Ray® Effect (Crooks *et al.*, 2016) **A:** Unloaded **B:** Loaded (Image open access)

In addition to the gripper being compliant to loads in the central region (as shown in Figure 2.5.16B), if the digit experiences a force or load at the tip, the structure does not deform in the same way, and it stays rigid. This allows the digit to be used in different ways depending on the type of object or required application - from flexing around large objects using the central part of the digit, to staying rigid and precicely picking up small objects with the tip.

2.6 Sensors

Fantoni *et al.* (2014b) gives an overview and classification of sensor principles in automated production processes. The first set is presence detection, ranging from contact methods such as a mechanical switch or an electrical circuit which is completed as the gripper comes into contact with an object. Contactless methods for presence detection could take the form of a laser, a proximity switch or vision system. Force-torque sensors provide more information than simply whether an object is present or not. They can provide feedback on the quality or performance of the grip through the amount of force or torque which is being applied. This could be locally from pressure sensors at the tips of the digits or strain sensors on the sides of the digits. Sensors mounted on the wrist can give the overall force or torque acting on the entire gripper, but provide little information on exactly what is happening at the tips.

In the context of this project, the contactless methods are of limited use since the 3D printed parts are often fully embedded within the powder. A contact sensor would provide feedback on object presence, but depending on the operating principle, it could be affected by the unfused powder. A wrist mounted force/torque sensor would give useful information on how the powder is affecting the movement of the gripper and its interaction with the powder overall, but it would be of little help when trying to assess detailed grip performance. From these sensing principles, a sensor mounted to the tips or digits of the gripper may be the most suitable way to get conformation that the object has been gripped, and to assess the performance of the grip.

2.6.1 Non-3D Printed Sensors

One of the most straightforward methods of gaining grip conformation would be a simple push button, mounted to the tip of the gripper, which would be depressed as force is applied to an object in the grasp. Although it is useful to know if something is or is not in the grasp, a simple on/off button is of limited use when trying to determine the grasp performance or the grip force which is being applied.

Force Sensing Resistors (FSRs) such as the one shown in Figure 2.6.1 are one way to gain more information about the interaction between the gripper and the object being gripped. As more force is applied, the air gap between the bottom semi-conductor surface, and top surface with interdigitating electrodes decreases, causing the resistance measured between the two contact pins to drop. The relationship between applied force and resistance approximately follows an inverse power-law characteristic, but there is a dead-zone at low forces where there is no response at all (under around 100g for this particular sensor). Although it could be possible to 3D print a sensor similar to this, if it was to be used without cleaning or assembly there would be loose unfused powder in between the conductive elements instead of air, which would likely have a negative effect on the sensor performance, as the air is able to easily flow out of a vent hole, which the powder would not.

Figure 2.6.1: Force Sensing Resistor (FSR)

Instead of placing a sensor in between the gripper digit and object, it is also possible to determine the applied contact force by measuring the strain or deformation of the digit as it contacts and interacts with an object. Strain gauges are one of the most common methods for measuring this deformation of an object as its surface expands or contracts. This expansion or contraction could be due to direct tensile or compressive loads, or a more complex load due to bending, twisting, or pressurisation. Most strain gauges are piezoresistive devices whose resistance changes

as they are strained. In the most basic setup, these strain sensors can take the form of a metal wire, or a rubber tube filled with mercury (Wilson, 2005), but for experimental stress analysis, industrial engineering applications and scientific measurement equipment, they usually take the form of a thin foil strain gauge (Omega Engineering Inc., 2018).

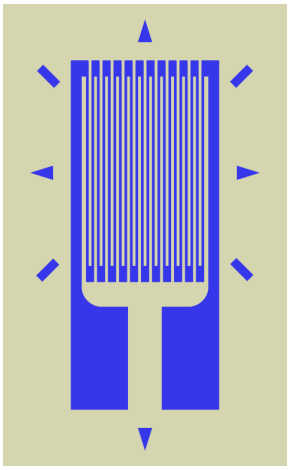

Figure 2.6.2: Strain Gauge by AnonMoos licensed under CC Share Alike 2.5

The geometry of a typical foil strain gauge is shown in Figure 2.6.2. The blue region is made from a conductive material which is what experiences a change in resistance (measured across the two large pads) as the sensor is strained. The conductive traces on the strain gauge are primarily oriented in the direction which requires the most sensitivity to elongation. The gauge usually forms part of a voltage divider circuit, which converts the varying resistance to a change in voltage, which can be measured using an analogue-to-digital converter attached to a microcontroller. Although single strain gauges can be used, many applications use multiple sensors in the form of a Wheatstone bridge, to increase sensitivity and compensate for unwanted effects due to temperature changes (Keil, 2017).

Wu *et al.* (2017) describes the development and hybrid force/position control of a compliant manipulator (Figure 2.6.3a). The gripper is actuated by pulling the tendon line which closes the tips. Once the force on the tendon is released, the gripper opens due to the elastic compliant mechanism. The actuation system is located at the base of the robot arm, which further reduces the size and weight

of the end effector. Two groups of strain gauges were attached to the large strain positions of the gripper, positioned based on FEA simulations using Solidworks. A load was applied to the gripper with the base fixed, and the resulting strain was observed (Figure 2.6.3b). Although the paper states that one set of gauges is capable of measuring the displacement of the tips, and another is placed to measure the clamping force, it is unclear how it is possible to separate these parameters for the compliant gripper design shown, as any amount of displacement will also cause a stress in the clamping force gauge region (as shown in Figure 2.6.3B), which will change the output of the strain gauges in this location, even when there is no change in clamping force. This means that the clamping force gauges would be somewhat dependant on the displacement, and it is also expected that the displacement gauges would be dependant on the clamping force as well. If these dependencies are much lower than for the intended parameter, it might not be an issue for the overall intention of the sensing principle, but it does give an insight into the complexities that can arise from having a sensing method that is based purely on the strain in a compliant mechanism. Figure 2.6.3c shows the test schematic where pressure sensors were placed on either side of an object to determine the clamping force, and a position sensor was used to measure the tip displacement. These external sensors were used to aid in the calibration of the clamping force and displacement strain gauges.

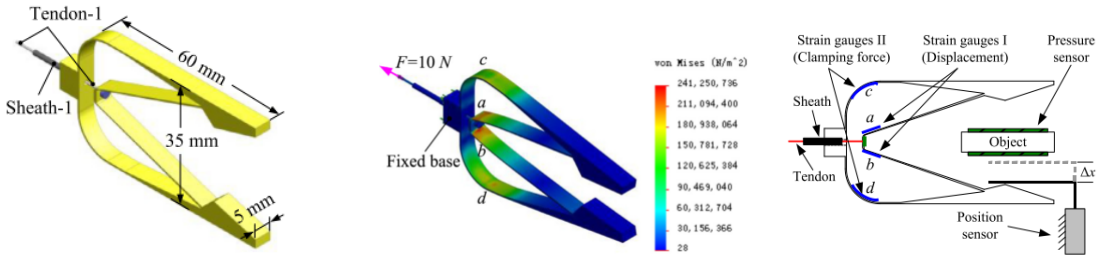

(a) Gripper Dimensions (b) Gripper FEA (c) Test Schematic

Figure 2.6.3: Wu *et al.* (2017) Compliant Gripper. Images used with permission from Elsevier.

Resistive flex sensors such as the one shown in Figure 2.6.4 are another way to measure how an object or joint is bending. They differ from typical foil strain

gauges in that they measure the flex over a larger region, rather than the strain in a small region. They are most frequently used in gloves for interacting with robots or virtual reality games. This type of sensor usually uses a conductive ink with a cracked surface. As the sensor is flexed, the cracks separate, causing an increase in the resistance (Saggio *et al.*, 2015). These sensors are usually used on gloves as part of a human machine interface, rather than for gripper based sensor systems.

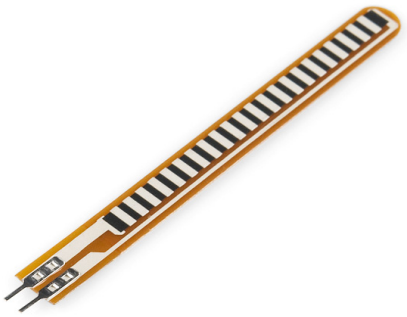

Figure 2.6.4: Flex Sensor by SparkFun Electronics licensed under CC BY 2.0

As shown in Section 2.5, most industrial robot grippers are made of separate components featuring rotating or sliding joints. For these applications, digital encoders and analogue potentiometers are often used. These can take the form of rotation sensors (Figure 2.6.5) (Platt, 2012). The digital sensors usually give a series of output pulses or signals throughout the rotation to indicate the position and direction, whilst the analogue potentiometers usually feature a wiper, which outputs a different resistance depending on the rotation angle. These sensors can be quite accurate, but are often one of the most unreliable electronic components (Walker, 2011), especially in environments where dust or debris is present. This could be problematic for a sensor which is intended to be used in or around unfused powder. These rotation sensors also have linear equivalents which work in a similar way, with a sliding contact/wiper rather than a rotary one.

(a) Rotary Encoder by SparkFun Electronics licensed under CC BY 2.0

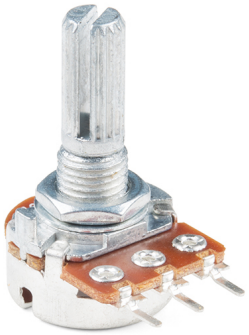

(b) Rotary Potentiometer by SparkFun Electronics licensed under CC BY 2.0

Figure 2.6.5: Rotation Sensors

2.6.2 3D Printed Sensors

Robotic grippers which use traditional manufacturing and assembly techniques feature sensors which are not 3D printed, and contain regular wiring and printed circuit boards. These are then assembled with the robotic gripper parts to create a device with sensing capability. One method which has been used to integrate sensory feedback more closely into 3D printed robotic grippers is to add metallic elements, whose resistance changes as the gripper is deformed. Figure 2.6.6a shows a soft pneumatic gripper in a pressurised (deformed) state (Adam Bilodeau *et al.*, 2015). Empty channels designed as part of the 3D printed gripper are filled with liquid metal before being sealed. These filled channels can be seen as darker coloured lines around the bottom edges of the gripper digits. These metallic channels act as a strain gauge, and the change in resistance can be measured over time as the gripper is pressurised. This is shown in figure 2.6.6b, which compares the resistance change with and without an object in the grasp. A similar technique to create embedded sensors and electrical connections has been shown by Muth *et al.* (2014), Espalin *et al.* (2014) and Lopes *et al.* (2012).

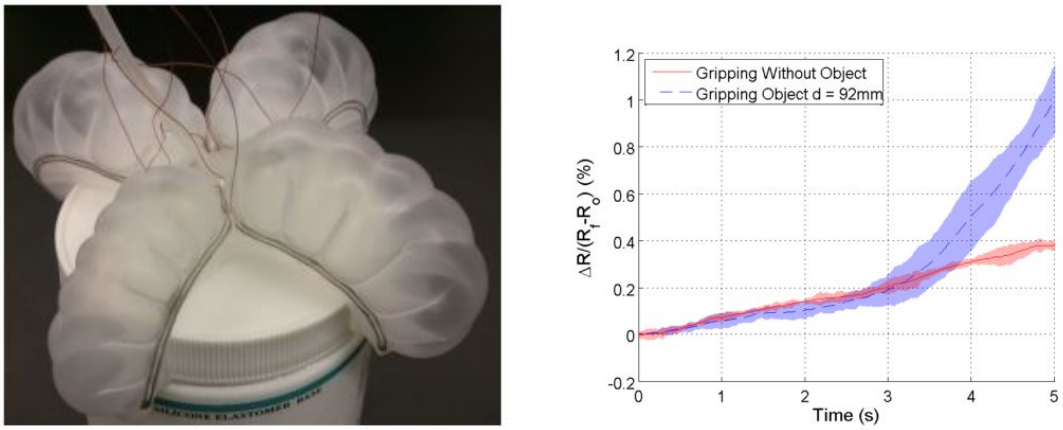

(a) Gripper in Deformed State

(b) Resistance vs Time for Sensor

Figure 2.6.6: Pneumatic Gripper with Embedded Strain Sensor (Adam Bilodeau *et al.*, 2015). ©2015 IEEE.

The results show that the embedded strain sensors can effectively determine whether or not an object is being grasped. This is useful for gripping objects embedded in a powder which are not easily identifiable using vision techniques. The manufacturing method for this example however takes multiple steps to create the gripper and then fill/inject it with the conductive material. For an MJF gripper, any unfused powder would also need to be removed from these channels, which could be time consuming or impossible depending on the geometry.

Leigh *et al.* (2012) showed an alternative method for creating piezoresistive sensors by 3D printing strips using a conductive filament, which when attached to flexible objects (such as a sheet of thin perspex) displayed changes in resistance as the object was flexed, similar to strain gauge or commercial flex sensor. When this research was carried out, conductive filament for FFF 3D printers was not commercially available, so the manufacturing process to create it was long and complex. In FFF 3D printing, multiple filaments with different material properties can be used to create a single part. Kwok *et al.* (2017) detailed the fabrication, characterisation and testing of a conductive filament for creating 3D printed circuits and sensors. A flex sensor was created using traces printed with a conductive filament, with a flexible filament to provide the support to the sensor whilst still allowing it to flex.

Dijkshoorn *et al.* (2018) shows a series of embedded sensors within 3D printed structures. These use multi-material 3D printing - combining non-conductive and new, commercially available, conductive filaments in an FFF 3D printing process. Figure 2.6.7a shows a planar and integrated complex strain sensor, 3D printed using non-conductive PLA (polylactic acid) along with sections of PLA containing a Carbon Black conductive filler. Figure 2.6.7b shows the results of a tensile test using one of these sensors.

(a) 3D Printed Strain Sensors (Dijkshoorn *et al.*, 2018) (Creative Commons Attribution 4.0)

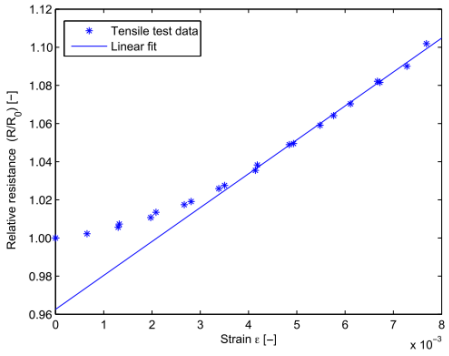

(b) Relative Resistance vs Strain (Tensile Test) (Dijkshoorn *et al.*, 2018) (Creative Commons Attribution 4.0)

Figure 2.6.7: 3D Printed Strain Sensors

A similar method was used by Eijking *et al.* (2017) in the creation of a whisker inspired tactile sensor. TPU (thermoplastic polyurethane) was used instead of PLA, with a conductive sensor on each side of the whisker (Figure 2.6.8a). A mechanical model was used to describe the expected changes in resistance, and a linear actuator was used to load the 3D printed whisker to validate the model. The results of this test are shown in Figure 2.6.8b. Both of these examples show that multi-material FFF 3D printing with conductive filaments can be used to create strain based sensors able to show changes in resistance from an applied load. However, it was also shown that both sensors had strong drift and hysteresis of the resistance over time. The load cases were also fairly simple, and no examples have been found using these types of 3D printed sensors within a robotic gripper.

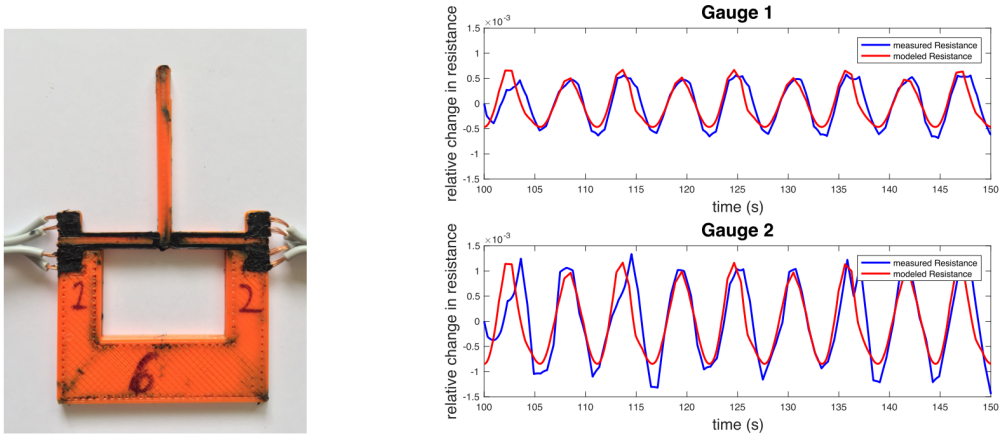

(a) 3D Printed Whisker Sensor

(b) Relative Resistance Change vs Time

Figure 2.6.8: 3D Printed Whisker Inspired Sensor (Eijking *et al.*, 2017). ©2017 IEEE.

Gooding and Fields (2017) tested a total of 97 3D printed strain gauge specimens, manufactured at a range of orientations and thicknesses, and compared test results to FEA simulations. It was found that the estimated resistance of the strain gauges differed substantially from the 3D printed specimens, likely due to the inconsistent extrusion of the conductive filaments, and stair-stepping effect of the FFF process. It was found that some of the hysteresis in these types of 3D printed sensors could be reduced by adding larger regions at the end of each loop of the conductive element.

HP has shown a small amount of parts which feature 3D printed strain gauges (Volkmann (2016), Molitch-Hou (2017) and Molitch-Hou (2016)). One example is a chain link which can measure the force of an applied load, and another is a small beam with a stain gauge on each side. These parts were not created using a commercially available MJF printer, and little technical information about their design or performance is known. Since the MJF process uses a single material for the raw powder, changing to a different material during the print process is much more difficult than a filament based process. This means that any changes to the material properties in the final part must come from a different material or agent laid down using the inkjet array. Casiraghi *et al.* (2018) investigated inkjet printing of graphene strain gauges onto paper. In one test, a strain sensor was printed onto

one side of a piece of paper, which acted as a variable resistor as the paper was flexed (Figure 2.6.9). This means that in the future, MJF printed strain gauges could be well suited for a gripper which is intended to be 3D printed in one-shot, without needing assembly, as they could be accurately printed in place.

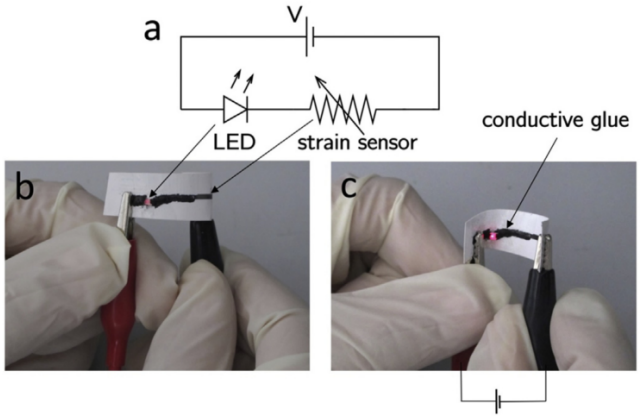

Figure 2.6.9: Inkjet Printed Strain Sensor. a) circuit schematic, b) system under tensile strain, c) system under compressive strain. Image from Casiraghi *et al.* (2018), used with permission from Elsevier.

2.6.3 Tactile Sensors

Tactile sensors are often used to gather more detailed information about the interaction between a gripper and an object. This information can be used to determine the position of the object in the grasp, its movement, and the forces that are being applied. The working principle behind these sensors varies widely, but the approaches often focus on creating an array of individual sensory elements (Chitta *et al.*, 2011). The changes in output or motion from these individual sensory elements are then compared across the array to determine the overall sensor output. Many tactile sensors utilise some form of statistical algorithm or artificial neural network to help classify the interaction, based on the output from the array of individual elements. Some examples of tactile sensors made up of many individual elements are BioTac, which uses electrodes within a conductive fluid (Figure 2.6.10a), and TacTip, which has white-tipped pins on the inside of a compliant rubber tip (Figure 2.6.10b).

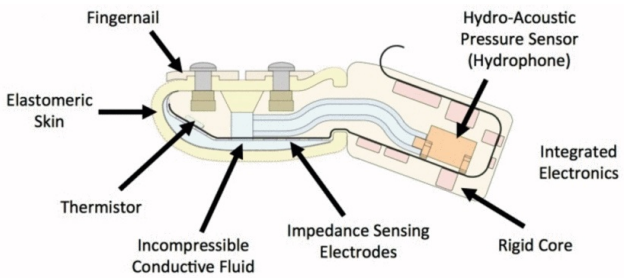

(a) BioTac (Jimenez and Fishel, 2014) ©2014 IEEE

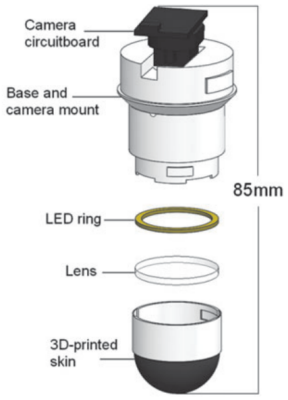

(b) TacTip (Ward-Cherrier *et al.*, 2018) CC BY 4.0

Figure 2.6.10: Tactile Sensors

Existing commercially available or open-source tactile sensors such as these are becoming more accessible and lower in cost, but they often still require a long manufacturing and assembly process, with a range of non-3D printable components inside the sensors to function.

2.6.4 Sensor Summary

From this sensor literature it is clear that commercially available strain and flex sensors could be well suited for a gripper operating in an environment with loose powder present. Whilst it has also been shown that some of these sensors can be created using 3D printing processes, they are currently larger than commercially available non-3D printed alternatives, with worse performance. As the focus of this project is on the gripper mechanism design and extracting objects from unfused powder, commercial sensors will be used, chosen based on their suitability for being 3D printable in the future. For example, as functional 3D printed sensors such as strain gauges have already been shown, using commercially available non-3D printed strain gauges will provide higher reliability for the early testing in this project, whilst still being a realistic step away from being fully 3D printed in the future.

Tactile sensors are able to provide more information about the interaction between the gripper and the object. Currently, all of the commercial available sensors feature a range of non-3D printable components within the digit/gripper itself, limiting their suitability for realistically being 3D printed in the near future. If this type of sensor could be created using only 3D printable components, the time and cost to manufacture the tactile sensor could be drastically reduced.

2.7 Actuation

Actuators are devices which apply a force or generate motion. The most common actuations are electric motors (Ida, 2014), which for robotic gripping devices apply force or movement either directly to the gripper, or indirectly via pneumatics and hydraulics (Fantoni *et al.*, 2014b). Electric motors are electromechanical devices which almost always operate using a current-carrying conductor placed in a magnetic field (Hughes, 2013). These often take the form of brushed or brushless DC motors, servo motors, and stepper motors. Although linear motors and actuators (like solenoids) exist, many linear motion requirements in robotics are fulfilled by rotary electric motors, with a gearbox or linkage to transfer the rotary torque to a linear force.

Current studies by Ellery (2018) and MakeSEA (2017) show progress towards creating fully 3D printed electric motors, but currently these devices have much lower performance than those which are not 3D printed, and still require manual assembly - often with many non-3D printed parts. Section 2.5.3 showed that 3D printed pneumatic and hydraulic actuators are already common, but a non-3D printed pump is most likely providing the pressurisation. This allows more of the gripping device itself to be 3D printed, but at the expense of shifting the non-3D printed hardware elsewhere.

Shape memory materials and piezo-electric actuators are also used in gripping devices, but they are less common and currently used most frequently in micro-gripper devices due to their relatively small displacement.

Since the focus of this project is the gripper mechanism and gripping technique, the actuator will either be an external electromechanical device which transfers motion to the gripper mechanism, or an embedded 3D printed pneumatic/hydraulic actuator which is pressurised from an external commercially available pump. A quick-release mounting interface for the gripper will be designed into the actuation system, to allow grippers to be added and removed easily, without a time-consuming integration process. In the future a suitable fully 3D printed actuator could be used to decrease this assembly step even further, and allow additional customisability to the system.

2.8 Literature Summary

This literature review has shown that there is currently no method for automated extraction of individual 3D printed parts from a powder based 3D printer (such as HP MJF). Current individual automated extraction methods only allow single parts to be removed from non-powder processes such as FFF or SLA which are often only used to print single parts instead of many parts simultaneously. Current extraction methods for powder based processes result in many parts connected to a common base, or individual parts in an unknown pose. This makes subsequent automated handling much more difficult, as if the position of the part is no longer known, collisions could occur when attempting to move or assemble it, or post-processing tasks such as cleaning could be performed incorrectly.

In order to extract individual printed parts in a known pose, a novel 3D printable impactive type gripper with compliant elements will be developed, and assessed using experimental part extraction tests from PA12 powder. These tests will aid in the development process, as no existing research has been found on how the powder will

directly affect the gripping process. Existing fundamental research on the interaction between solid objects and powder will be used to aid in the gripper mechanism development, and also applied in the assessment of qualitative and quantitative data recorded during the power extraction tests. Compliant mechanisms show the most promise for a one-shot 3D printed gripper, both in terms of performance in and out of the powder, due to limitations in creating conventional joints with tight clearances using 3D printing.

Although 3D printable sensors exist, they are often complex to manufacture and their performance is still lacking compared to those which are commercially available. Existing non-3D printed sensors will provide a reliable source of data for this project, chosen based partly on their applicability for 3D printing in the future. Similarly, fully 3D printable actuation devices which are not on the micro scale may be possible to manufacture, but existing devices still feature many non-3D printed components. In the case of 3D printed pneumatic and hydraulic actuators, although the final conversion to mechanical force is often achieved in a 3D printed device such as a bellow, the pressure is often being generated by a conventional pump. For these reasons, either a commercial actuator will be used as part of the gripping system as a whole, or a 3D printable pneumatic/hydraulic actuator will be integrated, with an external commercially available pump. Both will be trialled to determine which is most suitable for the task.

Chapter 3

One-Shot Printed Gripper Mechanism

This section details the development of a series of one-shot 3D printed gripping mechanisms, along with corresponding actuation systems. Following the project background and literature review, a list of requirements will be used to aid in the development.

3.1 Requirements and Scope

Creating a universal gripper which is capable of extracting and manipulating any possible part which is printable using MJF is not the aim of this research. This project will focus on creating a system which is able to extract a set of standard objects similar to those which are commonly printed using MJF in high volume. Initially, it is assumed that these objects have two relatively parallel faces 5mm to 50mm apart which are suitable for grasping. These objects should remain in a known pose after they have been individually extracted from the unfused powder. The allowable slip extracting an object from unfused powder should be similar to that of manipulating the same object when no powder is present.

It is assumed that the unfused powder will have an affect on the performance of the gripping interface between the digits and the part to be gripped, however the gripping mechanism should be designed in such a way that this unfused powder

does not affect or restrict the movement and operation of the gripper. The gripping system should be easily mountable to the end of a UR5 collaborative robot arm for testing purposes. The gripper mechanism should be suitable for one-shot printing using the MJF process, whilst also minimising the overall size and weight to save cost. Minimising the overall size, especially in the axis which moves through the powder, should also reduce any undesirable stagnant regions ahead of the gripper as it moves, reducing the drag force and any possible interactions with printed parts.

The unfused powder surrounding the printed parts will affect the coefficient of friction between the part and the gripper. As this coefficient is unknown, calculating the minimum required clamping force is not possible until initial tests are carried out. A ballpark figure will be calculated using the coefficient of friction of post-processed MJF parts, which will be used as a rough guide during the design phase. Frictional force can be written as shown in Equation 3.1.

$$F_f = \mu N \tag{3.1}$$

Where F_f is the frictional force, μ is the coefficient of static friction between the gripper tip and the object, and N is the gripping force. When lifting an object, this frictional force must be equal or greater than the weight of the object, which can be calculated as the object mass multiplied by the acceleration due to gravity, plus any additional acceleration due to being lifted. The minimum gripping force can then be written as shown in Equation 3.2 (Uemura *et al.*, 2019).

$$N > \frac{m(g+a)}{\mu} \tag{3.2}$$

Where N is the gripping force, m is the mass of the object, g is the acceleration due to gravity, a is the vertical acceleration of the gripper, and μ is the coefficient of static friction. Assuming an object size of 0.005m^3 with a density of 1010kg/m^3, a frictional coefficient of 0.6 for bead blasted MJF PA12 parts, and a vertical acceleration of 0.1m/s^2, the minimum gripping force is as shown in Equation 3.3.

$$N > \frac{m(g+a)}{\mu} = \frac{0.005^3 \times 1010 \times (9.81 + 0.1)}{0.6} = 2.085N \tag{3.3}$$

3.2 Mechanism Design

In the lead up to the creation of a complete one-shot printed gripper, a series of gripper mechanisms will be investigated. Their suitability for 3D printing in one-shot using MJF will be assessed, as well as how they perform at effectively grasping objects within a powder. Due to the increased difficulty in manufacturing assembled mechanical joints (e.g. revolute and sliding) compared to one-piece compliant mechanisms, and the lack of understanding of how these joints would perform within a powder, the initial gripper designs will feature compliant elements to achieve motion. If a compliant gripper mechanism is found to be unsuitable, classical mechanical joints will be investigated for further use.

Figure 3.2.1 shows a compliant hinge element, with a small thin flexible region with rigid sections on either side. This kind of compliant mechanism is commonly found on items such as lunch-box lids, to replace conventional pin hinges.

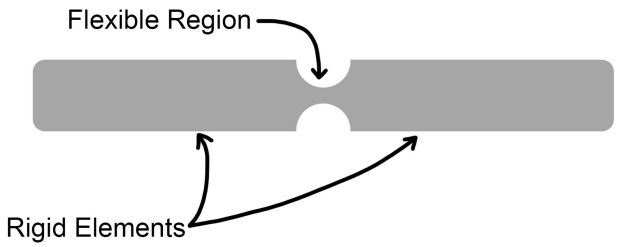

Figure 3.2.1: Compliant Hinge Element

The size of the compliant element can vary, depending on the desired deformation and stiffness, but most are usually at least an order of magnitude wider than they are thick (Figure 3.2.2). The length of the compliant region can also vary, from being concentrated in one small area to replicate or replace a conventional pin hinge, or a much more distributed compliant element, to reduce the stress concentration and allow the flex to happen over a much larger area (for example, a spring).

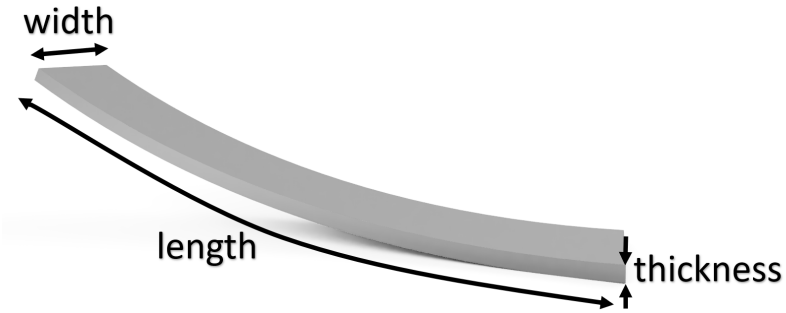

Figure 3.2.2: Compliant Element Size

Initially, compliant regions which are approximately 1mm thick and 10mm wide will be trialled, with rigid sections approximately 10mm thick and 10mm wide. For common 3D printing materials such as PA12, PLA, and PETG, these rough initial dimensions should allow the compliant regions to flex without a significant amount of force, while the rigid sections stay reasonably stiff. These dimensions will be varied along with then length of the compliant and rigid elements to achieve the desired amount of flex and movement of the mechanism.

Although it is possible to calculate the deflection of a simple compliant element such as the single beam shown in Figure 3.2.2 by hand, due to the complexity of calculating the exact deformation of an entire gripper including any tendon lines or interactions with objects, FEA simulations will be used as part of the design process to reduce the time and complexity of simulating the gripper mechanism.

3.2.1 FFF Design Considerations

Due to time and resource constraints, some of the prototype gripper mechanisms (and the majority of the non-gripper parts such as the actuator mount) will be 3D printed using an FFF process rather than MJF. The main design constraint that this process creates is that the printed parts are not isotropic, unlike those manufactured using the MJF process. This means that the orientation which a compliant element is 3D printed is much more important for an FFF process than for MJF.

The FFF process works by depositing material across individual horizontal layers

(the X-Y plane in Figure 3.2.3) laid down on top of each other (in the Z axis). Figure 3.2.3 illustrates three compliant elements on the bed of an FFF 3D printer. The first element is oriented vertically, which is the least desirable due to the fact that the FFF process produces parts which are weaker in between the individual layers. This means that the compliant element would be most likely to break between the layers as it is deformed. Geometrical errors and print failure are also more likely to be present on tall slender objects like this, especially for 3D printers where the bed (and thus part) move repeatedly in one of the horizontal axes during printing. Due to the small contact area with the bed, this part would likely also need an additional brim or support at the base. Whilst the second orientation may also need a brim to hold thin parts to the bed throughout printing, if the printed compliant element was intended to flex only in the X-Y plane, it would appear to be isotropic, as there is no flex across the individual layers (through the Z axis). Orientation 3 would be the easiest and most reliable to print this particular geometry, but the resultant compliant element may not act isotropically when deformed in the Z axis, and delamination could occur for certain geometries.

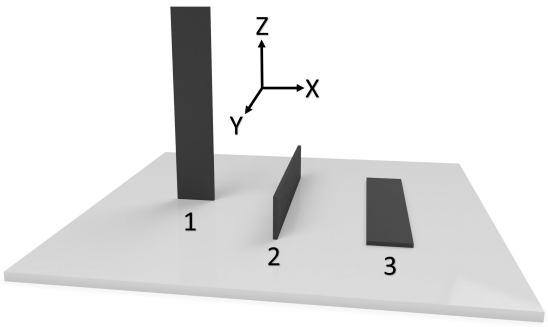

Figure 3.2.3: FFF Compliant Element Print Orientation

Unfortunately, for a one-shot 3D printed gripper, there may be other geometrical features present on the mechanism which require the part to be printed in a specific orientation. In some cases this could result in printed parts which feature some amount of anisotropy, causing a small difference in deformation compared to an MJF part of the same geometry. Due to the increased complexity in simulating FFF printed parts using FEA (Abbot *et al.*, 2019), all simulations will assume an isotropic material manufactured using MJF. All compliant FFF parts will be printed

in an orientation to maximise the apparent isotropy during gripper operation for that particular geometry.

3.2.2 Underactuated Gripping Mechanism

In the context of robot grippers, underactuation is where there are fewer sources of actuation than degrees of freedom, or joints (Birglen *et al.*, 2008). This can enable a range of objects to be gripped with relatively simple control, as there is not a dedicated actuation device for every joint. Existing underactuated grippers usually feature rigid sections which are connected with flexible joints, made of a separate material, which act as springs (Montambault and Gosselin, 2001). A tendon line is then passed through the rigid digits alongside the flexible regions, which causes the digit to bend once it is pulled (Ozawa *et al.*, 2009). Figure 3.2.4 shows tendons on the underside of a robotic hand Hussain *et al.* (2018). As part of the hand is already 3D printed, if the tendons could also be 3D printed in place, time could be saved during assembly. The same is true for 3D prosthetic hands from companies such as Open Bionics (2019) which are also partially 3D printed (Ultimaker, 2017).

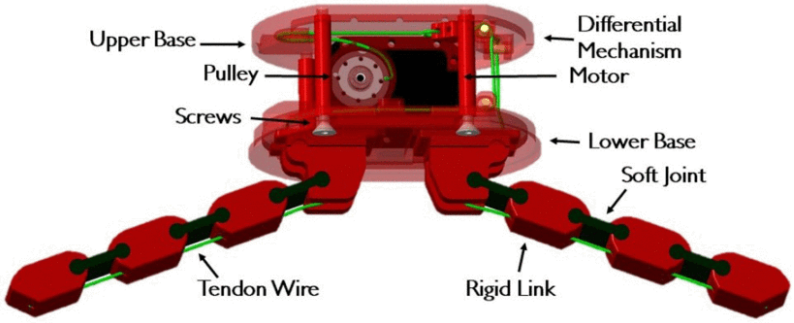

Figure 3.2.4: Partially 3D Printed Gripper with Tendons (Hussain *et al.*, 2018). ©2018 IEEE.

An initial prototype of an underactuated digit was manufactured on a Prusa i3 MK3S (Prusa Research, 2019), which uses the FFF 3D printing process. This process requires a support structure to be printed below hanging regions, but it is possible to 'bridge' certain straight line distances without support (3D Hubs, 2020a). Figure 3.2.5 shows a basic underactuated digit design. The large blocks are the

rigid sections, attached to each other by a thin flexible/compliant base. The tendon line is then printed from the end digit, through a channel in the others, to a pull tab within the main gripper body which can be attached to a linear actuator or similar. Pulling the tendon will create a bending force on the thin regions, causing the whole digit to flex. As there is only a single tendon line and actuator, this force causes bending in the regions with the least resistance (Wu *et al.*, 2009), allowing the gripper to conform to whatever shape it is grasping. In an FFF process, the print orientation plays a key role in the performance and manufacturability of such geometry. Due to the individual layers and lack of support, bridging can only be done parallel to the print bed. Printing digits perpendicular to the bed would be possible, but as the strength in this direction is much lower, the tendon and compliant regions would fail much more easily. Unlike many conventional tendon lines which are often made from fishing line (or similar) which buckle or deform almost immediately in compression, the 3D printed tendon line can still transfer force to the tip as it is stiffer and, even if it buckles, limited off-axis movement is possible within the digit channels. This allows the digit to bend and be controllable in both directions.

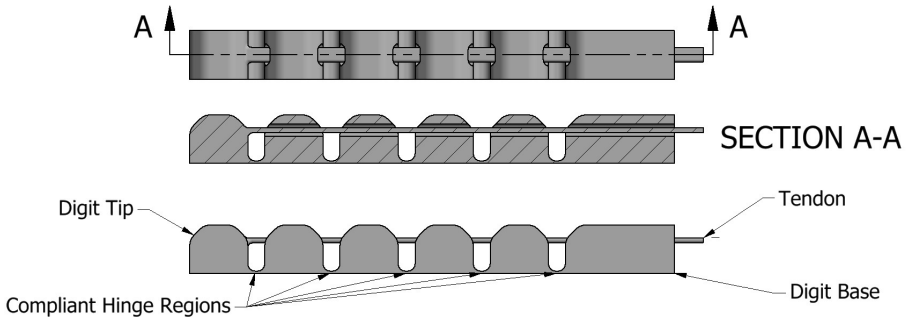

Figure 3.2.5: Underactuated Digit

FEA simulations within Ansys 2019R2 have been used to simulate the deformation of the underactuated digit to an applied load. Figure 3.2.6 shows the total deformation for a 4N load acting on the tendon. The maximum deformation is 39.6mm at an angle of 49°.

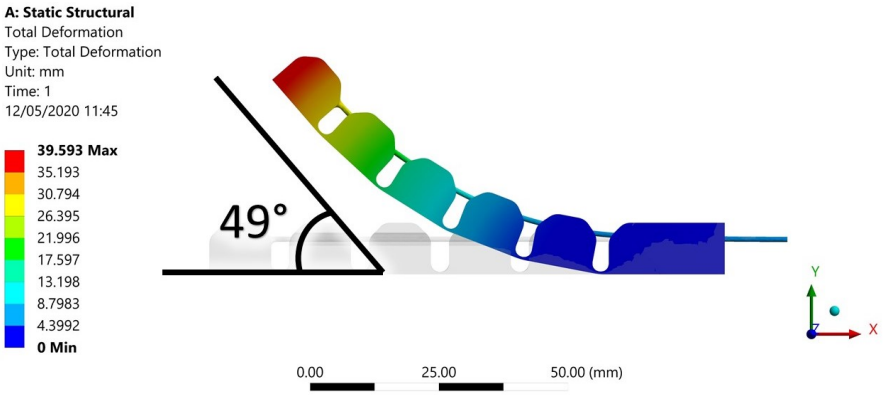

Figure 3.2.6: Underactuated Digit FEA Simulation

Figure 3.2.7 shows two prototype digits, with integrated tendons. The left design requires the tendon to be cut at the back (rightmost) wall before it can be pulled to bend the digit, the right design was printed with two independent base sections, allowing them to be pulled apart without cutting. The compliant regions in these prototypes were printed directly onto the printer bed, and the thickness was chosen based on the first layer thickness of the FFF machine, 0.3mm in this case. This allowed the sections to flex easily, whilst still being relatively robust.

Figure 3.2.7: Prototype FFF Digits

Another prototype digit was manufactured using HP's MJF process, shown in Figure 3.2.8. As in this powder based process the unfused powder provides support for the printed parts, no additional support structure is needed. This allows geometries to be printed which would be either impossible or require a complex, difficult to remove, support structure if printed using FFF, meaning an underactuated digit such as this can be printed in any orientation. The ability of the 3D printed tendon to transfer force in tension as well as compression can also be seen here, as the digit can be bent in either direction.

(a) Bend Closed (b) Straight (c) Bend Open

Figure 3.2.8: MJF Underactuated Digit Bend Test

Figure 3.2.9 shows three underactuated gripper digits. The first is 3D printed using the FFF process, and it can be seen that although the tendon line was designed as a single line, as the 3D printer passes from base to tip to create the geometry using the much smaller diameter nozzle, the unsupported middle section sags and cools. This results in many smaller individual strands, instead of a single solid tendon. These individual strands tend to flatten out from the original circular tendon cross section, into more of a band as the gripper is actuated, spreading the load between each strand. The second digit is 3D printed using the MJF process using the same tendon geometry dimensions. It can be seen that compared to the FFF process, it has been 3D printed as a single solid circular tendon, as designed. Visually it looks much smaller than the FFF tendon, however as the individual FFF strands have flattened, the overall cross-sectional area between the two is almost equal. Under high loading, the tendon line in the MJF digit snapped, which provided the inspiration for the third digit, which features a widened tendon for extra strength. As the tendon has been widened only in the axis perpendicular to the bending, there is only a slight increase to the bending stiffness, but a considerable increase in tensile strength.

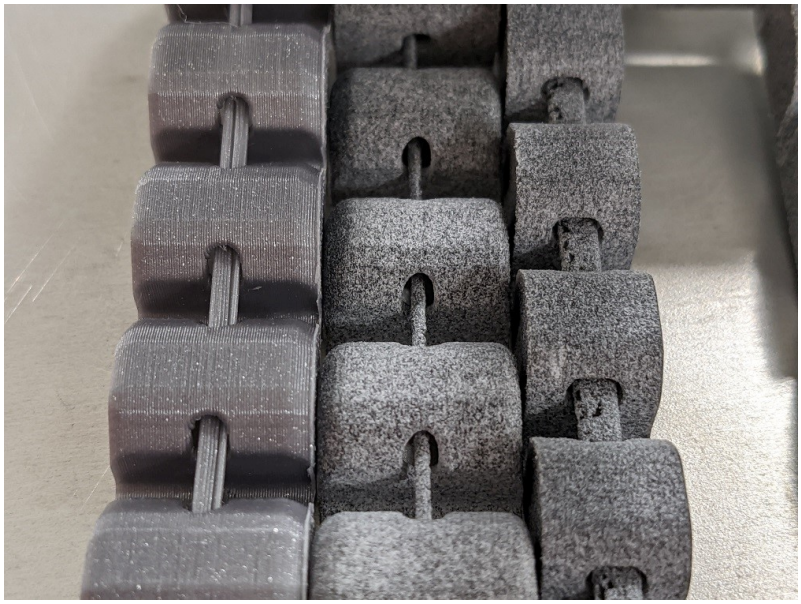

Figure 3.2.9: Left: FFF Tendon Line
Middle: MJF Tendon Line
Right: MJF Tendon Band

Figures 3.2.10 and 3.2.11 show an underactuated digit with the same simulated input, with and without an object in its path. It can be seen that for the unobstructed digit, the input force is distributed across each separate compliant region. However, once one of the rigid sections comes into contact with an un-deformable object, any further input force can only be distributed across the compliant regions after the contact point. In this case it only applies to one further region, but subsequent compliant sections would also continue to bend if present. The colour scale in both figures is logarithmic.

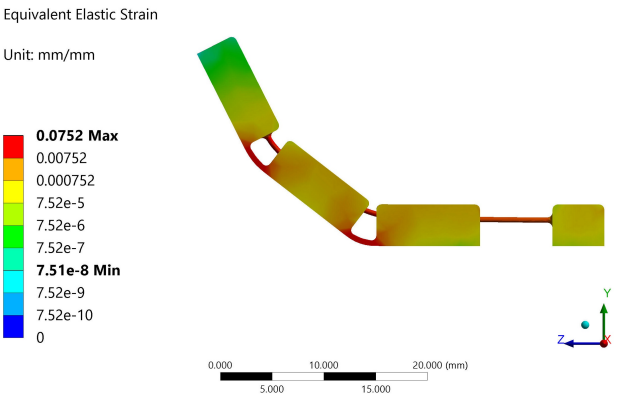

Figure 3.2.10: Unobstructed Underactuated Digit FEA

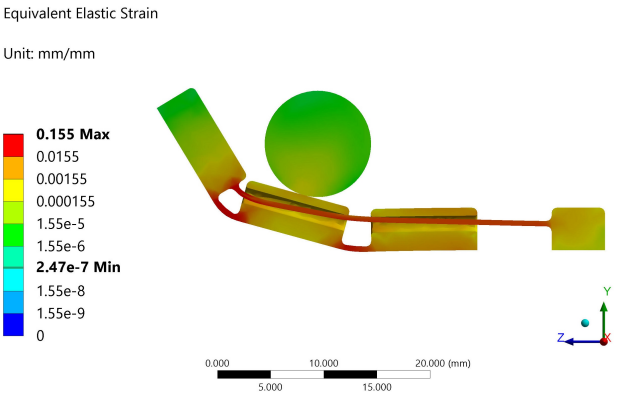

Figure 3.2.11: Obstructed Underactuated Digit FEA

An FFF prototype with three digits was manufactured and, once connected to a linear actuator, can be opened and closed to grasp a range of objects, as shown in Figure 3.2.12. Objects up to 200g have been successfully lifted using this gripper. The possibility of gripping a wide range of objects is key for general purpose gripping applications such as for prosthetics, or where objects are in an unknown orientation, but it can be less accurate for grasping objects which are intended to stay in a known orientation. It can be seen that the individual underactuated digits all flex in a different manner whilst gripping each object, even though there is only a single input.

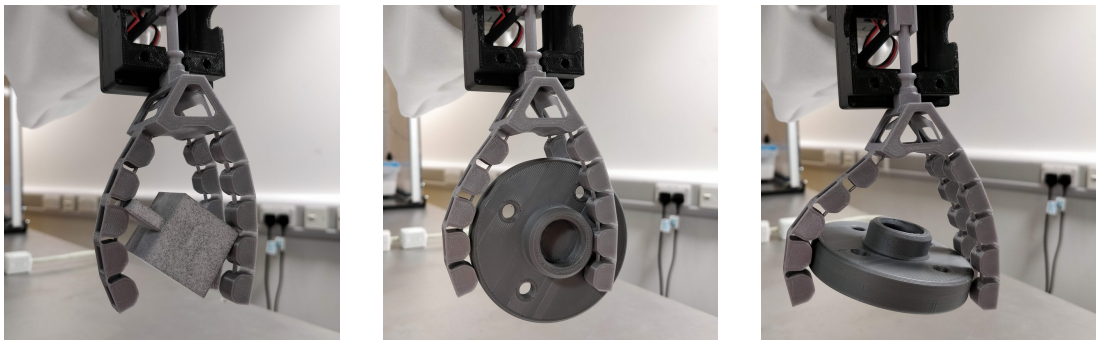

(a) Object 1 (b) Object 2 Orientation 1 (c) Object 2 Orientation 2

Figure 3.2.12: Underactuated Gripper Grip Test

This underactuated gripper performs well outside of the powder, but due to the underactuated design, without additional supports the digits would likely bend backwards as they penetrate the powder. In order to understand what pose the gripper digits are in, a separate sensor would need to be added to every compliant joint, adding complexity to the sensing system. Even if the digit pose could be understood, with only one input, there is limited control over how the digits grasp an object. Somewhat encompassing the object to extract it could also limit access to the part during subsequent post-processing steps such as cleaning. Due to its underactuated nature and encompassing grip, this mechanism may also not be ideal for studying the effects of the powder on the tips of the digits.

3.2.3 Explicit Mechanism

Although an underactuated gripper may be suitable for extracting an object embedded within a powder, a more explicit (i.e., more direct control of the tip location, compared to an underactuated digit) gripper mechanism could give a better understanding of the exact effect the powder is having on the grasp, and help extract the object in a known pose. These findings can then be used to aid in the development of other gripper mechanisms. To achieve this, the initial explicit gripper design will focus on a two-digit symmetrical mechanism.

An example geometry was created to produce a symmetric gripping motion from a simple linear input force. Figure 3.2.13a shows a 3D model of the test geometry, featuring a rigid base and pull tab, connected with thinner compliant elements. When a force is applied to the central pull tab, the two digits are pivoted about the sides of the base. This deformation can be seen in Figure 3.2.13b, which shows an FEA simulation of the model, with a 5N load applied to the pull tab in the -Y direction. This transient structural analysis was carried out using ANSYS 19.1 (ANSYS Inc, 2019). Once the material properties had been assigned, a fixed constraint was added to the base of the mechanism, and an input force was applied to the pull tab. One disadvantage with this design, is that although the tips do move closer together as desired, there is also a deflection of similar magnitude in the Y axis. This undesired deflection could be reduced or eliminated through experimenting with changes in the geometry.

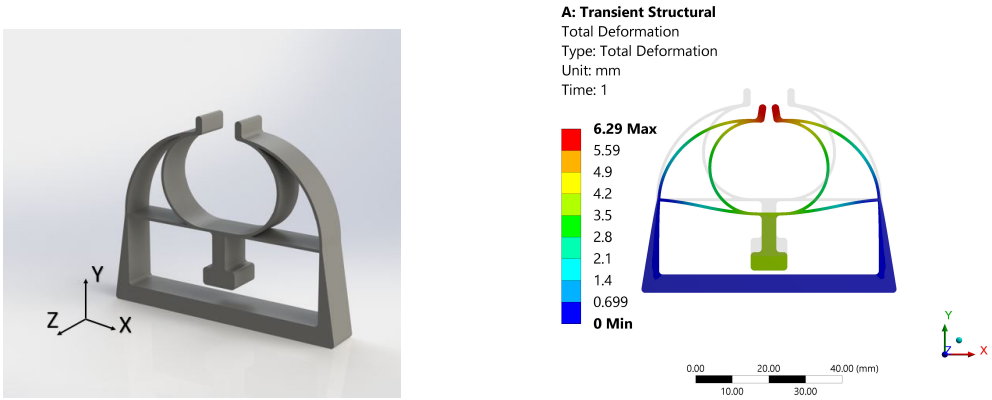

(a) 3D Model

(b) FEA Deformation

Figure 3.2.13: Linear Gripper Mechanism

Some prototype linear input grippers were printed using an FFF printing process in a PLA material (Figure 3.2.14). These printed prototypes feature a hole in the base where a rod can be inserted to push the tab, opening the digits. Both feature the same basic design, with a common mounting element. Part of the mechanism was removed from one of the prototypes, which reduces the force required to actuate. This means that the grippers can be adapted whilst keeping the same interface with the actuator and robot arm. As these grippers were printed flat on the bed of an FFF 3D printer, the compliant elements act isotropically, as the flex only occurs within the plane of each layer, instead of through the layers.

Figure 3.2.14: Linear Gripper Design Prototypes

Figure 3.2.15a shows a revised linear input gripper design, which uses the same input and mount interface, but a slightly different mechanism geometry. This results in less deflection in the undesired axis compared to the previous design. Similarly, slight changes in the geometry allow the gripper to respond differently to the same input. The rightmost prototype was manufactured using the MJF process. Figure 3.2.15b shows the simulated deformation of the gripper from a 5N input force from above. This results in a 7mm deflection of the push tab, and 20mm of deflection of each digit. Although this gripper has flat tips and a non-parallel acting mechanism, as it grips an object, the tips flex to align with the sides of the part, due to the compliant nature of the mechanism. The FEA results also show a contact force between the digits of over 10N, which is 5x the theoretical required minimum shown in Section 3.1.

(a) Prototypes (printing process from left to right: FDM, FDM, MJF.)

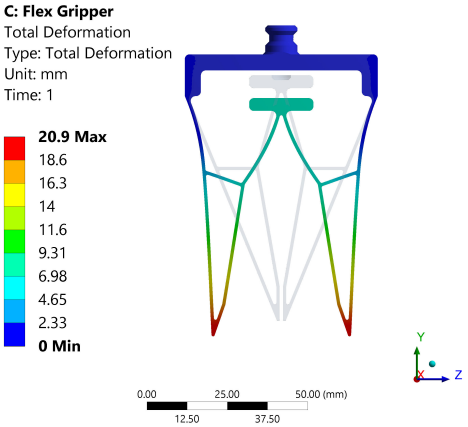

(b) FEA Deformation

Figure 3.2.15: Revised Linear Gripper

A comparison between the MJF and FFF prototype grippers is shown in Figure 3.2.16. At the circular region on the base of each gripper, the difference in layer height between the two manufacturing processes can be seen. The FFF process shows easily visible layers, compared to the MJF part with much smoother curves. This means that the MJF gripper more closely matches the geometry of the 3D CAD model.

Figure 3.2.16: MJF and FFF Comparison

3.2.4 Concentrated vs Distributed Compliance

Figure 3.2.17 shows the deformation of two grippers. Figure 3.2.17a features rigid elements with compliant regions concentrated as hinges. Figure 3.2.17b is the same gripper but with sections which distribute the compliance. The same 5N load is applied to the tab of each gripper in the -Y direction. It can be seen that the 5N load results in approximately the same deformation of the input tab and tips for both mechanism designs.

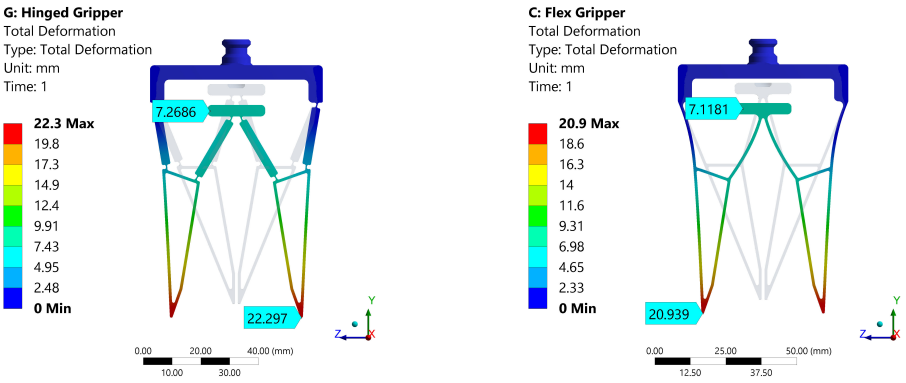

(a) Concentrated Compliance

(b) Distributed Compliance

Figure 3.2.17: Deformation Comparison between Concentrated and Distributed Compliance Gripper

Figure 3.2.18 shows a capped isosurface of each gripper with the coloured regions experiencing an equivalent (von-Mises) stress over 10 MPa. It can be seen that the maximum stress experienced in the regions of concentrated compliance is almost 5x higher than in the distributed compliance gripper. This is a significant difference, considering how similar the overall deformation is. As the yield strength of many common 3D printing materials such as PLA, PETG, and Nylon is around 50MPa, this would cause the concentrated compliant regions to plastically deform or break completely.

(a) Concentrated Compliance (b) Distributed Compliance

Figure 3.2.18: Concentrated vs Distributed Compliance Equivalent Stress Capped IsoSurface (over 10 MPa)

One observed benefit to the concentrated compliance design is that as the compliant region is much smaller, the stiffness of the part to deflections in other axis is much higher. This removes the need for additional structural geometry in some cases such as in the IAM 3D Hub (2018) gripper (Figure 2.5.15). Figure 3.2.19 shows a simulated comparison between deformation of the concentrated and distributed compliance gripper mechanisms after a 5N load is applied to the side of the tab (in the x axis). It can be seen that the distributed compliance regions allow much more deflection in this axis than the concentrated compliance regions.

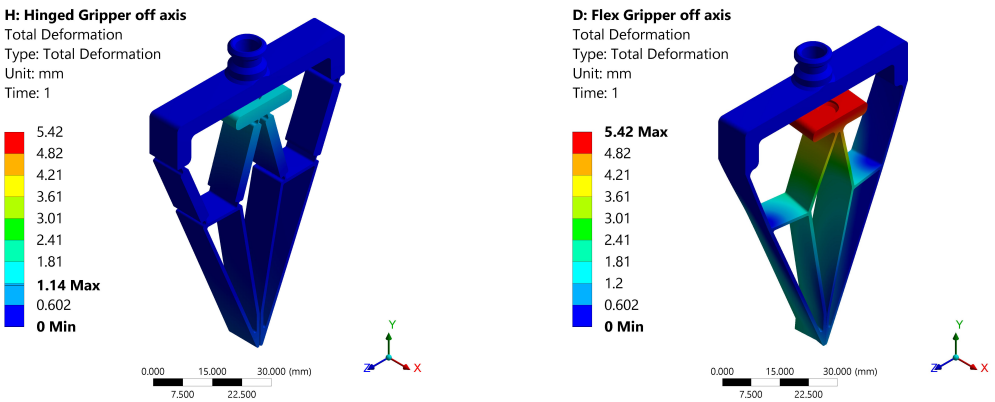

(a) Concentrated Compliance (b) Distributed Compliance

Figure 3.2.19: Comparison of off-axis deformation. Colour scales are matched to make comparison easier.

Both gripper designs were manufactured from PETG using the FFF 3D printing process (Figure 3.2.20). Actuating the 3D printed compliant grippers by hand showed that they act in the same manner as the simulated grippers, with a similar amount fo deflection in the intended direction, but much less stiffness in other axes on the gripper with distributed compliance.

Figure 3.2.20: Prototype FFF 3D printed grippers

As expected from the much higher stress experienced on the concentrated compliance gripper, plastic deformation occurs during operation, causing the gripper to not return to the original position (Figure 3.2.21). To prolong the lifespan of such a gripper, the deformation should be limited to keep within the elastic limit.

Figure 3.2.21: Plastic Deformation on Concentrated Compliant Gripper

Although the concentrated compliance mechanism shows less off-axis deformation, the much higher stress experienced in the compliant elements makes designing, simu-

lating, and testing the deformation of the mechanism more difficult. Concentrating the compliance to a small region creates a joint which more closely resembles a conventional revolute joint, which can be helpful for understanding the motion of the mechanism when actuated, but would require external sensors such as encoders or potentiometers to measure the angle at each joint. Distributing the compliance across a larger region means the strain in this section can be measured more easily using strain gauges or flex sensors. Being able to understand the relationship between the strain in these compliant regions and the deflection or clamping force at the gripper tips could more easily enable the creation of a one-shot printed gripper with embedded sensors. A downside of a distributed compliance mechanism is that for some complex load cases, the elements can flex or buckle in unexpected ways. To avoid this, each gripping mechanism should be tested whilst gripping a range of objects to determine its safe operating limits.

3.3 Actuation

As the focus of this project is the gripper mechanism and not the actuation device, this project will feature a actuation system which is independent to the gripping mechanism. This will either take the form of a completely separate electromechanical actuator which the gripper mounts to, or a pneumatic/hydraulic actuator which may be 3D printed as part of the gripper, even if the design is independent - this means the gripping mechanism will be the same, regardless of the actuation principle.

3.3.1 Pneumatic Actuation

Pneumatic actuation is commonly used for industrial grippers, and also in some 3D printed gripping devices, including those manufactured using MJF. A prototype mechanism was designed, based on the IAM 3D Hub Gripper shown in Figure 2.5.15. Based on FEA simulations (Figure 3.3.1) and a non-functional test prototype, it was decided that this type of Bourdon tube gripper is more suited to low force gripping

tasks such as pick and place (e.g. for PCB assembly), as large forces make controlling the grip difficult, as the coils easily flex in undesirable directions.

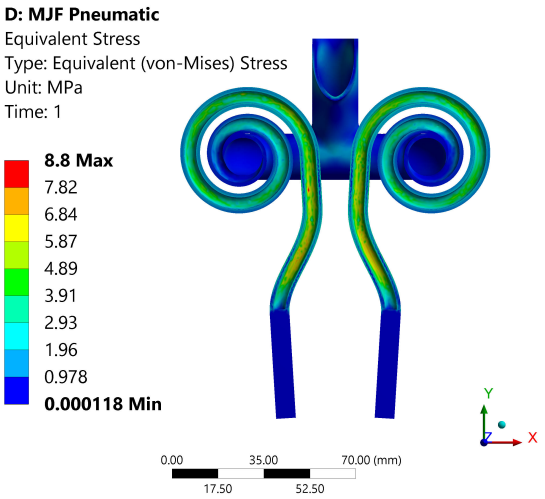

Figure 3.3.1: Pneumatic Bourdon Tube Gripper FEA

Figure 3.3.2 shows the previously designed distributed compliance gripping mechanism, extended to include an embedded pneumatic actuator, based on a bellow design. This gripper features the same compliant elements and mounting geometry, with an extended centre to fit the bellows mechanism. This means any relationship between strain and deflection or clamping force in the compliant region should be identical to the gripper without the embedded pneumatic actuator.

(a) External View

(b) Cutaway View

Figure 3.3.2: Gripper Mechanism with Embedded Pneumatic Actuator (3D CAD Model)

Figure 3.3.3 shows the strain experienced by the pneumatic gripper during a FEA simulation. The applied internal pressure was set to a vacuum of 0.6 atm. The simulated stress and strain are within the allowable elastic range for the HP PA12 material.

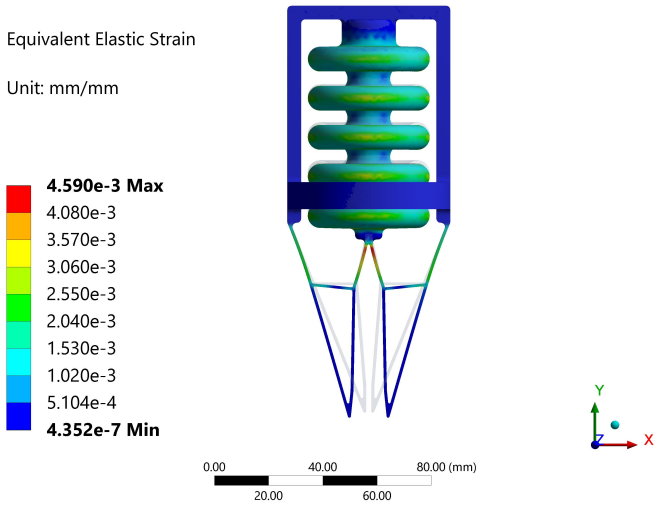

Figure 3.3.3: Pneumatic Gripper FEA

This gripper was printed using the MJF 3D printing process, shown in Figure 3.3.4. It can be seen that the MJF powder is able to preproduce the complex geometry of the 3D model very accurately. Although the powder which was surrounding the gripper during the printing process has been effectively removed on the exterior surfaces, some amount of powder was still present inside the bellows of the pneumatic mechanism. Due to the small opening, post-processing the gripper to completely clean this region is challenging.

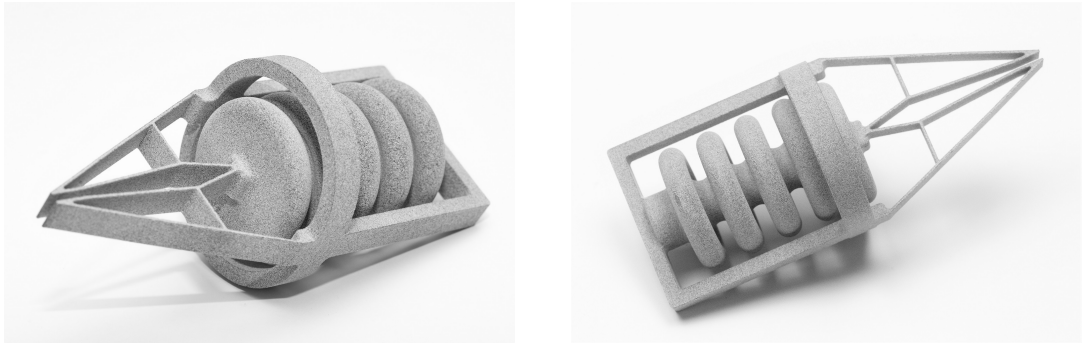

(a) (b)

Figure 3.3.4: Gripper Mechanism with Embedded Pneumatic Actuator

Figure 3.3.5 shows the gripper movement, able to open with positive internal pressure, and close with negative internal pressure to grasp an object.

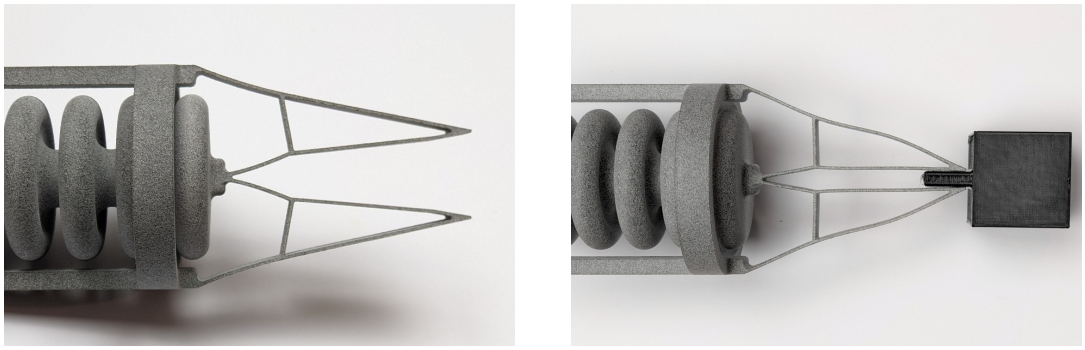

(a) Open (b) Closed

Figure 3.3.5: Gripper Operation

Although the embedded pneumatic actuator shows promise, its priority was lowered, mostly due to the fact that working with novel pressurised actuators in close proximity to loose PA12 powder could pose a safety hazard, as if the right concentration of powder-air is achieved it can be combustible/explosive. It is also much harder to control reliably and smoothly than a purely electromechanical actuator. As the mechanism below the actuator is identical between both actuation methods, this pneumatic design could be developed further in the future once it can be tested with less risk.

3.3.2 Electromechanical Actuation

Figure 3.3.6 shows a small solenoid acting as an actuation device for the gripper mechanism. When attached to a 12V power supply, the solenoid actuates and pushes the input tab of the gripper. Although this low-cost solenoid can easily be actuated using a transistor and a microcontroller such as an Arduino (2019), the speed of actuation is fixed and there is no fine control of the exact displacement. The holding force of this solenoid is 20N, but the actuation force is less, and also not linear throughout the actuation stroke.

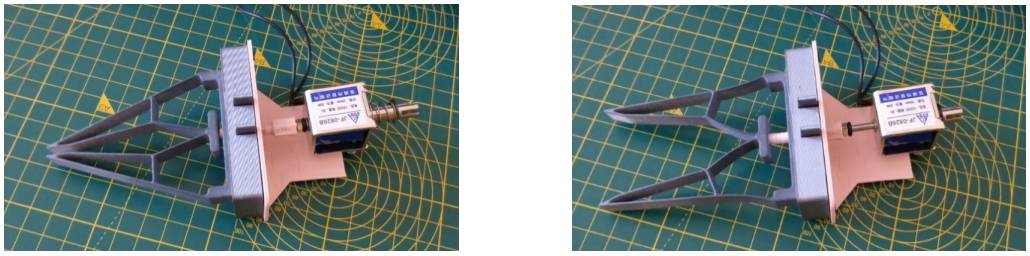

(a) Gripper Closed

(b) Gripper Open

Figure 3.3.6: Prototype Solenoid Actuator Mechanism

Although the solenoid shown here is capable of opening the gripper mechanism, more control over the position of the digits and the speed of actuation is needed to reliably grip objects from within the powder. Figure 3.3.7 shows a gripper mechanism attached to a small servo motor. As the servo turns it pushes on the end of a rod which passes though the mount, actuating the gripper. When attached to a microcontroller, the position of the servo can be controlled in 1° increments, allowing much more precise control of the gripper, compared to the solenoid. However, this method of conversion from rotary to linear motion is not ideal, as it relies on the elasticity of the compliant mechanism to return to the closed position. As the compliant mechanism alone produces a relatively small grasping force, the servo arm would need to be attached to the input rod to apply enough force to lift most 3D printed objects, however this kind of linkage could add backlash or additional assembly steps.

Figure 3.3.7: Servo Actuator Mechanism

Rather than a motor with a rotary output, a linear actuator was tested and found to be the most suitable electromechanical method of applying the linear displacement to the input rod. This actuator is controlled in the same way as a standard servo motor, allowing easy control using an Arduino or similar microcontroller. This actuator provides a much larger stroke length than is needed for this specific gripper, but this allows other mechanisms with larger strokes to be tested in the future if needed. Figure 3.3.8 shows the linear actuator with an attached gripper, mounted to a UR5 robot arm.

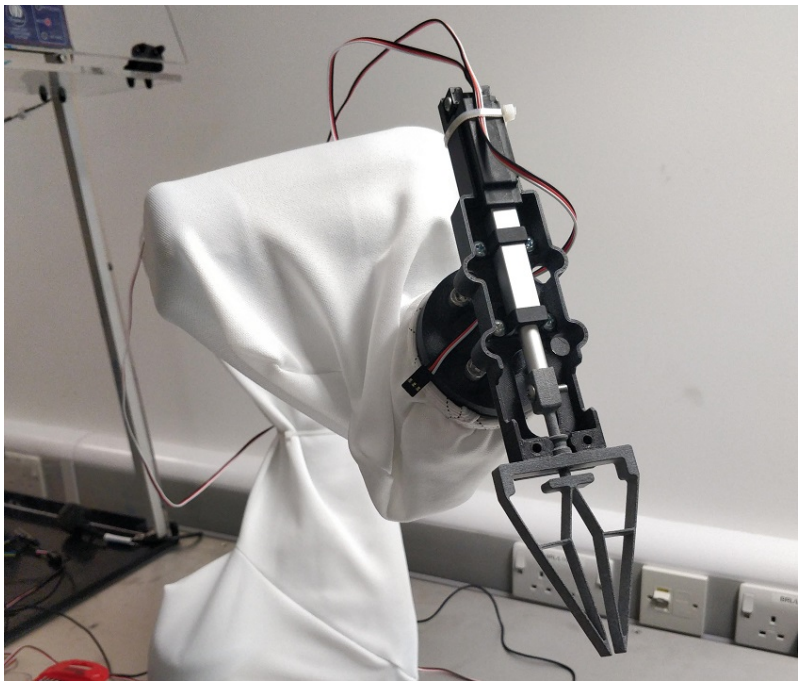

Figure 3.3.8: Initial Gripper Testing

After initial testing an alternative linear actuator was chosen, with the same size and performance, but without a built-in controller. Instead, the motor and linear potentiometer pins were exposed directly, meaning a custom closed-loop control system could be developed using the Arduino microcontroller and a H-bridge motor driver. This allows increased accuracy of the position, and it means that the exact closed-loop position is known, rather than trusting the requested position has been achieved.

3.4 Grip Force Measurement

In order to measure the grasping force of the 3D printed mechanism, a grip force gauge was created. This force gauge is made up of two back-to-back load cells, connected to a HX711 load cell amplifier and an Arduino. Figure 3.4.1 shows this force gauge being gripped by one of the 3D printed explicit grippers.

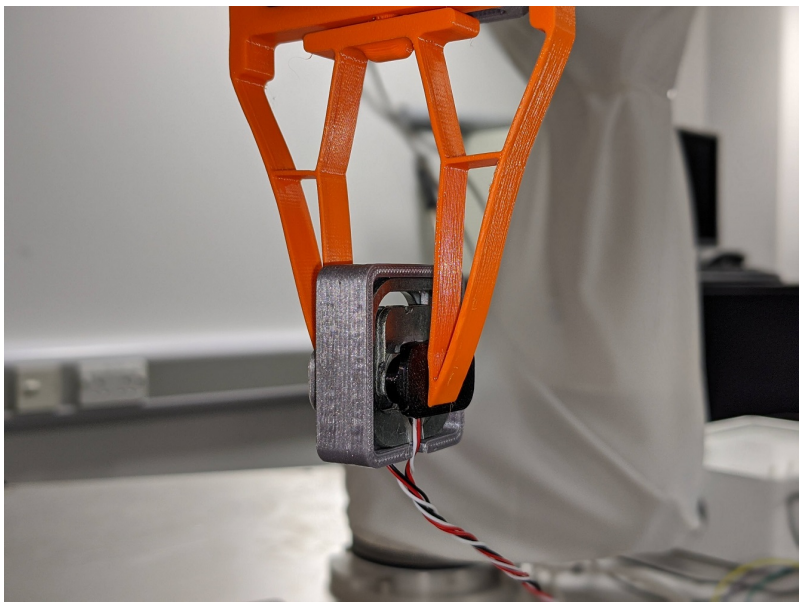

Figure 3.4.1: Grip Force Gauge

To calibrate the force gauge, it was placed on a flat surface next to a set of high precision weighing scales. Various objects were then placed on the scales and on the force gauge, and the values were plotted using Microsoft Excel (Figure 3.4.2). It can

be seen that there is an almost perfectly linear relationship between the mass output from the weighing scales and the output from the grip force gauge. The gradient of this relationship can then be used to calibrate the force sensor. Once calibrated the force sensor was accurate to under 2% across the range tested, compared to the precision scales. The calibrated grip gauge output can then be converted from mass in grams to force in newtons. As the calibration was done with the gauge vertically oriented, there will be a slight difference in output when gripped horizontally, due to the mass of the sensor itself, however this is only small (in the region of 10g) and can be eliminated using a simple offset or tare function.

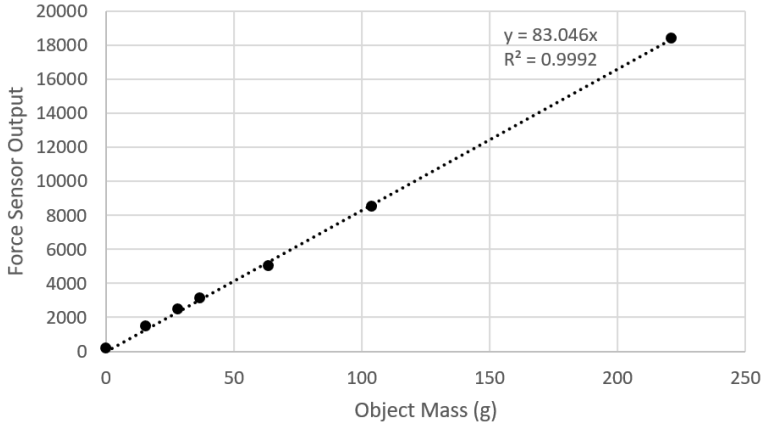

Figure 3.4.2: Grip Force Gauge vs Weighing Scales

Using this grip force gauge, the explicit compliant 3D printed grippers have achieved 4.2N, or around double the estimated minimum required clamping force of 2.085N, calculated in Section 3.1.

Chapter 4

FEA Validation Using Visual Tracking

In order to validate the FEA simulations, visual tracking will be used to understand if the 3D printed gripper mechanism deforms in the same way as the simulated one, for a given input displacement. Being able to accurately simulate the compliant gripper allows alternative designs to be tested, and enables the gripper to be modified and tailored to the task, without needing as much physical testing before use.

The visual tracking method is based on measuring the motion of a series of discrete points on the gripper as it opens and closes, and comparing that to a simulation of the same gripper with points in the same location.

4.1 Gripper Visual Tracking Hardware

A black gripper was 3D printed with a series of small posts across one side, which were coloured with white marker. This gripper was then mounted to a static actuator, where any fasteners were covered in black tape, and the background was covered in a black fabric (Figure 4.1.1).

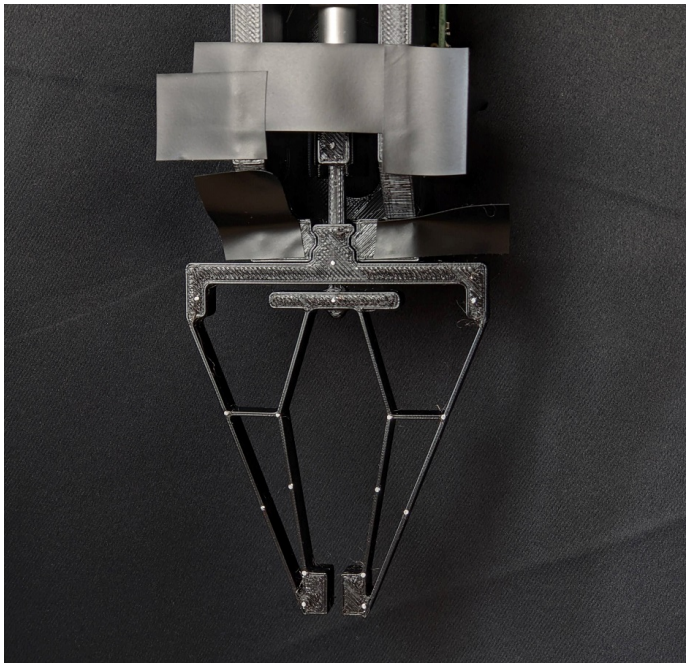

Figure 4.1.1: 3D Printed Gripper with White Tracking Points

A 4K camera was then pointed at the gripper (Figure 4.1.2), and connected to a desktop PC using a 4K video capture device. The gripper was lit with a soft-box light, and the camera ISO, shutter speed and aperture were set to minimise noise at a relatively dark exposure, to make image thresholding easier with a dark background and light white markers.

Figure 4.1.2: High Resolution Camera Pointed at Gripper

4.2 Gripper Visual Tracking Software

A program was then written using Python and OpenCV to find and track the points as the gripper opens and closes. A camera calibration was carried out to reduce lens distortion. This was done using the OpenCV chess board image and accompanying functions to find the distortion coefficients and camera matrix, which can be used in all subsequent tests with the same camera to undistort the captured images/video frames. On the first frame of the video, a region of interest is specified around the expected location of each point on the gripper in the frame. The image is then converted to grayscale, and binary thresholding is used to segment the white points from the rest of the image. The centroid of each contour within the regions of interest is then found, giving the co-ordinate of each white point on the gripper.

To track the movement of the points in subsequent frames, the location of each individual region of interest is updated using the co-ordinates of the point found within it on the previous frame. This means the individual regions of interest 'chase' the points as they move, ensuring that the individual points are tracked and labelled consistently.

Figure 4.2.1 shows a sample frame from the visual tracking, with the individual regions of interests shown in green, around the white points on the gripper. As mentioned previously, a low exposure was purposely chosen which makes the white points easier to track, which means the actual gripper is more difficult to see in the image.

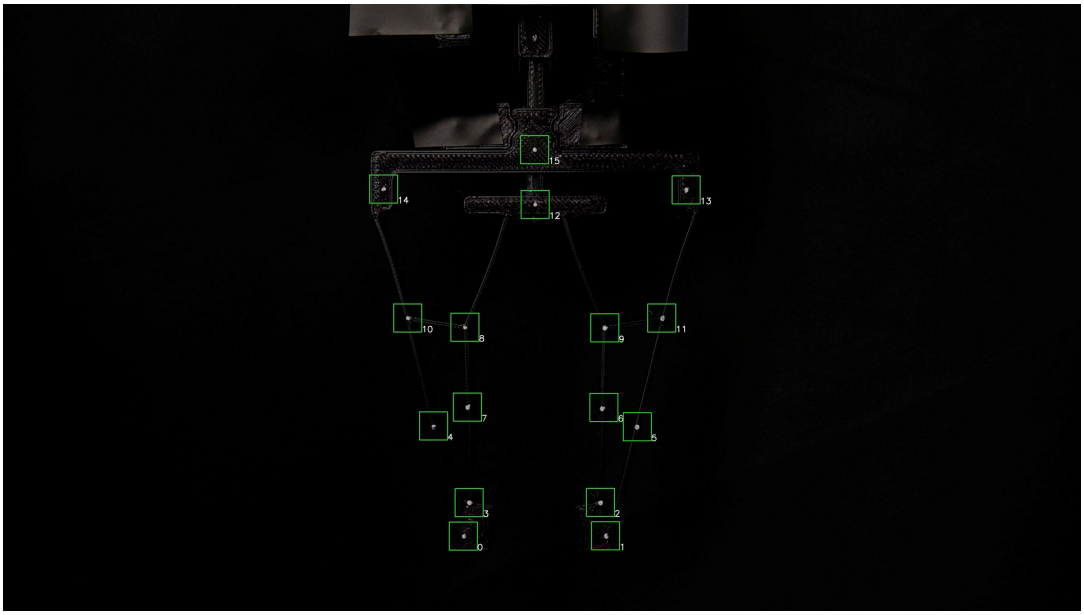

Figure 4.2.1: Visually Tracked Points on Gripper

The co-ordinates of each point are then saved for every frame of the video in a .csv file for comparison with FEA data using Microsoft Excel. As the visually tracked co-ordinates were calculated in pixels, the data was scaled to mm based on the known distance between two points which are relatively far apart and rigid in relation to each other (points 13 and 14 in Figure 4.2.2), to match the FEA units. The distance between points 12 and 15 can be used to record the initial gripper input position, and the distance between 0 and 1 can be used to help calculate the gripped object width.

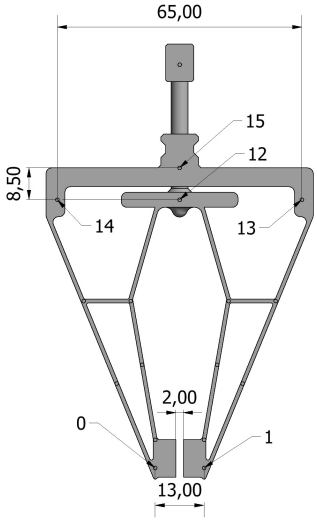

Figure 4.2.2: 3D CAD Model Scale Locations and Dimensions

4.3 Finite Element Analysis

The same 3D model with small posts which was used to 3D print the gripper was imported into ANSYS (Figure 4.3.1), and each of the post faces were individually labelled to match with the visual tracking labelling.

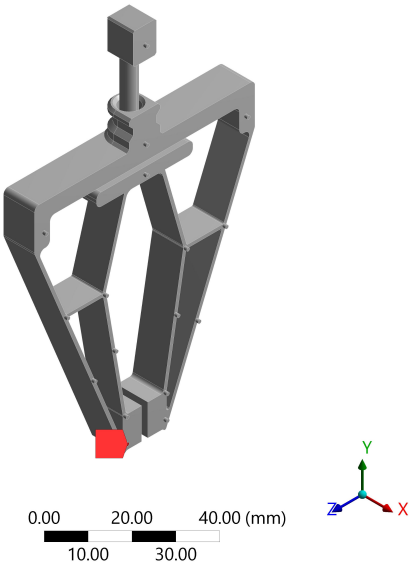

Figure 4.3.1: Gripper 3D Model

A transient structural simulation was conducted, with a fixed constraint at the gripper mount, and an input displacement of 3mm applied to the input block (the

same as in the experimental setup). Figure 4.3.2 shows the output deformation of the gripper, with one of the points highlighted. For each labelled point on the gripper, the vertical and horizontal displacement was exported at a series of time points throughout the simulation.

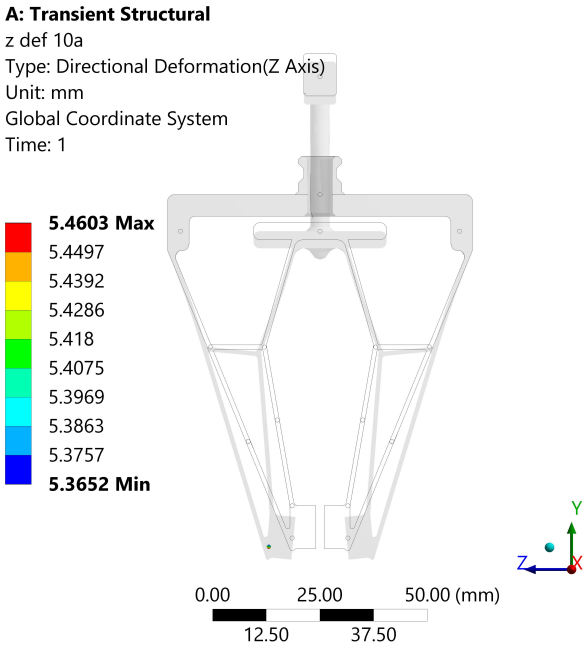

Figure 4.3.2: Simulated Gripper Deformation

4.4 Visual Tracking vs FEA Results

The point data from the visual tracking and the FEA was analysed using Microsoft Excel. Figure 4.4.1 shows the FEA point paths, overlaid with the visually tracked point paths. The visually tracked points have been converted from pixel position to mm, and offset to make point 15 the origin. As the individual FEA paths were relative to each start location, they have been offset to match the CAD point location relative to point 15. From this plot it can be seen that although there is some error in the path locations for some points, the overall movement looks to be very similar. This error in the initial point locations between the simulated and real gripper could be due to dimensional errors in the 3D printed gripper, or a slight misalignment of the camera to the gripper.

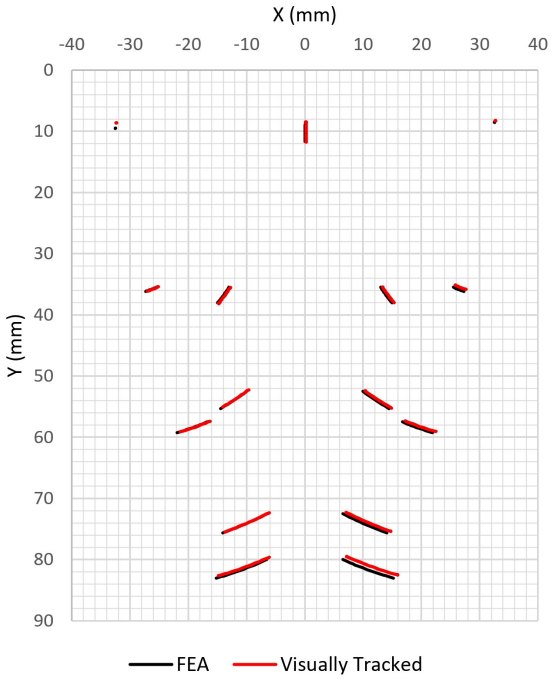

Figure 4.4.1: Comparison of FEA and Visually Tracked Point Paths for an Open and Close Movement.

Figure 4.4.2 shows the relative movement of points 0 and 1 during and open and close gripper movement, comparing the visual tracking and FEA. It can be seen that when the point start locations are matched, the visually tracked point movements align almost perfectly with the simulated point path. The visual tracking test was carried out 6 times, showing that there is good repeatability of visual tracking system, which matches well with the simulated movement.

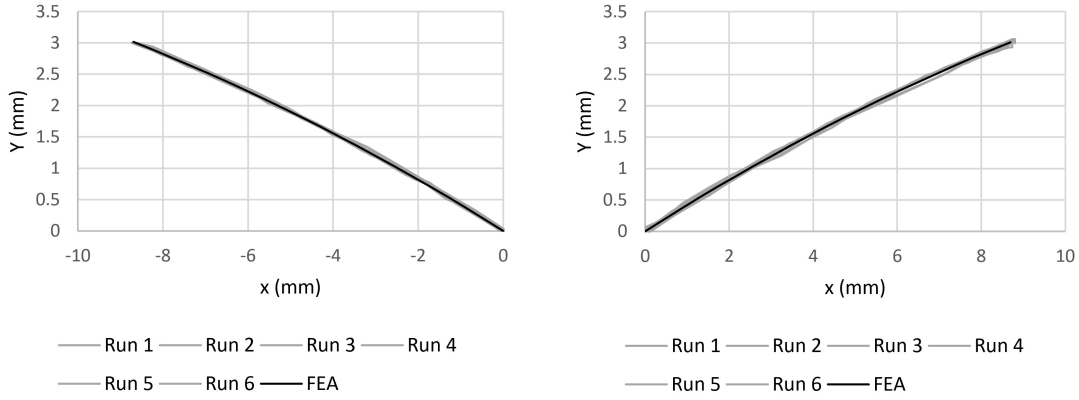

(a) Point 0

(b) Point 1

Figure 4.4.2: Individual Point Path Comparison between FEA and Visual Tracking

In order to expand the comparison to include not only the unrestricted motion of the gripper opening and closing, but also the deformation whilst gripping objects, the FEA simulation needed modification. As the gripper is already 'closed' in the unstressed state, the object was modelled below the gripper within ANSYS Geometry Modeller, and then multiple steps were added to the transient simulation to raise the part up into the grasp region, once the gripper had opened.

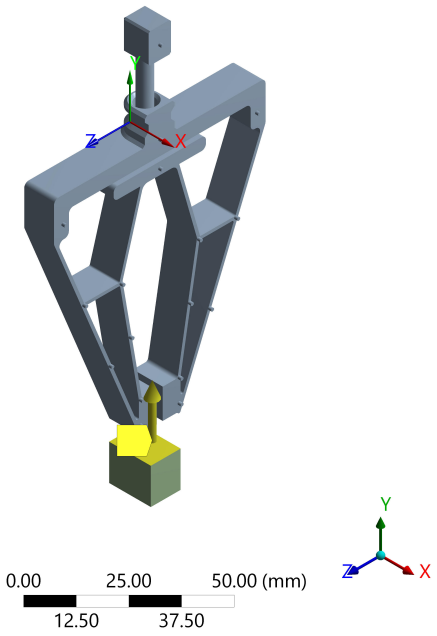

Figure 4.4.3: FEA Object Start Location

Contact regions were also added, one region for each contact location on either side of the object/gripper digits (Figure 4.4.4). These allow the gripper to interact with the object as it is grasped, instead of just passing through it.

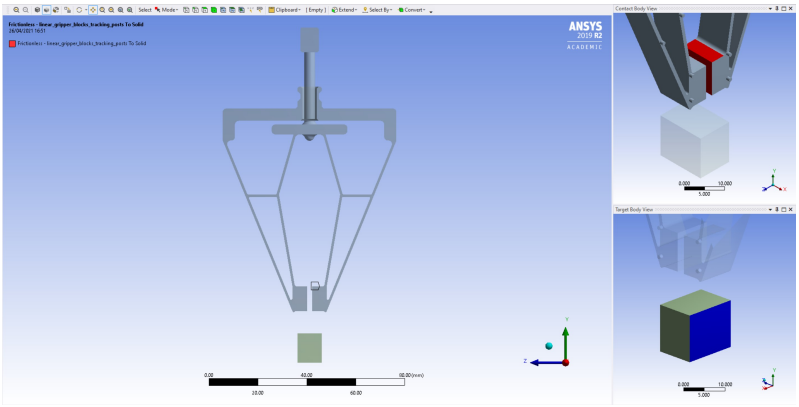

Figure 4.4.4: FEA Contact Region

Figure 4.4.5 shows points 0 and 1 during an open and close movement, with a 5mm wide object in the grasp. It can be seen that the path is almost identical to the previous case without an object, but with the addition of a small deviation at around ±1.5mm. This deviation and its location is expected, as at the start of the test the gripper digits are spaced 2mm apart, meaning each side should only return to 1.5mm from the origin whilst gripping a 5mm object. As expected, the FEA paths are symmetrical, with the deviation occurring at exactly ±1.5mm. However, the visually tracked points are not quite perfectly symmetric about the start location, with one of the points returning slightly closer to the origin, and the other slightly further away. Again, this is likely due to either a misalignment in the visual tracking setup, or a slight geometrical error in the physical 3D printed gripper, causing some asymmetry in the compliant mechanism.

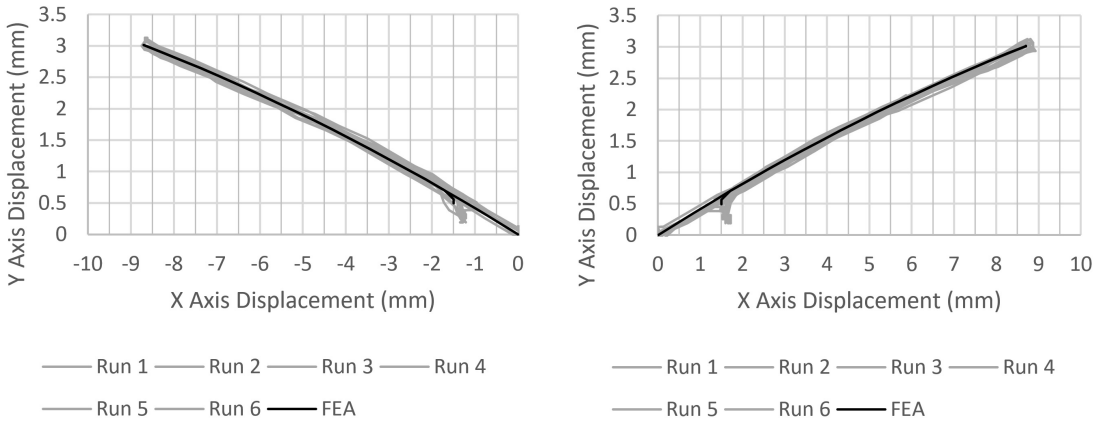

(a) Point 0

(b) Point 1

Figure 4.4.5: Comparison of FEA and Visual Tracking for 5mm Object Grip

As the actuator continues to move even after the gripper contacts the object, the digits are not able to move closer, and so the compliant elements flex in the next 'easiest' direction, which is why the point begins to deviate in the vertical axis until the actuator stops. This vertical deviation post-contact is larger for the visually tracked points compared to the FEA simulation, which is due to the FEA object being constrained in the vertical axis, whereas the real object is not, and it can freely move as it is grasped.

Figure 4.4.6 shows the same comparison but with a 10mm wide object. As expected, the deviations from the unrestricted path occurs at ±4mm (the object width minus 2mm initial gap). Again, the FEA shows good symmetry between the two digits, but there is a slight difference between the visually tracked data from one side to the other.

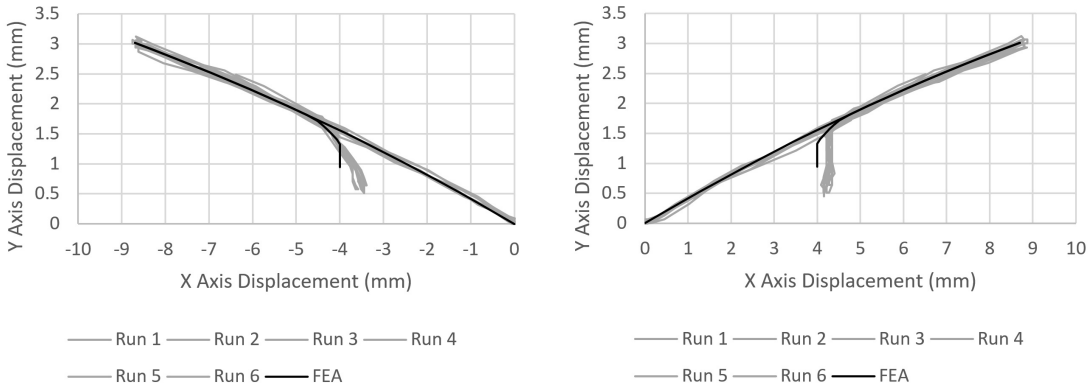

(a) Point 0

(b) Point 1

Figure 4.4.6: Comparison of FEA and Visual Tracking for 10mm Object Grip

The results from this point tracking test between a 3D printed and simulated gripper show that the compliant mechanism can be simulated to a high accuracy, especially in unrestricted movements when no objects are in the grasp. When objects are grasped, the points tracked on the real gripper are shown to be not quite symmetrical due to dimensional or alignment errors, but the overall movement is still as expected from the simulation.

Being able to accurately simulate compliant 3D printable grippers before manufacture means time can be saved when testing the gripper, and the design can be iterated or tailored to the gripping task before it is even physically manufactured.

In the future this simulation could be extended to include how the gripper performs when grasping solid objects buried in unfused powder, however as no physical testing data is available to validate these simulations, this cannot yet be done. As the focus of this project is the physical 3D printed gripper and how it performs at extracting real 3D printed objects from unfused powder, the results from this project could be used to help validate future simulations on similar interactions.

Chapter 5

Sensors and Measurement Methodologies

As the gripper is intended to be used to extract objects from within unfused powder, a visual tracking system such as the one used to validate the simulations is not suitable for operation in a powder, as the markers will not always be visible. Because of this, additional sensors are needed to help understand the position of the gripper, and how it is interacting with the object within the unfused powder, when it cannot be seen.

As found in the literature review, many commercial grippers use rotary or linear encoders and potentiometers to measure the angle or displacement of joints in the gripper mechanism. As the compliant gripper does not contain conventional rotating joints, and the unfused powder may have a negative effect on the internal contacts of many potentiometer or encoder types, a sensor which does not contain any sliding or rotating interfaces, that also has the potential for 3D printing in the near future, would be the ideal choice.

As the compliant elements flex when the gripper opens and closes, a sensor applied to these regions could allow the amount of flex to be related to the gripper position, or the force that is being applied in certain load cases.

For initial testing, commercial sensors will be used to measure the amount of flex or strain in the compliant elements. Commercial sensors allow physical testing of the mechanism to be carried out to verify the design, as a step towards manufacturing the gripper in one-shot with embedded 3D printed sensors.

5.0.1 Flex Sensor

One commercial sensor capable of measuring the relative flex in the compliant region is a resistive flex sensor such as those made by Spectra Symbol Corp. (2019). Figure 5.0.1 shows a flex sensor which has been adhered to the side of a 3D printed gripper mechanism. The sensor acts as a variable resistor when flexed. When connected to an Arduino as part of a voltage divider circuit, the flex sensor can be used to determine if the gripper is open or closed, by comparing the voltage divider output in each position.

Figure 5.0.1: Flex Sensor Mounted to Gripper Mechanism

Figure 5.0.2 shows the analogue input on an Arduino as the gripper is opened and closed. Since flex sensors like this are designed to sense a flex from 0° to 180°, there is a noticeable amount of noise present in the output, due to the relatively small flex as the gripper opens and closes. The actuator position is also shown to highlight the relative noise on the flex sensor compared to the input position. The actuator position is measured from an onboard linear potentiometer. It can be seen that the flex sensor output is also not quite symmetrical during the open and close operation, indicating that there is some hysteresis present in the flex sensor. Although the

resolution of the analogue reading is relatively low, it is still clear when the gripper is in either the fully open or closed position. Unfortunately, as this sensor is mostly intended for use on large flexing objects like gloved fingers, it covers almost the entire length of the compliant gripper. This is not ideal, as the compliant regions do not flex consistently along their length, as the lower half of the gripper only flexes when a gripping force is applied to an object. This means it is difficult to accurately determine the strain or flex in a specific location on the compliant element. To ensure that smaller regions of flex can be measured independently, an alternative sensor is required.

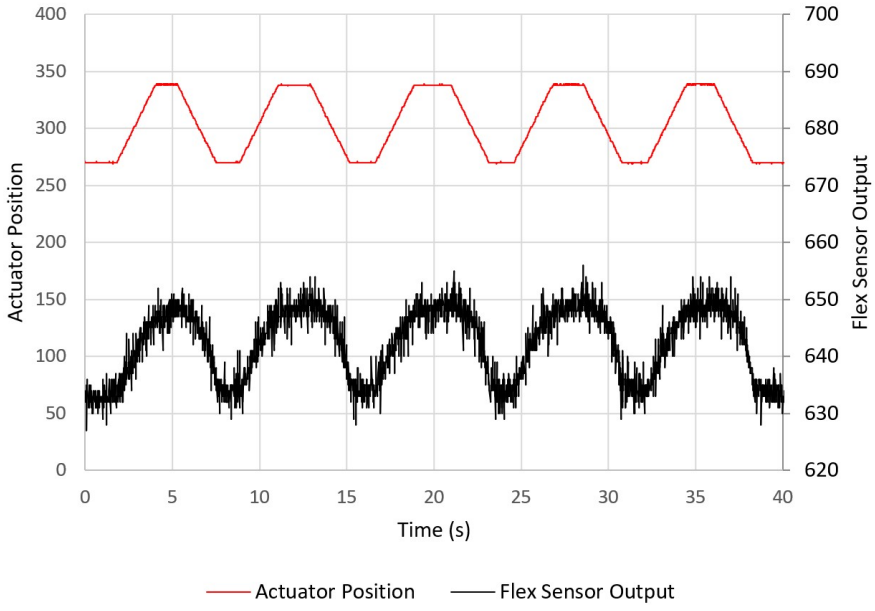

Figure 5.0.2: Flex Sensor Output Compared to Actuator Position

5.1 Strain Gauge

One method to more accurately measure the flex in the compliant regions of the gripper is to use a strain gauge. These are smaller and are often used to measure the strain in metal and composite structures, so they are potentially much more suited to accurately measuring the flex in this region. Initially, a single strain gauge and amplifier board was used on the gripper, as shown in Figure 5.1.1a. This setup was chosen for its simplicity and ease of use for showing how the strain varied during

individual tests. Although it is relatively reliable for the duration of a single test or a series of tests carried out at the same time (e.g. during a single afternoon), there are issues with the setup for long term, calibrated, reliable results. This can be due to a change in the amplification gain on the device itself, or due to a change in temperature on one day compared to another. Instead, a strain measurement system which uses multiple strain gauges connected to a HX711 amplification board (Figure 5.1.1b), will be used. This allows for temperature compensation, and all offsets and gains can be applied consistently in software. This results in more accurate calibration of the strain gauge output, meaning exact numerical values from tests carried out on different days can be compared, instead of just the overall trend.

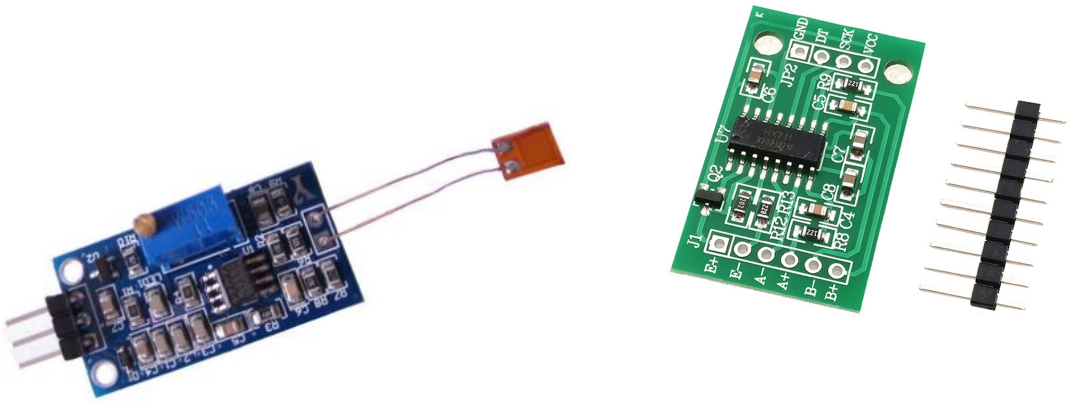

(a) Initial Strain Gauge and Amplification Board (b) HX711 Board

Figure 5.1.1: Strain Gauge Amplification Boards

Figure 5.1.2 shows a strain gauge adhered to the upper part of the compliant gripper mechanism, which flexes as the gripper opens and closes. Another strain gauge can be seen behind, on a much thicker part of the gripper that experiences less flex, and it is placed perpendicular to the minimal flex that does occur. This means that this 'passive' gauge will experience a negligible change in strain compared to the 'active' gauge, and can be used as part of the voltage divider circuit for temperature compensation. Both gauges are connected to the HX711 board, along with two 330Ω resistors (close to the strain gauge resistance of 350Ω) to complete the voltage divider circuit.

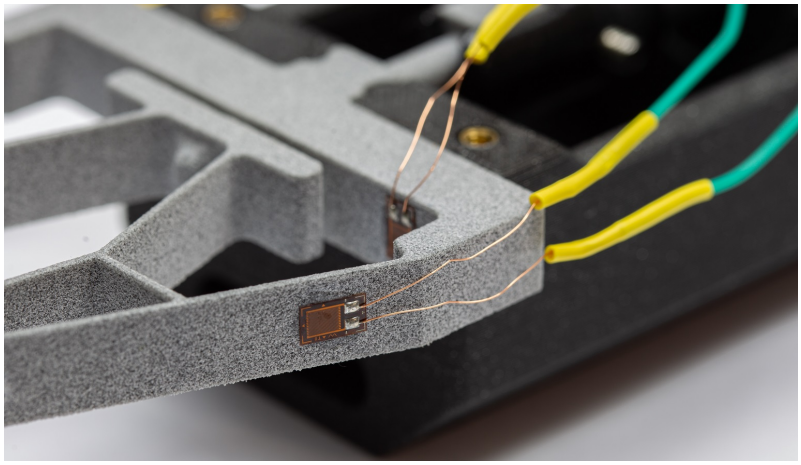

Figure 5.1.2: Strain Gauge Mounted to Compliant Gripper

The strain output compared to the actuator position is shown in Figure 5.1.3. It can be seen that the resolution of the strain input is very high, and the output follows the actuator trend closely with almost no noise. This shows that the performance is much greater than the previously tested flex sensor.

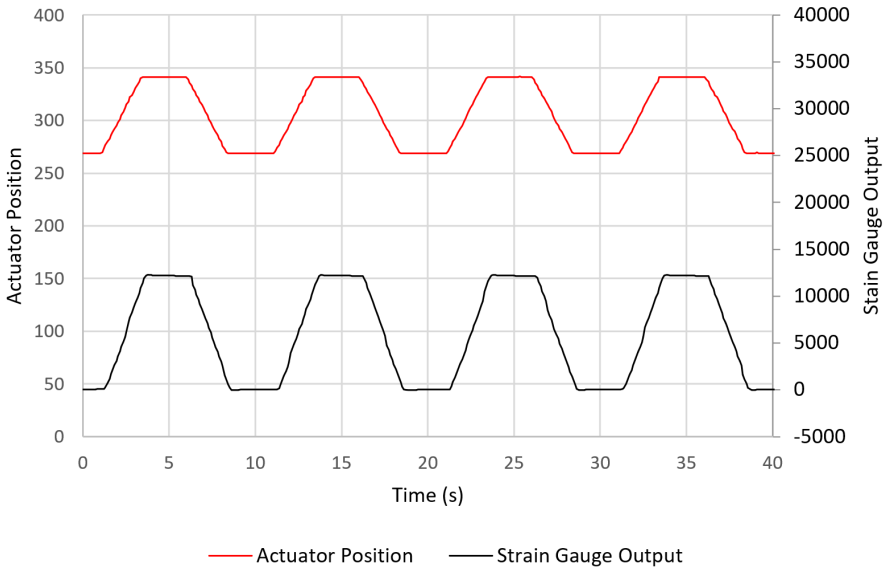

Figure 5.1.3: Strain Gauge Output Compared to Actuator Position

5.1.1 Simulated vs Experimental Strain

Being able to simulate the amount of strain experienced by the gripper can aid in the design process, as it allows the location of the strain gauge to be chosen based

on what needs to be measured, e.g. the gripper position or grasping force. To understand how the strain gauge output compares to calculated or simulated strain in a 3D printed flexing object, a simple cantilever beam bending test was carried out. The strain can be calculated from the applied stress and Young's Modulus of the material, as shown in Equation 5.1. Where ε is the strain, σ is the stress, and E is the Young's Modulus of the material.

$$\varepsilon = \frac{\sigma}{E} \tag{5.1}$$

The bending stress at the gauge location can be calculated using Equation 5.2 where σ is the stress, M is the moment, y is the distance from the neutral axis (in this case, half the height of the beam cross-section), and I is the second moment of area of the cross-section about the neutral axis.

$$\sigma = \frac{My}{I} \tag{5.2}$$

The moment at the gauge location (Figure 5.1.4) can be calculated for a cantilever beam using the applied force, and the distance between that force and the gauge, as in Equation 5.3. Where M is the moment, F is the applied force, and d is the distance between the applied force and the gauge location.

$$M = Fd \tag{5.3}$$

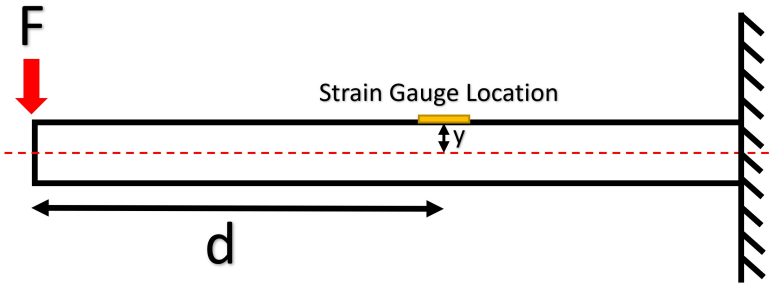

Figure 5.1.4: Beam Side View

The second moment of area for a rectangle can be calculated using Equation 5.4, where I is the second moment of area, and b and h are the width and height of the cross-section (Figure 5.1.5).

$$I = \frac{bh^3}{12} \tag{5.4}$$

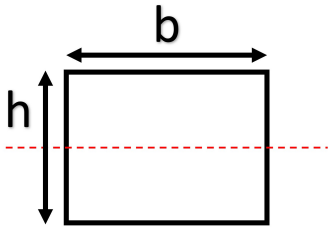

Figure 5.1.5: Beam Section View

A 150mm long cantilever beam with a 5mm x 5mm cross-section was fixed to the side of a desk with a load applied 5mm from the end, and a strain gauge mounted at 75mm (Figure 5.1.6). The force on the beam was created using a bottle of water, with a set of precision scales used to measure the weight before each test[1].

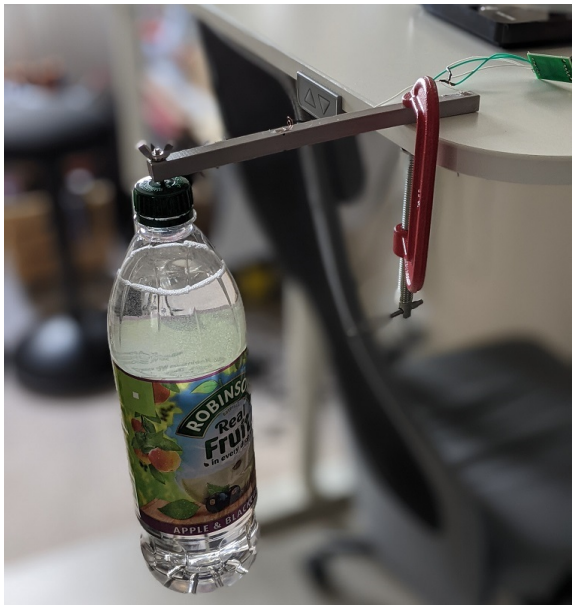

Figure 5.1.6: Simple Beam Bending Test

[1]This method was chosen over a set of calibrated engineering weights following lab access restrictions at the time of testing due to COVID-19.

Figure 5.1.7 shows the strain gauge configuration used for this test. The active gauge is placed in the location where the desired strain is to be measured, with the gauge aligned with the direction of flex. As strain gauges also experience a change in resistance due to changes in temperature, a second passive gauge is placed in an unstressed region of the part to compensate for any temperature changes. A Wheatstone bridge circuit is formed using these two gauges along with two resistors of a similar resistance. A HX711 load cell amplifier is used to provide the input excitation voltage, and to measure the output voltage of the bridge circuit, sending it to an Arduino microcontroller for recording and analysis.

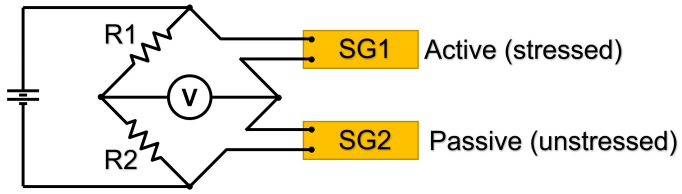

Figure 5.1.7: Quarter Bridge with Temperature Compensation Strain Configuration

Figure 5.1.8 shows a 3D model of the same beam geometry within ANSYS, with the strain gauge location specified on the beam. A fixed constraint was applied at the same location as the desk edge, and a point load was applied at the bolt hole at the end of the beam. An element of the beam at the same location as the experimental gauge was selected as the location to output the simulated strain.

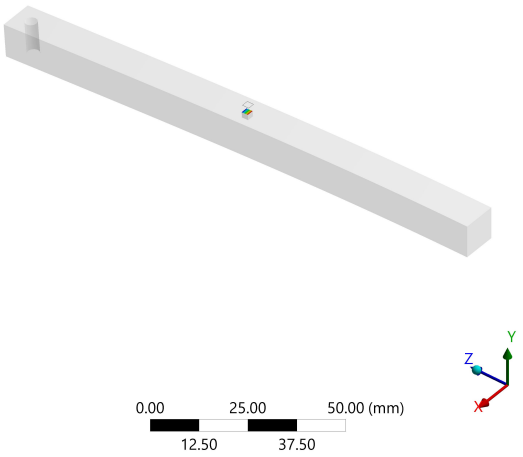

Figure 5.1.8: Beam Bending FEA

Figure 5.1.9 and Table 5.1 shows the results from the simulated and measured strain compared to the calculated strain. It can be seen that the output is linear across the range tested, with an almost perfect match between the calculated and simulated strain, with a relatively small error between those and the measured data. This shows that in a simple static scenario, the FEA simulation and experimental strain matches well with the theoretical strain for a point load at the end of a cantilever beam.

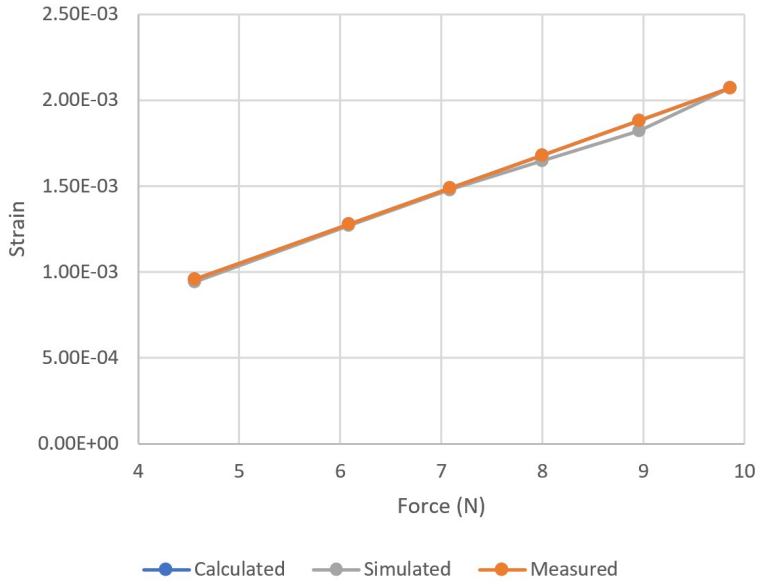

Figure 5.1.9: Beam Bending Strain Results

Force (N)	Calculated Strain	Simulated Strain	Measured Strain	
				error
4.562	9.579E-04	9.580E-04	9.422E-04	**-1.642%**
6.082	1.277E-03	1.277E-03	1.269E-03	**-0.622%**
7.083	1.487E-03	1.487E-03	1.478E-03	**-0.651%**
7.995	1.679E-03	1.679E-03	1.647E-03	**-1.903%**
8.957	1.881E-03	1.881E-03	1.820E-03	**-3.252%**
9.859	2.070E-03	2.070E-03	2.070E-03	**0.000%**

Table 5.1: Beam Bending Strain Results

Experimental and simulated strain for a cantilever beam can also be compared without knowing the force, stress, or Young's Modulus if the beam deflection is known, using the following equation:

$$\varepsilon = \frac{3\delta dy}{L^3} \tag{5.5}$$

Where ϵ is the strain at the gauge location, δ is the maximum deflection of the beam, d is the distance from the applied force to the gauge, y is the distance from the neutral axis to the gauge, and L is the length of the beam. This equation can be derived from those listed at the start of this subsection, plus the following equation for the maximum deflection of a cantilever beam:

$$\delta = \frac{FL^3}{3EI} \tag{5.6}$$

This means that if the beam is deformed by specifying a deflection at the end rather than a force, the same strain will be present independent of the material stiffness. As the Young's Modulus varies between different materials, such as those printed in PLA/PETG using FFF, and those printed in PA12 using MJF, this causes the same force to result in a different amount of strain. However, if the gripper is displacement controlled rather than force controlled, changing the gripper material will not affect its deformation or motion for a given input displacement, so long as it acts isotropically and is kept below the elastic limit. This means that the Young's Modulus of the 3D printed grippers does not need to be known to simulate how they will deform in operation.

5.1.2 Object Width Measurement using Strain Gauge

Another strain gauge was adhered to the side of a 3D printed gripper, as shown in Figure 5.1.10. As there is almost no strain in this lower compliant region when the gripper mechanism opens and closes, instead of being used to measure the gripper

position, this gauge location is more suited to measuring the gripping force. If the gripper mechanism input displacement is kept constant across a range of objects, each with a different width, then a larger force will be applied to the wider objects. This will cause the strain in this compliant region to be higher for a wider object, if the gripper's input displacement is kept equal.

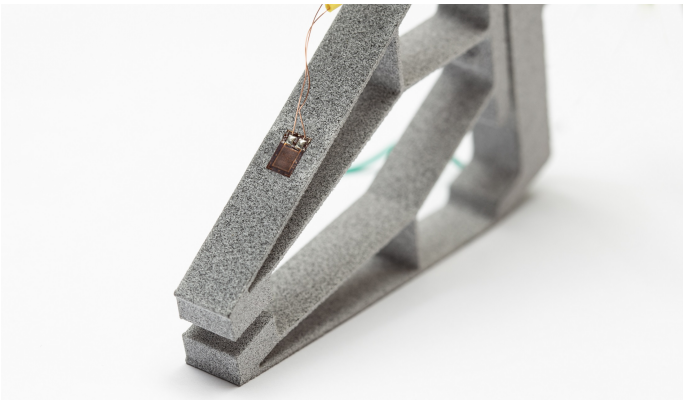

Figure 5.1.10: Strain Gauge Mount

In order to relate the strain in this region to the object width, a grip block with varying stepped widths was created, which can be gripped in succession to measure how the strain varies (Figure 5.1.11).

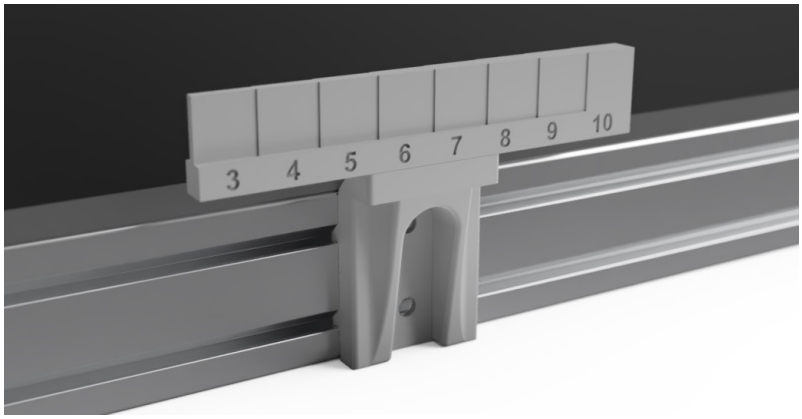

Figure 5.1.11: Fixed Grip Width Gauge

Figure 5.1.12 shows a sample output from one of these object width tests, starting at 10mm and going down to 3mm. For each test a rise in strain can be seen whilst the gauge is gripped, before it drops again whilst the gripper releases and moves to the next width. It can be seen that the wider the object, the higher the strain output is.

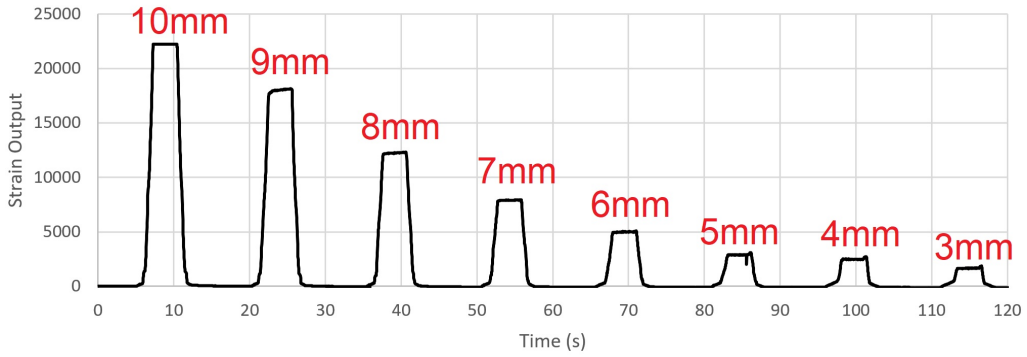

Figure 5.1.12: Strain Output vs Time (10mm to 3mm widths)

The same gripper geometry and a subset of object widths was also simulated using ANSYS FEA. Figure 5.1.13 shows the strain output from the simulated gripper, alongside the experimental strain recorded from the same object widths. The experimental strain has been scaled to match the same range as the simulated strain. It can be seen that once scaled the trend is very close, showing that the simulated and 3D printed compliant grippers are deforming in the same way when grasping objects of various sizes.

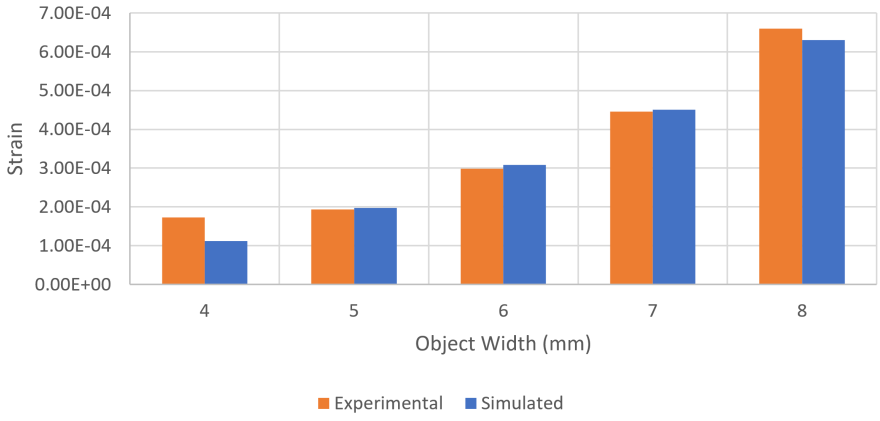

Figure 5.1.13: Simulated vs Experimental Strain whilst Gripping Objects

5.2 Force Sensing Resistor

As their name suggests, Force Sensing Resistors (FSRs) such as the one shown in Figure 5.2.1, are sensors that experience a change of resistance across two pins when

a force is applied. As a force is applied, the air gap between the semiconductor surface and interdigitating electrodes reduces, causing the resistance to drop.

Figure 5.2.1: Force Sensitive Resistor (FSR)

To test the FSR, it was adhered to the digit of a 3D printed gripper, and the grip gauge shown in Section 3.4 was grasped. A voltage divider circuit was used to measure the change in resistance using an Arduino microcontroller. Figure 5.2.2 shows the FSR mounted to the digit of a 3D printed gripper, with the wires loosely held in place using cable ties, to prevent damage to the FSR or connections. The wires are able to move freely as the gripper opens and closes as to not affect the sensor output or gripper movement.

Figure 5.2.2: FSR on 3D Printed Gripper

Figure 5.2.3 shows the resistance output change for the FSR, compared to the force output of the grip force gauge. It can be seen that the relationship is not linear and the hysteresis is quite pronounced. There is also a deadzone at low force where there is no output measurable. This means that although the FSR is usable for basic applications that need to detect if a force is being applied, it is not suitable for accurately measuring the quantity of that force reliably or repeatedly. For this reason, commercial FSRs such as this will not be explored further for this project.

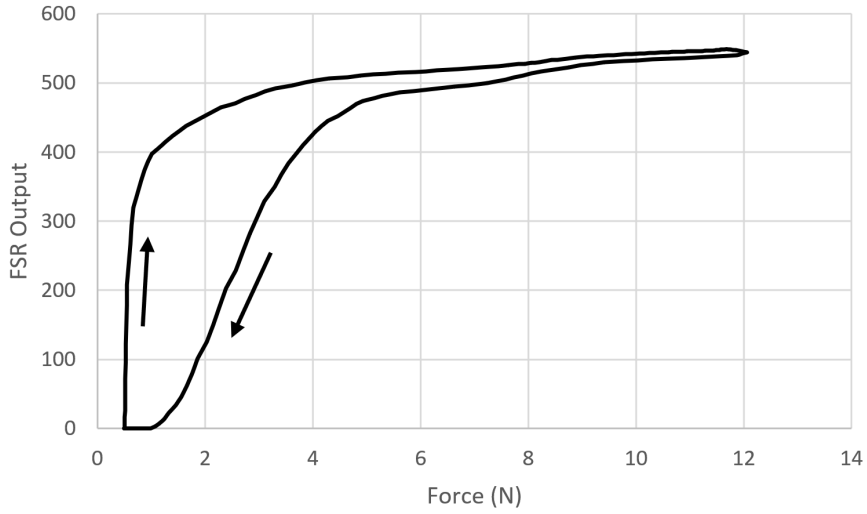

Figure 5.2.3: FSR vs Force

Chapter 6

Extracting 3D Printed Objects from Unfused Powder

Following the initial tests of the gripping mechanism, its performance at grasping and extracting 3D printed parts from a powder will be assessed. As no existing literature was found about the effect that powder has on the gripping process when attempting to extract a solid object from within it, initial testing will be focused on attempting to extract a cleaned 3D printed object, i.e. one that does not have powder caked to the side of it, but nonetheless extracted from within virgin PA12 powder, i.e. powder that has not been through the MJF process. Once this has been done, additional testing will be carried out to see what the difference is when using uncleaned 3D printed parts, surrounded by aged powder which *has* been through the MJF process.

Testing with cleaned objects in virgin power is also much less resource intensive, as the same objects can be tested repeatedly, re-cleaning between tests. Once an uncleaned object direct from the MJF process is gripped, the caked powder is disturbed, meaning each object can only be used once for reliable quantitative testing.

Although the flowability is lower for aged powder which has already been through the MJF process, it has also been shown to be less consistent through the volume of the powder (Sillani *et al.*, 2019), and the powder recycle rate (the amount of powder which is re-used for subsequent printing) is not always fixed, which could affect results. Galati *et al.* (2020) showed that the molecular structure, shape, and

surface of the aged/recycled powder is unaltered compared to the virgin powder. This means that although there will be some differences between using virgin and aged powder, the difference should be minor, and the consistency of initial testing using virgin powder can allow results and trends in the data to become more clear.

6.1 Test Setup

As it is not feasible to source a complete MJF 3D printer and post-processing station for this testing, a custom test rig was created for extracting parts from PA12 powder (Figure 6.1.1). The rig features a fume/particle cabinet (1) (Bigneat Ltd, 2020), with both fume and particulate filters, containing storage for powder (2) and a tray which can be filled with powder for testing (3). The custom end-effector, comprising of the actuator (4) and gripper (5), is mounted to a UR5 robot arm (6) (Universal Robots, 2019) which is fixed to the top work surface. The robot is able to reach inside the cabinet to the tray, to extract objects. The gripper and actuator are connected to a custom control box (7) and PC for data collection (8). The control box also sends commands to the robot arm controller, whose motion is programmed using the pendent (9).

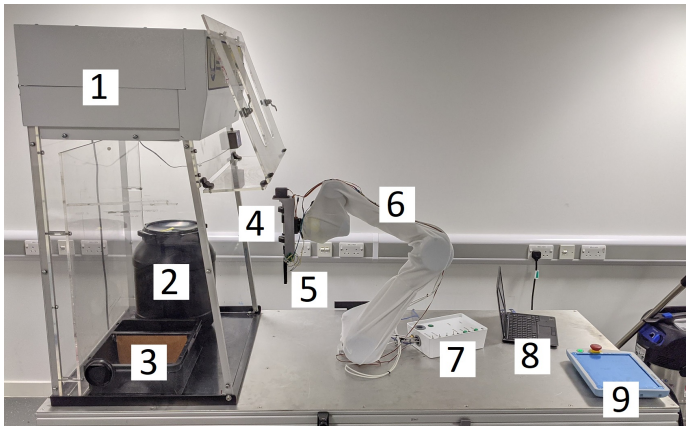

Figure 6.1.1: Object Extraction Test Rig
1: Fume Cabinet, 2: Powder Storage, 3: Test Tray, 4: Actuator, 5: Gripper, 6: Robot Arm, 7: End effector Control Box, 8: Data Collection PC, 9: Robot Arm Control Pendant

Figure 6.1.2 shows a high-level overview of the control setup. The robot arm and end-effector both have dedicated control boxes which are able to send and receive basic signals from one another. First, the path of the robot arm is programmed using the touch-screen pendant, as a series of distinct set of waypoints and movements, e.g. moving towards the object, moving away from the object, moving out of the cabinet. The program then waits until it is instructed to move by the end-effector control box. The end-effector control box contains an Arduino Mega which is programmed using the Arduino IDE on a nearby laptop. The end-effector control box also features drivers for the end-effector actuators and a series of buttons and switches for control, plus space to accommodate other boards as necessary for sensors attached to the gripper.

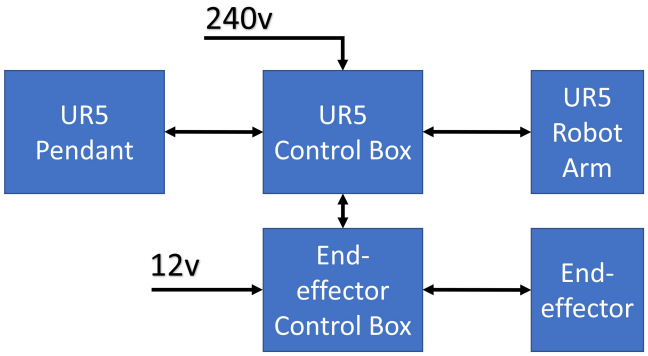

Figure 6.1.2: Test Rig High-Level Schematic. Arrows indicate a power and/or data connection.

6.1.1 Test Parts and Powder

Test parts for the extraction tests have been printed using the MJF process (Figure 6.1.3). These parts are a 30x30x30mm cube with a 24x15x5mm tab on the top face. The initial tests will attempt to grab the tab to extract the part.

Virgin PA12 powder for testing has been supplied by HP which is stored in large drums below the test rig. Using virgin powder allows the tests to be repeated many times without needing to source new test parts or powder every time.

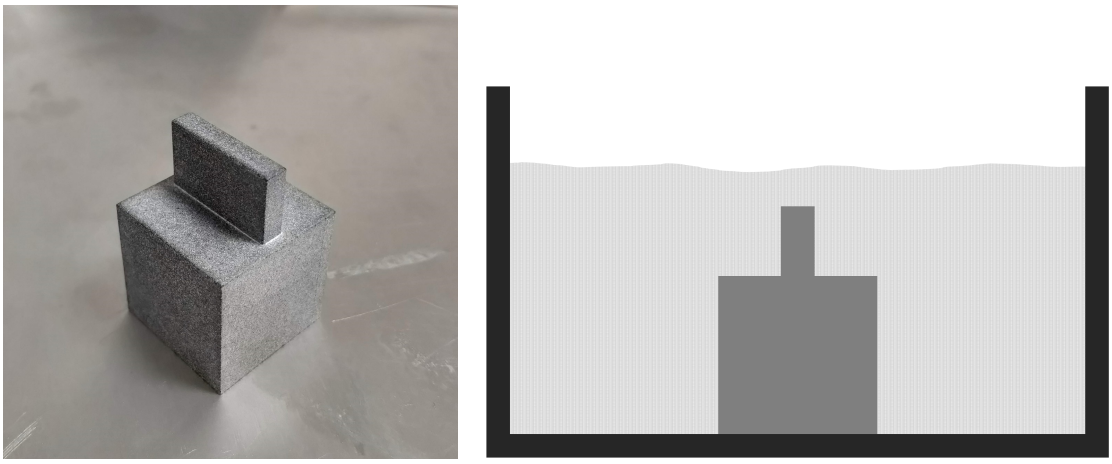

(a) Test Object Outside of Powder (b) Illustration of Test Object in Powder

Figure 6.1.3: Test Object

6.2 Test Method

In order to create repeatable results, a test procedure will be followed to ensure that the part is located in the same place before every test.

1. Ensure necessary PPE is being worn, and the fume/particle cabinet is turned on.

2. Manually place the test object into the grasp of the gripper mechanism attached the robot arm.

3. Use the robot arm to place the test object into the empty tray.

4. Release the test object, and move the robot arm back away from the object and tray.

5. Pour virgin PA12 powder around and on top of the test object slowly, ensuring there are no clumps and that the object does not move.

6. Use a depth gauge to ensure that there is an equal amount of powder around/on top of the test object before each test.

7. Start the automated gripping control program to attempt to extract the test object from the PA12 powder, whilst logging any relevant data, such as the actuator position and strain gauge sensor output.

8. Once the test has finished, clean the object and tray of any unfused PA12 powder, ready for the procedure to restart.

This procedure should ensure that the printed test object is placed in a known consistent location each time, surrounded by a consistent amount of unfused powder.

6.3 Underactuated Mechanism

When attempting to extract an object using the underactuated gripper, contact with the powder causes the digits to flex, as the tendon does not hold each joint rigidly. This means the exact position of the digits within the powder is unknown. Once the gripper is actuated and the tendon line is pulled, the object is not extracted when the robot arm lifts the gripper from the powder, as the digits are not able to move all of the way through the powder to grasp it.

It was found that repeatedly actuating the gripper resulted in the digits gradually being able to move through the powder more and more, eventually encompassing the test object within it. This meant that the object could be extracted, but the process was slow and inaccurate, resulting in objects that were in an unknown pose once removed. Figure 6.3.1 shows two frames from a video of this repeated actuation extraction, where after 7 actuations, the object is beginning to be lifted as the digits encompass the object.

(a) Initial Actuation (b) 7th Actuation

Figure 6.3.1: Underactuated Gripper Part Extraction using Repeated Grasp Actuations

If a sensor was placed on every joint, it might be possible to measure the exact position of each digit, but as the mechanism is underactuated it is still not possible to actively control how the digits flex at each joint, only what the overall flex is across each digit. This means that even with more feedback, the performance of the gripper would not be improved, and the pose of the object would still remain uncontrollable.

6.4 Explicit Mechanism

In order to attempt to extract a 3D printed solid object from unfused PA12 powder in a known pose in a single actuation, the explicit gripping mechanism will be tested. It is thought that the explicit mechanism digits will be able to penetrate the unfused powder more easily than the underactuated mechanism, as they are stiffer in the vertical direction, with a smaller cross-section, and the contact is focused in one location rather than having to encompass the object.

6.4.1 Test Gripper and Sensor

Figure 6.4.1 shows the strain sensor setup for this series of tests. An active gauge is adhered to the lower compliant region of the gripper, and a passive gauge is adhered to a location on the gripper which experiences almost no strain during operation. Both gauges are attached to a HX711 module, which uses a Wheatstone bridge circuit to convert the changes in resistance from the gauges as they strain into a signal that can be read by the Arduino, and logged to a nearby PC via USB.

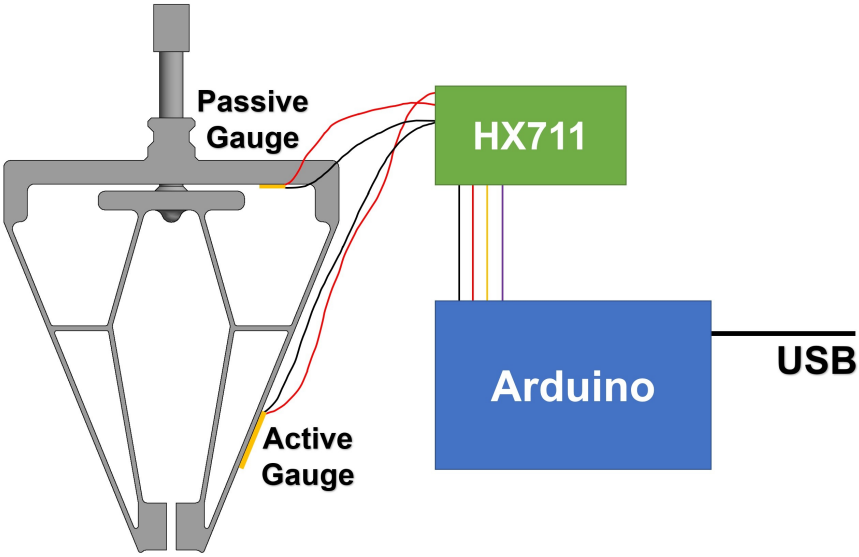

Figure 6.4.1: Explicit Gripper Mechanism

6.4.2 Baseline Test Without Powder

Figure 6.4.2 shows the strain output from gripping the object with no powder present. It can be seen that the strain rises at around 10 seconds as the object is gripped, where it remains almost unchanged until it is released. The small rise in strain at around 20 seconds is due to a horizontal movement of the robot arm as part of the object extraction path, causing a slight change in the reaction force and an increase in strain on one side of the gripper. The test was carried out six times, with each showing a similar output, both in the overall trend and scale of the strain output. The strain output for this graph has been scaled relative to the

average strain during the grasp of this test. This means subsequent comparisons with powder present can be shown relative to the strain output when no powder is present. The strain was scaled by simply dividing by the average strain during the first part of the grasp.

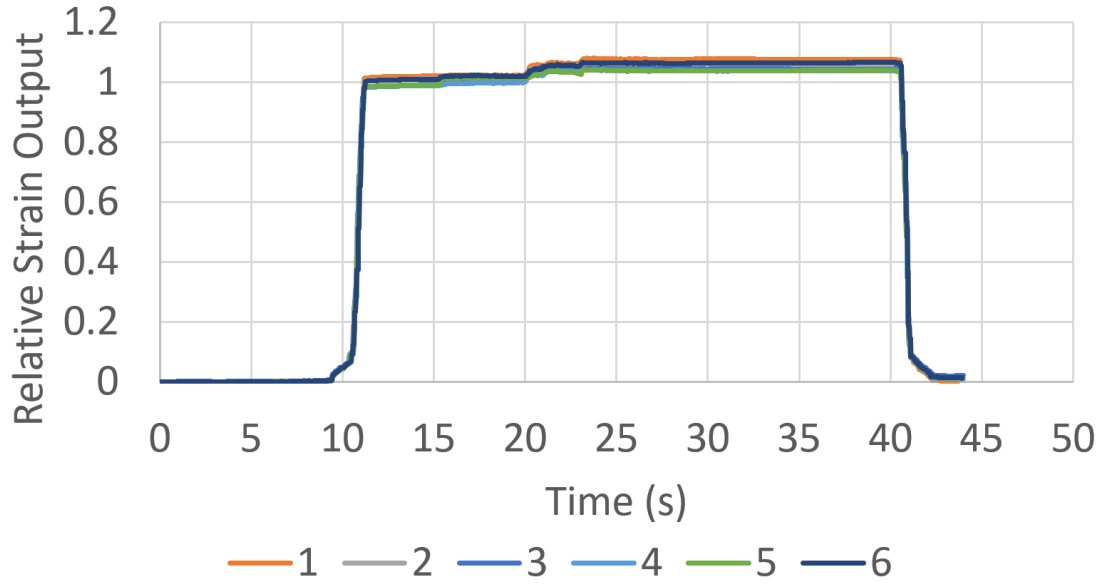

Figure 6.4.2: Object Grip Outside of Powder

6.4.3 Object Extraction from Virgin PA12 Powder

Figure 6.4.3 shows the strain output from gripping the same object but this time completely covered in virgin PA12 powder. It can be seen that there is a high initial strain output relative to the test with no powder, followed by a period where the strain slowly declines until it reaches a steady output until the object is released. The initial flat region of high strain is due to an equilibrium between the applied grasping force, and the compacting of the powder around the object before it is lifted. As soon as the gripper begins to move upwards (at just after 15 seconds) to extract the object, the force chain network through the powder, between the gripper and the object, becomes unstable and the digits are able to move again. During this region where the strain output declines, loose unfused powder is continuously falling from between the object and the gripper as it is lifted, causing the part to

slip (Figure 6.4.4), until a stable force chain network through the powder is found again. Although in these tests the object did not completely fall, it is visibly a lot more unstable in the grasp. It should also be noted that after this period of slip, although the strain plateaus, it does so at a higher level than would be expected for that object width if no powder was present. This is due to the fact that there is still some amount of powder between the object and the gripper, causing the strain output to equal that of a larger solid part. Although the overall trend was consistent for each of the six tests, the exact slip speed and behaviour during the region of instability was not consistent.

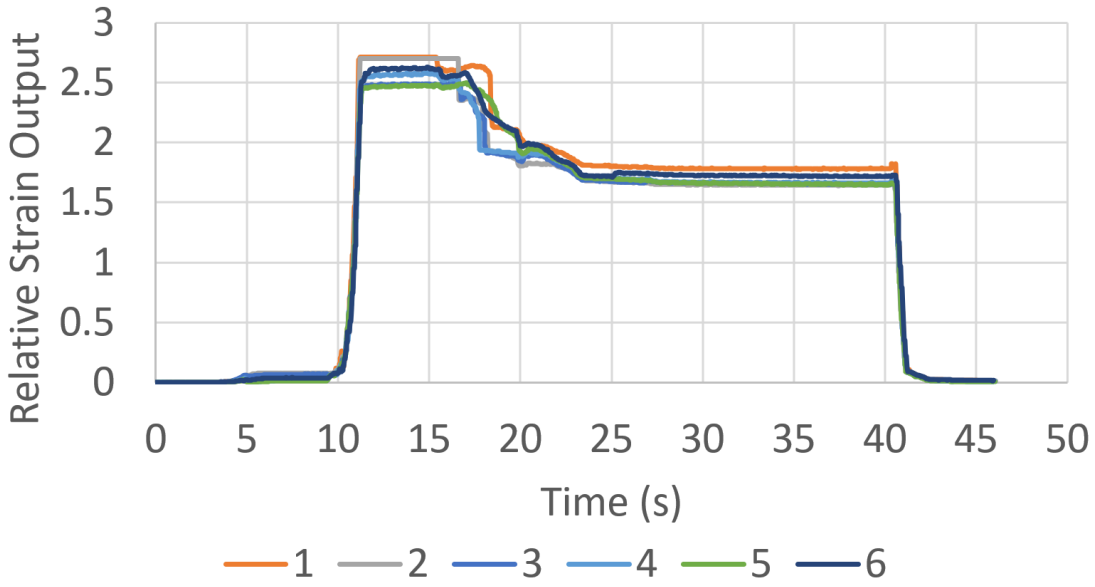

Figure 6.4.3: Object Grip Inside of Powder

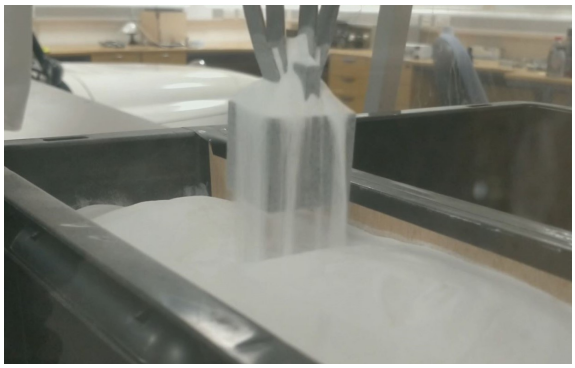

Figure 6.4.4: Object Slipping in Grasp

This initial test shows that although it is possible to successfully extract 3D printed solid objects from within virgin PA12 powder with a 3D printed gripper, there is instability in the grip, and the perceived object width is much larger than expected (around 2.5x). Simply increasing the gripping force does not necessarily help either of these issues, and excessive gripping force is not ideal for delicate parts. The increased strain experienced by the gripper will also reduce the fatigue life, due to an increased stress level. This means other methods of reducing the slip and perceived object width, without increasing the gripping force, would be most beneficial. The slight change in pose during the slip also means that errors could be introduced to any subsequent automated part handling.

Chapter 7

Improving Grip Performance

As the flat tips grasp an object surrounded by powder, the powder is compacted against the sides of the part. This increases the perceived size of the object and can cause the grip to become unstable as the object is moved. Reducing the distance between the gripper and object (i.e. less powder between the tip and the side of the object) gives the sensors a better understanding of the object size, and increases the stability of grasp. If the strain output and slip are reduced to the same level as that when no powder is present, this allows future grippers to be designed and tailored more easily, without the need to fully simulate the powder. Reducing the slip also means that the part stays in a known pose as it is extracted.

7.1 Modified Gripper Motion

As distributed compliance mechanisms such as the explicit gripper allow some amount of flex in more than just the intended direction, changes to the direction of the input motion also result in changes to the direction of the output motion. Figure 7.1.1 shows one modification to the standard linear input. The black arrows show the original input required to open and close the gripper in the conventional manner, and red arrows illustrate an additional torque being applied to the input rod, causing it to twist. This twisting motion causes the digit tips to move in the direction perpendicular to the gripping direction. As the torque acts through the centre of the symmetrical mechanism, the tips move in opposing directions. This

allows the tips to rub against each other (or against an object being gripped) which could allow them to move through some of the powder around the object. Movement in the other directions is also possible, but this is limited by the specific geometry at the gripper mount in this case.

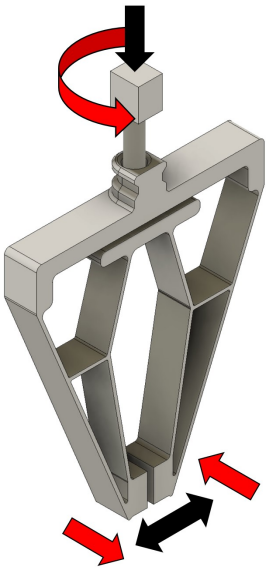

Figure 7.1.1: Twisting Input Motion

Although no additional joints or compliant elements have been added to the mechanism itself, to allow both the linear and rotational input to be controlled separately an additional actuator is needed, and the original input must also be modified to allow the rotation to occur. To achieve this, the linear actuator was mounted between two bearings, allowing it to rotate along its length, whilst remaining constrained in the vertical linear input axis. Figure 7.1.2 shows two initial mechanisms which were trialled for rotating the actuator. The first uses a lever which is pushed by two small servos - one for each rotation direction. This method worked but it was quite bulky and required both servos to be matched and positioned well to avoid backlash. The second design used a gear to allow a single servo to rotate the actuator in both directions. Again, although this worked, the gears also caused some backlash, making it harder to control the rotation accurately.

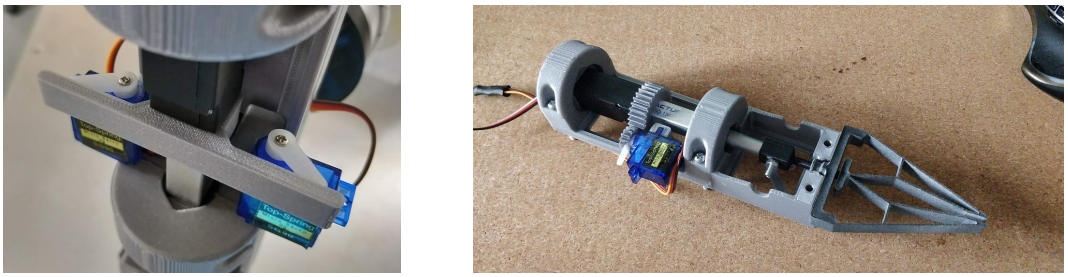

(a) Lever (b) Geared

Figure 7.1.2: Initial Input Twisting Methods

The final input twisting mechanism features a larger servo, mounted with its rotation output aligned through the centre of the linear actuator. This allows it to directly drive the rotation without the need for additional levers or gears[1]. As the gripping force is applied to the bearings and not the servo, it is able to rotate the actuator even at high gripping forces. A coupler between the gripper mechanism and actuator allows both a linear force and a twisting torque to be transmitted. Currently, the gripper is held in place with a small plate and two bolts, but this could be replaced by a compliant spring or motorised lock to allow grippers to be changed faster.

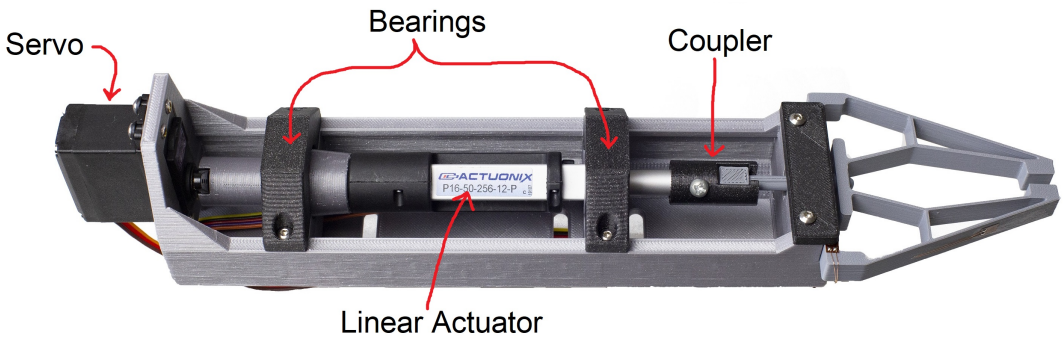

Figure 7.1.3: Final Twisting Input Mechanism

The servo is connected to the same Arduino based control system as the linear actuator, and it is setup to twist backwards and forwards as the gripper closes to grasp the object within the powder. The twisting motion stops very shortly after the gripper has closed, and will remain in this position for the remainder of the extraction movement.

[1]There are internal gears within the servo, but these have significantly tighter tolerances than an external 3D printed gear, resulting in a negligiible amount of backlash at the servo output.

Figure 7.1.4 shows an object extraction test carried out in the same way as in Chapter 6, but with the addition of the twisting during the grasp. Although the initial rise in strain is slightly lower than without any twisting, it is still approximately 2.25x the strain experienced when no powder is present, and some gradual slip still occurs once the robot arm begins to move. One of the effects of attempting to twist the digits against the object is that as the powder does not hold it rigidly, the twisting motion often just moves the object around, instead of moving through the powder against it. At higher gripping forces, the increase in friction between the tips and the object cause the tips to stop moving in relation to each other, and the twisting input simply causes the compliant elements to flex in another direction.

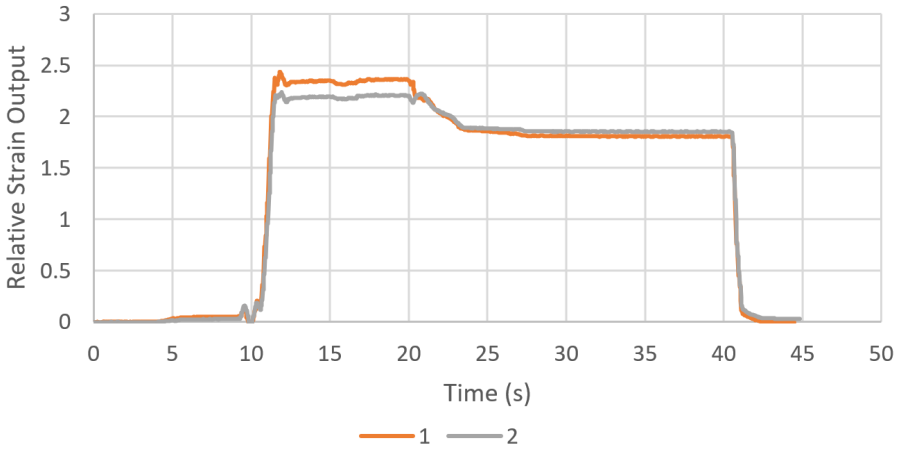

Figure 7.1.4: Object Grip Inside of Powder with Toothed Gripper

Due to the limited effectiveness of this twisting input technique, other methods will be trialled to reduce the initial rise in strain and subsequent slip that occurs during the object extraction process.

7.2 Modified Tip Geometry

As simply increasing the gripping force does not help the powder flow from in between the gripper tips and the object to be extracted, and excessive forces can break delicate parts, a revised tip geometry that decreases the contact area will be trialled, which should in turn increase the stress on the powder without increasing the overall

gripping force. To do this, a 'toothed' gripper was created, by adding a series of tabs extending perpendicular to the face of the gripper (Figure 7.2.1). This increase in stress applied to the powder should allow the tips to pass through the powder close to the side of the object more easily.

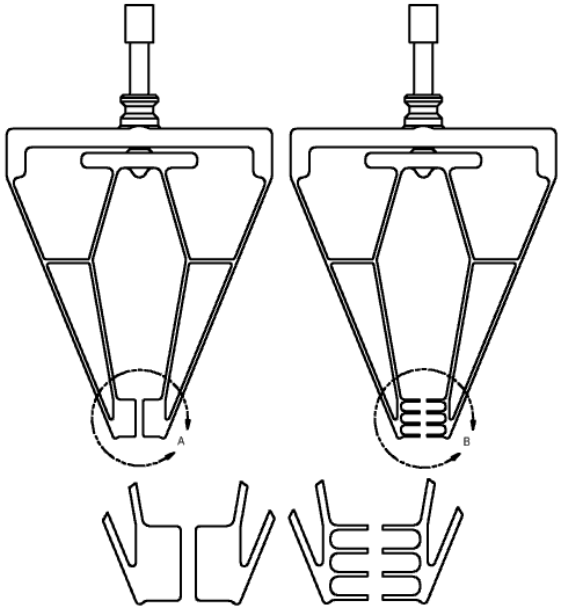

Figure 7.2.1: Flat vs Toothed Gripper Tip

Figure 7.2.2 shows the strain output from grasping a series of object widths from 3mm to 10mm with the flat and toothed grippers. It can be seen that both follow the same trend, with an error trend that decreases as the object width and strain increases. This error is small enough that although the tip geometries differ, the rest of the mechanism is identical and so the strain outputs can be compared for the gripping process.

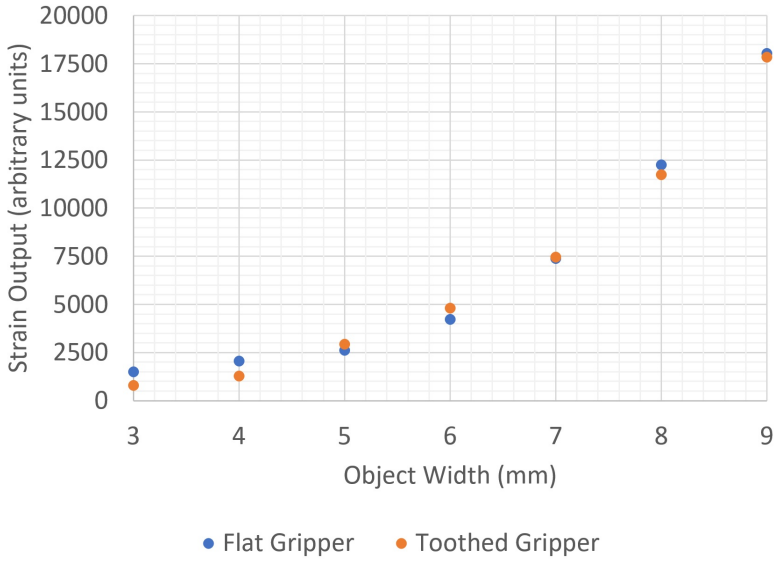

Figure 7.2.2: Flat vs Toothed Gripper Strain Response

Figure 7.2.3 shows the strain output whilst gripping the same object as before, but with the toothed gripper. It can be seen that there is still an initial rise in strain much greater than what would be expected with no powder present (2-2.3x), but this time once the object is moved there is a rapid movement of the tips as the powder becomes unstable, instead of a prolonged region of gradual slip. Although the instability is not completely removed, the only time it happens is when there is a change in direction such as the object being lifted (just after 15s) or being moved to the side (at around 20s), as this causes the force chain path through the powder to become unstable, but a new one is always quickly found, unlike with the flat tips where the part is almost continuously slipping. By the time the object is moved away from the tray of unfused powder, the level of strain is almost exactly equal to that when no powder is present. This indicates that the tips are now passing though essentially all of the unfused powder surrounding the object, aside from the large initial strain before it is extracted. Whilst this is certainly an improvement from the flat tip geometry, an ideal solution would result in no increase in the level of strain when compared to a case where no powder is present, at any point of the grasp.

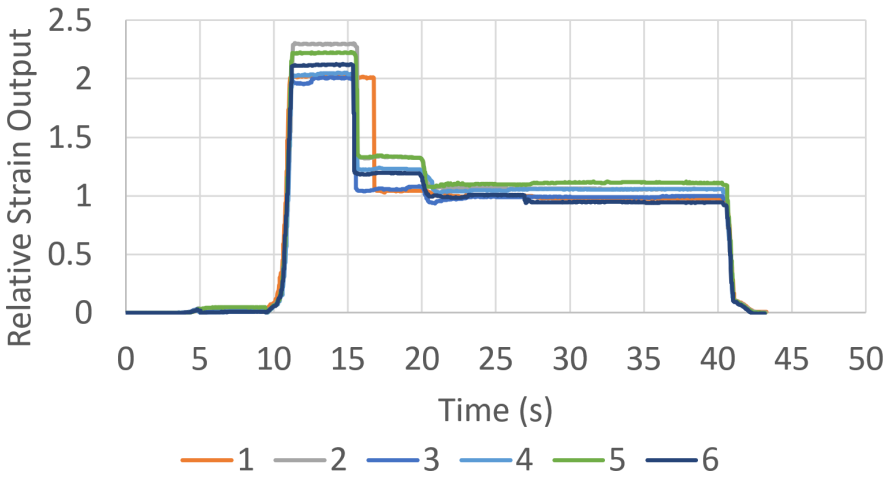

Figure 7.2.3: Object Grip Inside of Powder with Toothed Gripper

7.3 Digit Vibration

Dunst *et al.* (2018) showed that vibration can be used to increase the flowability of powders and separate agglomerates by reducing the internal friction forces. Wu *et al.* (2020), Matsusaka *et al.* (1996) and Kollmann and Tomas (2002) showed that vibrating a powder delivery tube allowed for a more consistent and higher flow rate through the nozzle. Vibration is also used in the HP Automatic Unpacking Station to help separate the solid objects from unfused powder by allowing them to move more easily though the unfused powder. At that scale however it causes the pose of the object to become unknown, as the entire build volume is vibrated at once. This is also not ideal for delicate objects, as individual objects could collide with each other within the powder, even if they were initially separate. Localising the vibration to the tip of the gripper should allow it to move more easily through the powder immediately surrounding the object, but without a change in the pose of the object to be gripped, or those which may surround it.

To achieve this, a small sealed brushed DC vibration motor (Figure 7.3.1) was mounted to the end of the digit, which can be activated during the gripping process. The vibration frequency of this motor is approximately 200Hz at 5V. For the following tests, the vibration was enabled as the gripper began to close, and dis-

abled approximately one second after the object was gripped. A small block was added to house the motor, which only connects at the base of the digit, meaning the compliant element is unaffected.

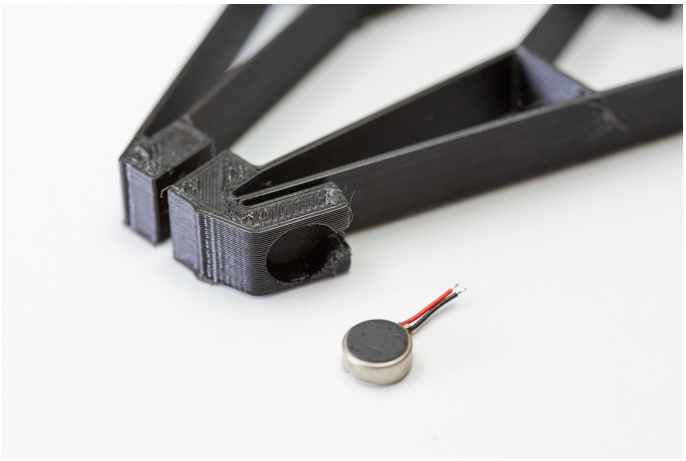

Figure 7.3.1: Mini Disc Vibration Motor

Figure 7.3.2 shows the strain output from gripping the same object surrounded by PA12 powder with the flat tip gripper, but with vibration. It can be seen that vibrating the tip as the object is grasped removes the large initial rise in strain and subsequent slipping that occurred in the previous tests. There are still some slight changes in strain as the vibration is enabled and as the object is moved, but these are relatively minor compared to the increase in strain for same test without vibration. For the gripper with flat tips, the addition of vibration did not cause the tips to move any closer to the object by the end of the test, it only removed the slip as the object was moved.

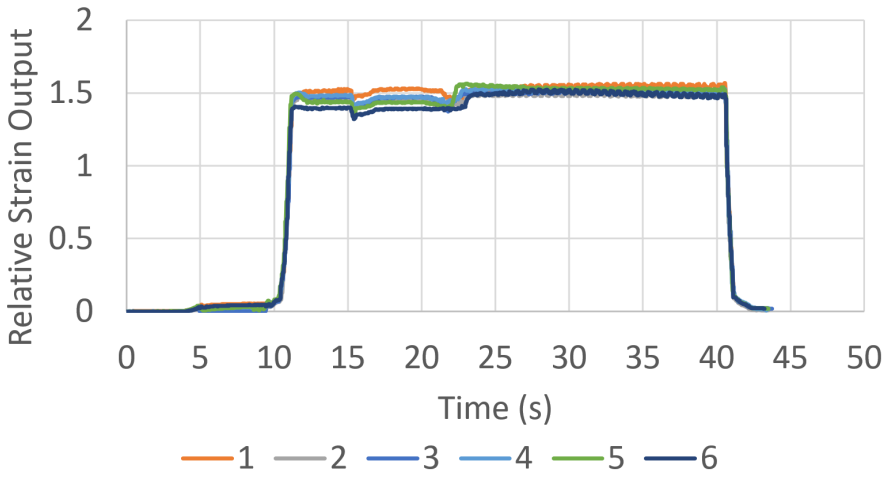

Figure 7.3.2: Object Grip Inside of Powder with Flat Gripper and Vibration

Figure 7.3.3 shows the strain output from an identical test, but with the toothed gripper. This setup shows the same overall trend as the flat tip gripper, but this time the strain output does not rise higher than what would be expected when gripping the object with no powder present. This means that no slip occurs as the object is extracted, and the perceived object width is identical to that of the same object with no powder present, even before the object is lifted.

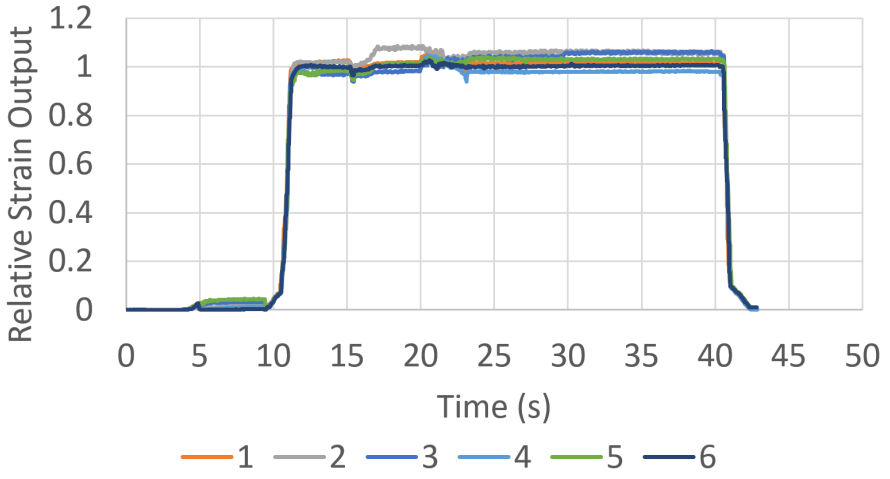

Figure 7.3.3: Object Grip Inside of Powder with Toothed Gripper and Vibration

Figure 7.3.4 shows the averaged strain output from each series of tests. Here it can be seen more clearly how the twisting motion has a minor effect and still produces a gradual slip, the toothed tip geometry reduces the overall increase in relative strain

output, and how the vibration reduces the initial rise and subsequent slip of the strain output. It also shows clearly how the combination of toothed geometry and vibration results in essentially the same relative strain output as when no powder is present, eliminating the instability and increased perceived object size.

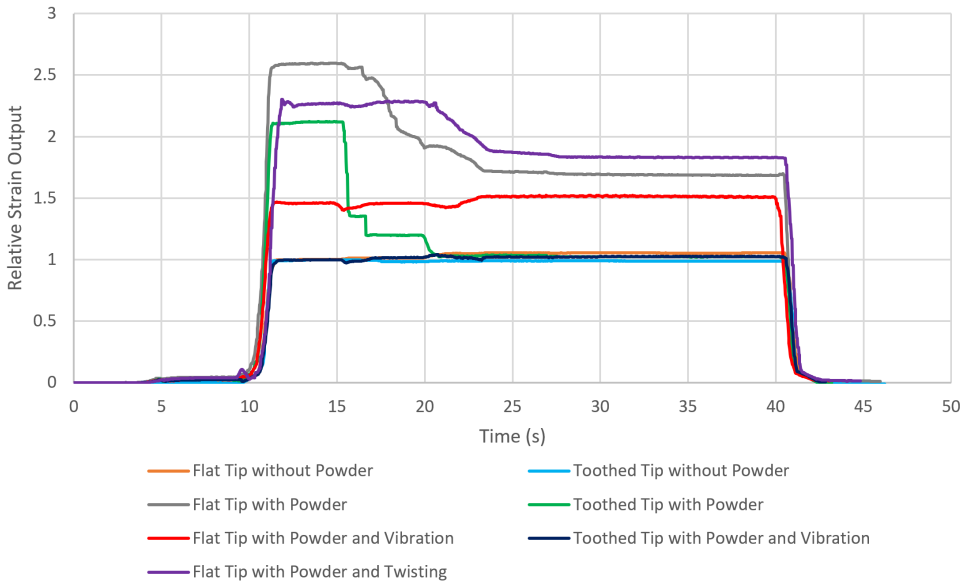

Figure 7.3.4: Comparison of Averaged Relative Strain Output Results

Configuration	Powder	Twisting	Vibration	Relative Strain Output
Flat Tip	N	N	N	1x
Toothed Tip	N	N	N	1x
Flat Tip	Y	N	N	2.6x
Flat Tip	Y	Y	N	2.3x
Flat Tip	Y	N	Y	1.5x
Toothed Tip	Y	N	N	2.1x
Toothed Tip	Y	N	Y	1x

Table 7.1: Comparison of Averaged Relative Strain Ouput Results

7.4 Object Slip Comparison

Although the strain perceived by the gripper using a combination of toothed geometry and local vibration has been shown to equal that of an object which is not surrounded by unfused powder, the current strain gauge setup is not able to measure how much the object is actually slipping during the grasp.

As the object is completely surrounded by powder before it is extracted, it is difficult to measure exactly how much it has slipped as it is grasped and lifted. To solve this, a thin structure was added to the object (Figure 7.4.1) which extends above the powder, whilst still allowing the gripper to grasp it as normal. A fiducial marker can then be placed on the exposed part of the structure, which can be tracked using a camera during the test. Another marker is also placed on the gripper, and the relative distance between them can be measured and compared to help understand how much the object has slipped during extraction (Figure 7.4.2). The additional structure has been designed to be symmetrical as to not cause any rotation of the object during the extraction, and as thin as possible to reduce the amount of added mass and surface area, whilst keeping enough stiffness to minimise any deformation between the tracking marker and grasp location as the object is moved.

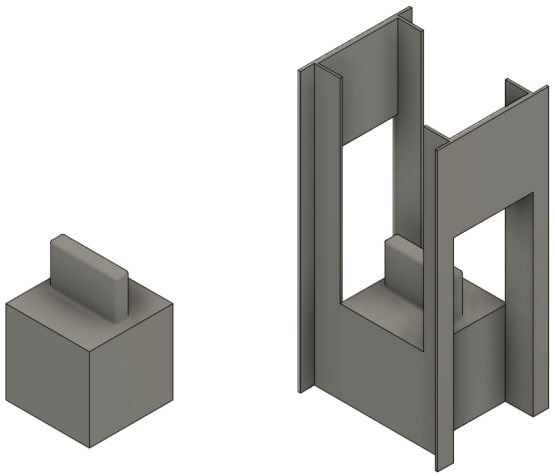

Figure 7.4.1: Object Including Tracking Marker Stand

The gripping process is filmed using a 4K camera with known calibration parameters, and OpenCV (OpenCV Team, 2021) is used to detect and estimate the pose of the ArUco (Garrido-Jurado *et al.*, 2014) fiducial markers placed on the object and gripper. The pose estimates of each marker are saved to a CSV file for every video frame, for further analysis in Microsoft Excel.

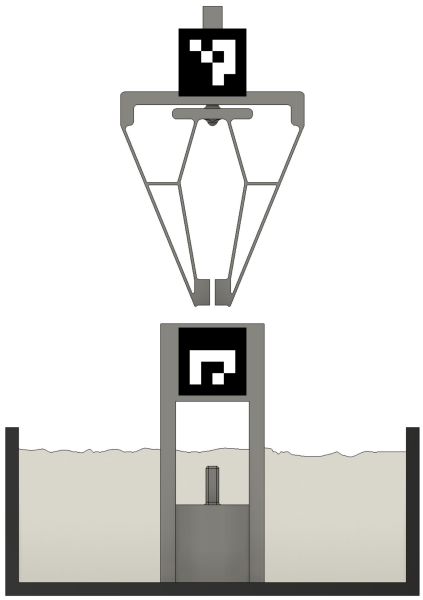

Figure 7.4.2: Tracking Marker Object within Powder

Figure 7.4.3 shows the change in vertical position of the gripper and the object, as it is extracted from the tray without powder present. The vertical position has been offset so that the object starts at 0, and the gripper is at 0 when it reaches the bottom of its movement (at the point where the grasp begins). It can be seen that the gripper and object start 120mm apart, and the gripper moves down to grasp the object. As the object is lifted, the vertical position of it and the gripper change at the same rate, and rise together. Any slip during the extraction will cause the final vertical position of the object to be lower than the vertical position of the gripper at the end of the test.

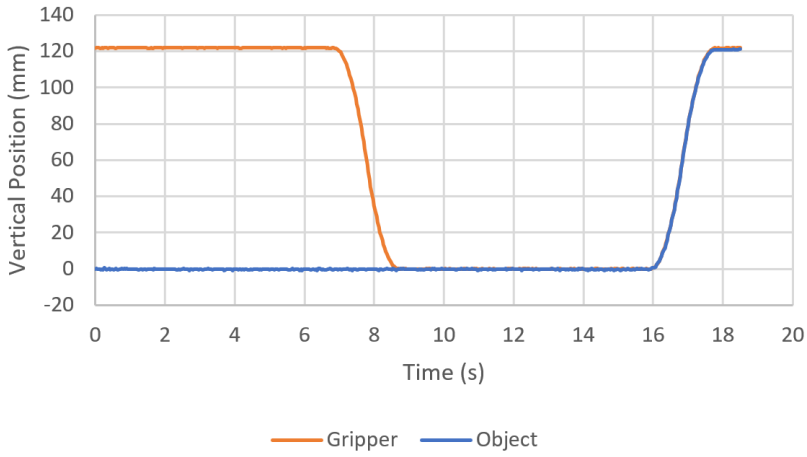

Figure 7.4.3: Relative Movement of Gripper and Object during Extraction (without powder)

7.4.1 Results

The same test was carried out with the object covered in virgin PA12 powder, using the standard flat tipped and the toothed grippers, both with and without local vibration at the tip. Figure 7.4.4 shows three frames from one of the extraction tests. The estimated pose axes from OpenCV can be seen, which are recorded and used to determine the amount of slip at the end of the extraction. Due to the test setup the dark gripper is not clearly visible against the dark background, but as only a clear view of the two markers are required, this is not an issue.

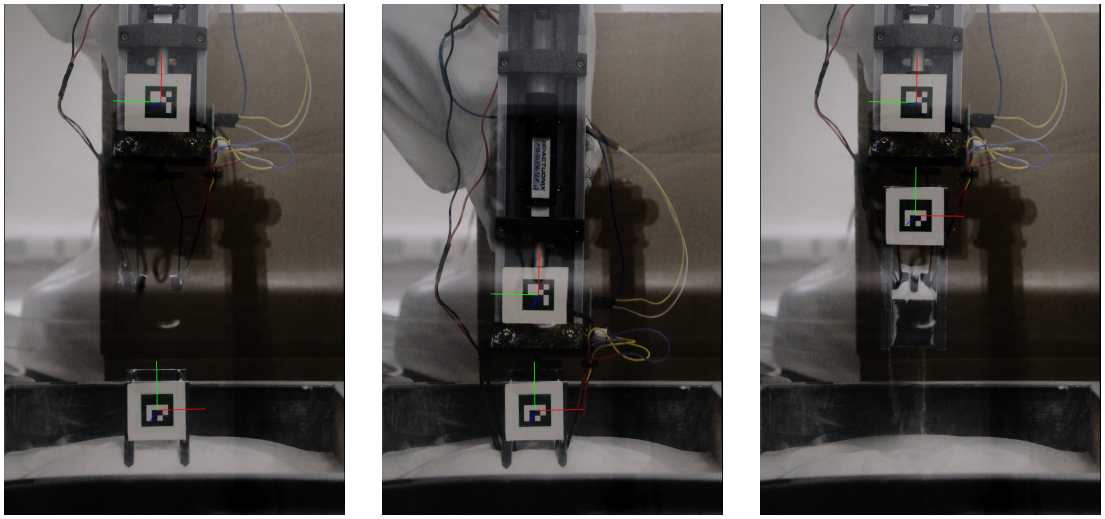

(a) (b) (c)

Figure 7.4.4: Pose Tracked Object Extraction

Figure 7.4.5 shows a comparison between the measured vertical slip. It can be seen that the object slips by 3.51mm when surrounded by powder, using the flat tip gripper with no local vibration, compared to only 0.19mm with no powder present. Although the object does not completely fall from the grasp, a slip of this magnitude could easily cause issues if the object pose needs to be known for subsequent automation or assembly processes.

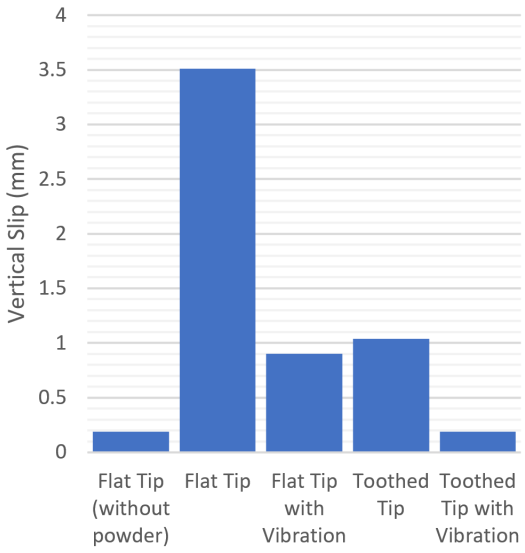

Figure 7.4.5: Vertical Slip Comparison

Applying local vibration or using the toothed gripper causes the slip to reduce by a similar amount, down to 0.90mm and 1.04mm respectively. Although this is an improvement, it is still approximately 5x the amount of slip as when no powder is present. These results are similar to the measured strain data, showing a result somewhere between a test with the standard gripper, and a test with no powder present.

Using a combination of toothed tip geometry and local vibration causes the vertical slip to reduce to 0.19mm, the same as the measured slip with no powder present. Again, this matches well with the strain data, which showed the same amount of strain whilst gripping an object with no powder and one with powder using toothed tip geometry and local vibration.

Chapter 8

Aged Powder and Caked Objects

Although it has been shown that a one-shot 3D printed compliant gripper is able to extract cleaned 3D printed solid objects from virgin PA12 powder, the MJF process produces parts which are surrounded by not just loose unfused powder but some caked powder directly around each printed part. The printing process does also slightly change the properties of the unfused powder, meaning that the slip/clumping/flowability characteristics of this 'aged' powder will vary slightly compared to virgin powder which has not been through the MJF process. Figure 8.0.1 shows a series of blocks with tabs, sent directly from the MJF process, without being cleaned or post-processed.

Figure 8.0.1: Caked Objects in Aged Powder from MJF Process

8.1 Aged Powder & Clumping

During the MJF process, the build volume is heated to a temperature close to the material melting temperature (Figure 2.2.1). A fusing agent and detailing agent are then selectively sprayed across each layer of powder, to fuse and prevent fusing of the powder into solid parts. This process results in a change in the material properties of the unfused powder which surrounds the printed parts, compared to virgin powder. This includes a reduced flowability, and small regions of clumping. As shown in Figure 8.1.1 these clumped regions can form 'blocks', but these are relatively fragile, and can easily be broken apart, and when rubbed together by hand will return to visually the same as the bulk unfused powder.

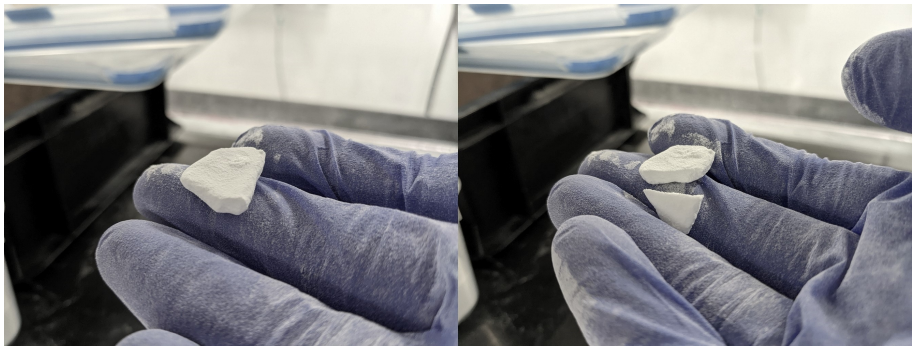

Figure 8.1.1: Aged Powder Clump

Figure 8.1.2 shows the strain output whilst extracting an object with no powder present, compared to virgin PA12, and aged PA12 powder. The strain output has been scaled relative to the average strain when no powder is present. It can be seen that both the virgin and aged powder both cause an initial strain output of approximately 2.6x the strain when no powder is present. There is then a gradual decline in the strain output as the object is extracted and it slips in the grasp, as powder falls from between the gripper and object. The duration of this slip looks to be similar between the virgin and aged powder, but the strain output for the aged powder tests does not drop as low as for the virgin powder. This is likely due to the lower flowability present in the aged powder. It can also be seen that the three tests without powder follow an almost identical trend, but there is some variability in the tests with powder surrounding the object. This variability is increased with the aged powder when compared to the virgin powder.

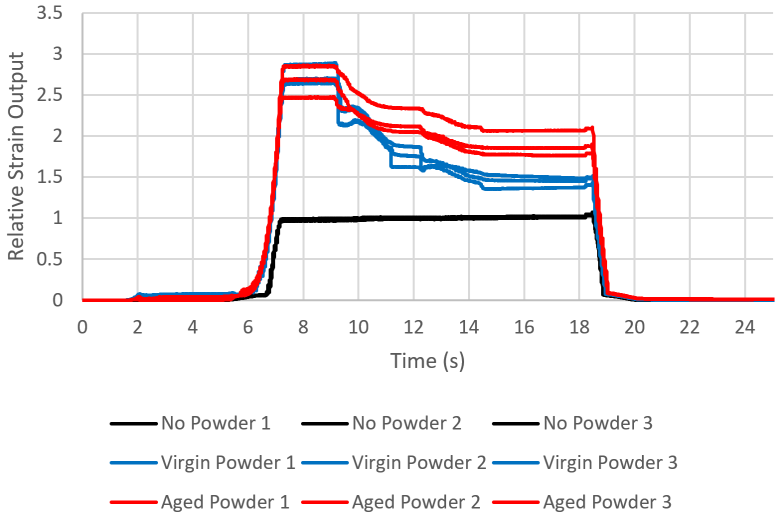

Figure 8.1.2: Relative Strain Output when Grasping a Cleaned Object from Virgin and Aged PA12 Powder Using the Flat Tipped Explicit Gripper Mechanism Without Vibration

8.2 Caked Objects

Figure 8.2.1 shows an object directly after removal from the MJF process, still caked in unfused powder, alongside another object of the same geometry which has been cleaned by hand, to remove the excess caked/unfused powder. Although this caked powder can be removed entirely using a small brush or similar tool, it does not simply fall off due to gravity, as the bulk of the unfused powder does. Figure 8.2.2 shows an illustration of a solid printed object surrounded by unfused powder at the end of the MJF process. The caked powder forms a rough boundary around the solid printed part, which is then surrounded by much more loose unfused powder, filling the rest of the build volume. It is expected that the caked powder directly surrounding the object will affect the performance of the grip, but it is not known how.

Figure 8.2.1: Caked Object (left) vs Cleaned (right)

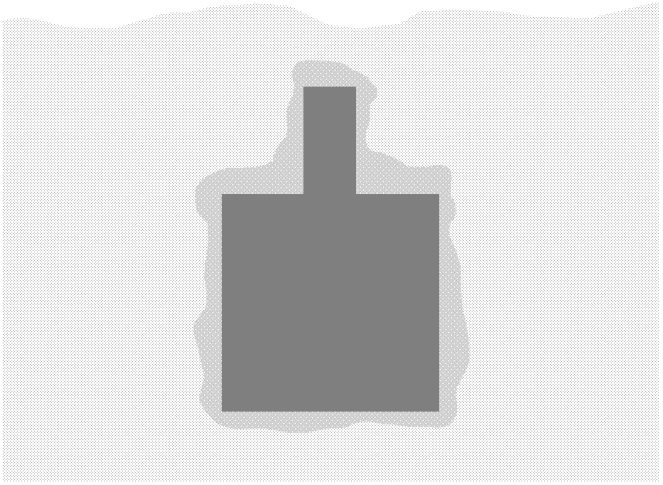

Figure 8.2.2: Illustration of Uncleaned Object in Unfused Powder

8.2.1 Grasping Caked Objects

To gain an initial understanding of how the caked powder reacts when it is gripped, some initial tests were conducted outside of the unfused powder, by just gripping the caked object. Figure 8.2.3 shows a caked object after being grasped by the gripper with flat tips. It can be seen that there is a flat spot on either side of the tab, where the flat tip made contact. As the gripper was not able to move through the caked powder, it compacted it more between the tips and the object. It can be seen that

the sides of the object do not look the same. This is due to the inconsistency of the caked powder which surrounds the parts.

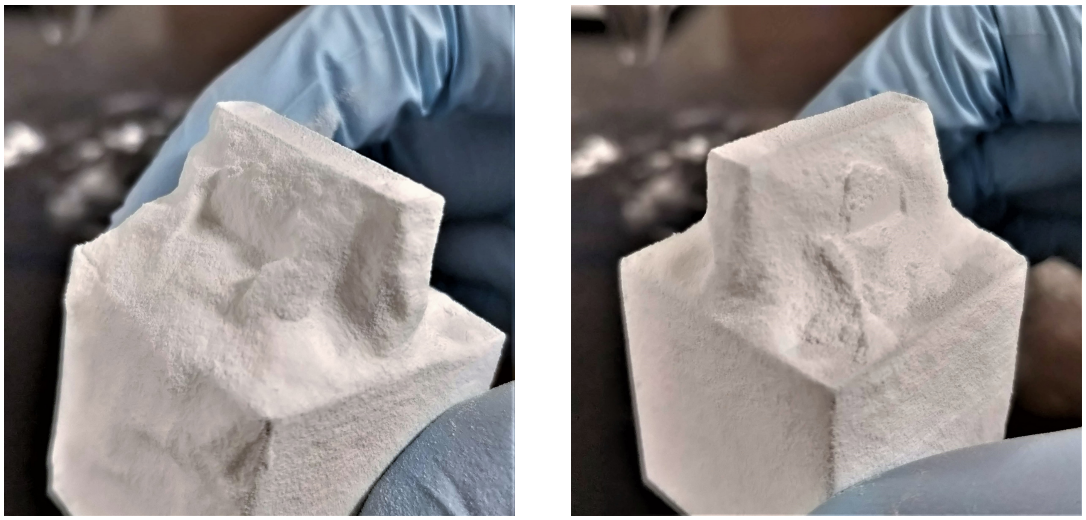

(a) (b)

Figure 8.2.3: Uncleaned Object after Grasp with Flat Tipped Gripper

Figure 8.2.4 shows another caked object being grasped with the toothed gripper. It can be seen that the toothed geometry is able to somewhat penetrate the caked powder surrounding the object, rather than just compressing it like the flat tips.

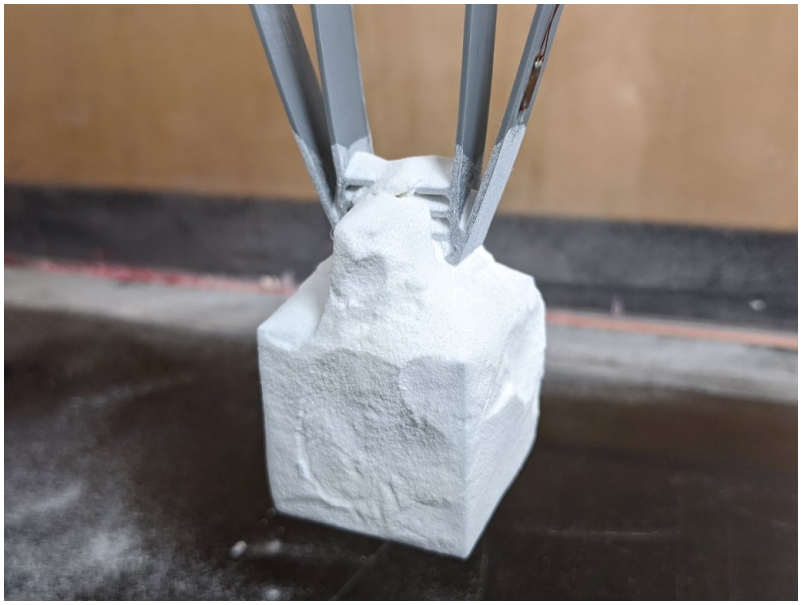

Figure 8.2.4: Toothed Gripper and Uncleaned Object

The side of an uncleaned object after being grasped with the toothed gripper with local vibration is shown in Figure 8.2.5. It can be seen from the tooth marks that the gripper tips are able to pass through a substantial amount of the caked powder.

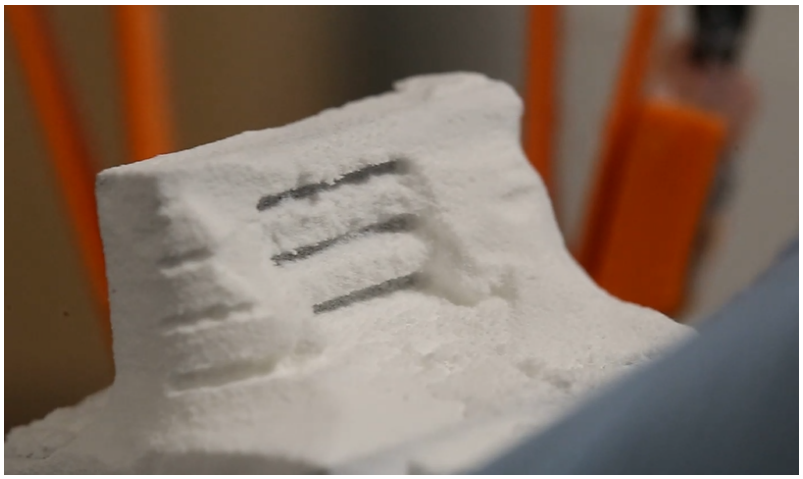

Figure 8.2.5: Side of Uncleaned Object after Grasp with Toothed Tip and Vibration

8.2.2 Extracting Caked Objects from Aged Powder

Figure 8.2.6 shows the strain output (relative to that experienced by gripping a clean object with no powder present) whilst grasping a series of caked objects surrounded

by aged powder, compared to cleaned objects in aged powder, using the flat tipped gripper with no vibration. It can be seen that in all cases, grasping objects that are still caked in powder result in a substantial increase in the amount of strain experienced by the compliant gripper. There is also an increase in the variability between tests, which correlates with the inconsistent amount of caked powder which surrounds the printed parts. In all cases there is an initial rise of strain as the gripper approaches the object, as the digits are flexed due to the interaction with the caked powder, which does not happen when extracting cleaned objects. Once the gripper begins to move to lift and extract the caked object, there is a prolonged region of slip, consistent with tests with the flat gripper with cleaned objects.

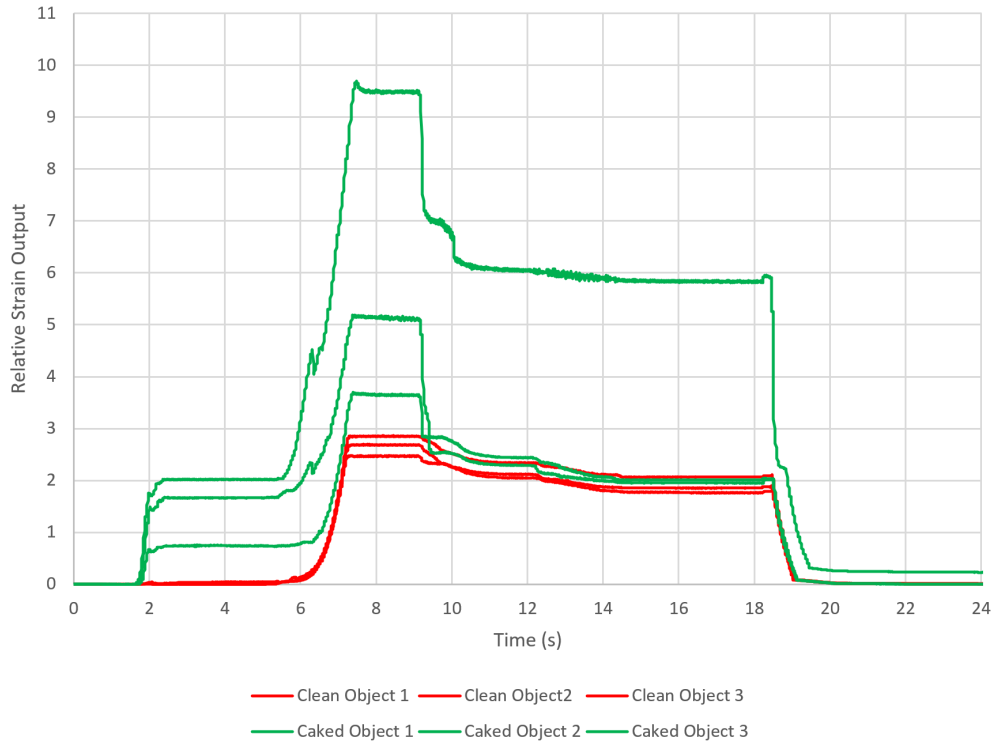

Figure 8.2.6: Relative Strain Output for Extracting Cleaned Objects Compared to Caked Objects, in Aged Powder using Flat Tipped Gripper

Following the success of using a toothed gripper with local vibration to reduce the slip and increased relative strain output when extracting cleaned objects from virgin powder, the same gripper was tested with caked objects in aged powder. Figure 8.2.7 shows three extraction tests using a flat tipped gripper, and three using the toothed gripper with local vibration. It can be seen that some of the trends seen previously

are still valid, but the overall result is not as clear. As before, the toothed gripper with vibration is effective at removing the initial rise as the gripper is closed, as well as any sharp or prolonged slip as the object is lifted. However, in this case it does not result in a relative strain output that equals that of gripping the same object without powder present. It is also not a clear improvement over the flat gripper without vibration in all tests. It can be seen that as with the previously shown caked grasp result, there is a much wider variability compared to when grasping cleaned objects. Like the flat gripper, there is also an initial strain experienced as the digits contact the caked powder directly surrounding the object but before the gripper closes (2-6 seconds), however the toothed gripper with vibration strain can be seen to decrease during this period, as the vibration is allowing some of the caked powder to move, as opposed to the flat gripper without vibration where this initial strain does not change.

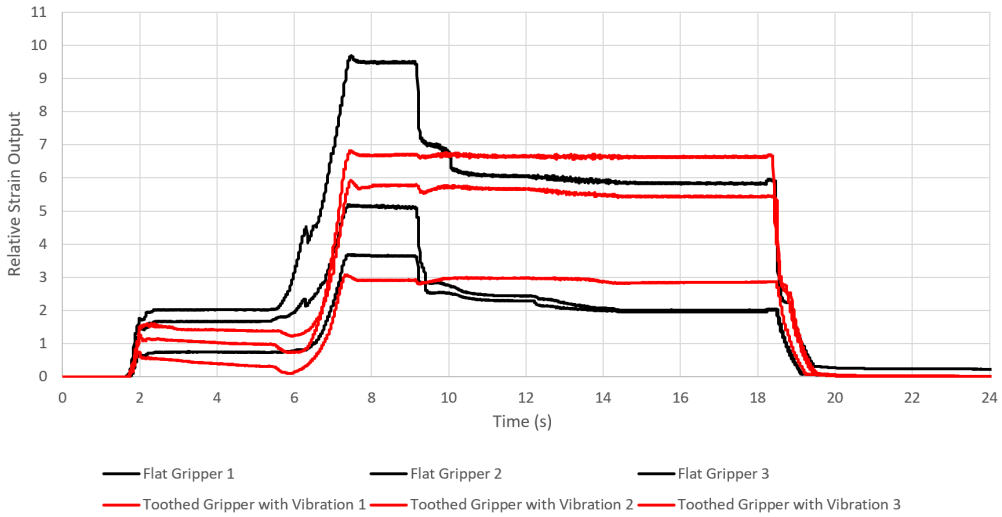

Figure 8.2.7: Relative Strain Output for Extracting Caked Objects in Aged Powder using Flat Gripper and Toothed Gripper with Local Vibration

Although the strain output is shown to be much higher than for the same object without powder present, the caked objects were successfully extracted from aged powder in every test that was carried out. This means that the one-shot 3D printed mechanism and gripping technique are effective at reliably extracting individual caked objects from unfused powder, even if the output from onboard sensors are inconsistent and dissimilar to that of cleaned objects.

8.3 Extracting Multiple Objects

As an additional demonstration of the gripper's ability to extract objects in a known pose from unfused powder, multiple caked objects covered in aged powder will be individually extracted from a container, and placed next to the container in a pre-specified location. The objects used for this test will be ones which have been previously grasped for the caked object strain testing shown above, and so are not usable for additional quantitative tests, but are still useful for this further demonstration.

For this test, a series of objects will be placed into an empty container, each in a known location. Unfused aged powder will then be poured over them. To automate the extraction of multiple objects, a program was written on the UR5 robot arm, which starts by moving the gripper to the first object location. Once in position, a command is sent to the gripper control box, and the object is grasped. The gripper control box then sends a confirmation back to the UR5 once the object is grasped, and the UR5 lifts the gripper and object, and moves to a new location outside of the powder. Once in position, the UR5 sends another command to the gripper control box to release the object. The process then repeats for each of the objects which are to be extracted.

As printed objects are surrounded by a region of caked powder which is not as loose as the bulk of the powder after printing has finished, if two objects are printed close together, the caked region can cause the parts to appear to be joined (Figure 8.3.1), until the caked powder is cleaned or a small force is applied, and the objects fall away from each other. Clearly, separate objects that act as if they are a single object are not ideal from an automated extraction process. In this multiple extraction test, all objects will be placed with at least 25mm separation which is larger than the caked region which has been found to surround any of the sample objects. No literature has been found describing the thickness of the caked powder surrounding parts.

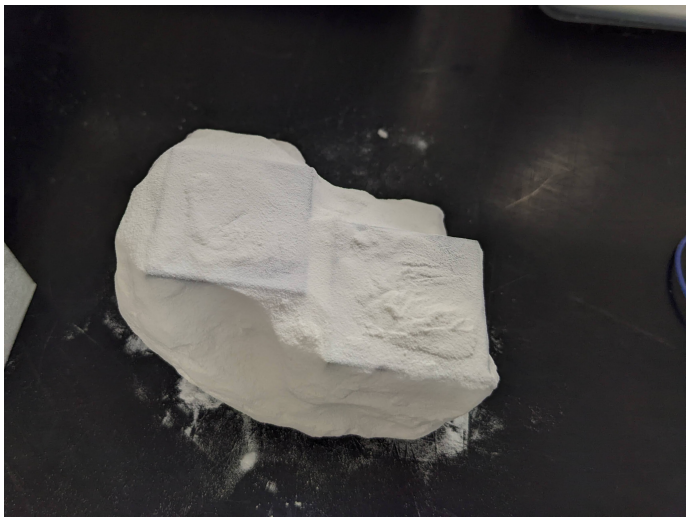

Figure 8.3.1: Caked Objects Printed Close Together

Figure 8.3.2 shows 9 objects placed into an empty tray. The variability of caked powder between the objects is clearly visible, along with some evidence of being previously grasped as part of previous testing. Once the objects had been placed into the empty container in a known pose (as they would be within the 3D printer post-printing), aged powder was gently poured over them until they were all completely buried.

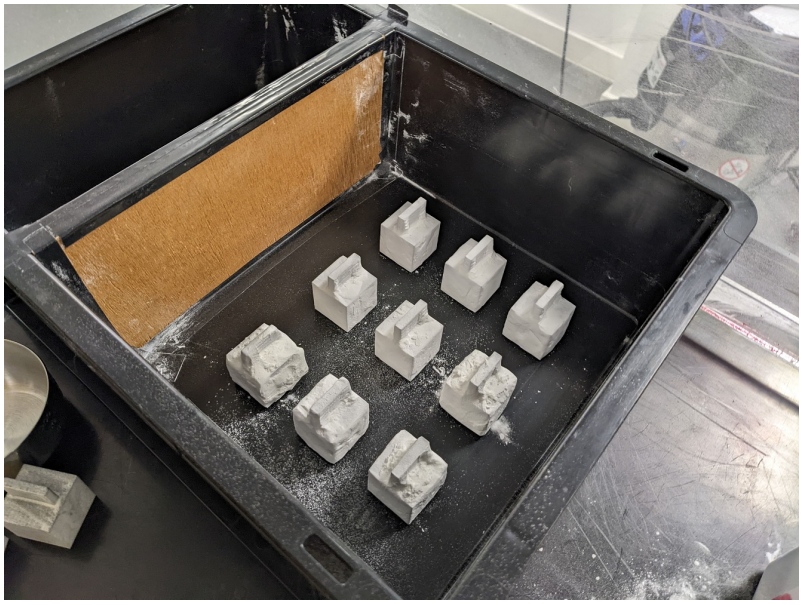

Figure 8.3.2: Pre-grasped Caked Objects in Empty Container

The automated test could then be started. Figure 8.3.3 shows an image taken during the test. It can be seen that the toothed gripper is able to pass through the powder and is contacting the side of the object, with minimal powder between. Powder can be seen filling the gaps between the tabs, and piled on top of the tips and object, with a small amount falling during the movement.

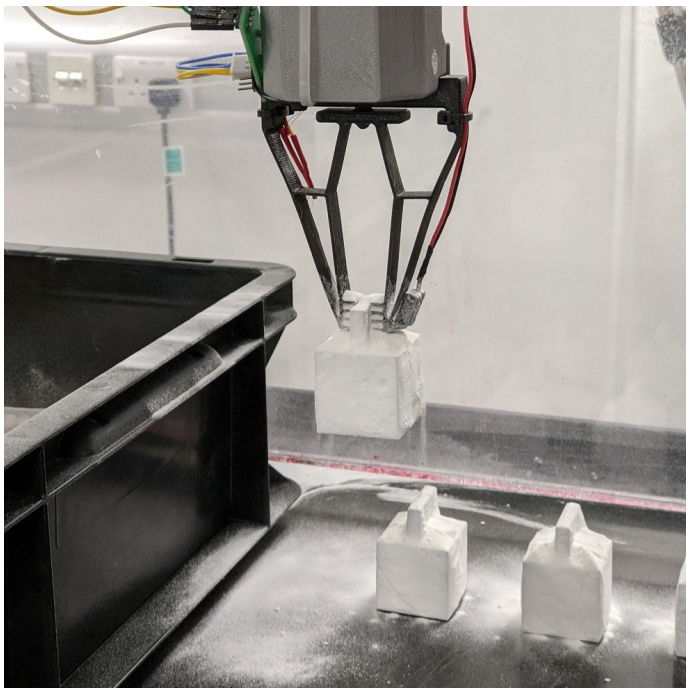

Figure 8.3.3: During Multiple Object Extraction

Figure 8.3.4 shows the 9 caked objects after being extracted from the aged powder. It can be seen that each was extracted successfully, and placed in a known location alongside the container. Each object is visibly well aligned in the expected location, indicating that there was minimal slip or change in the object pose during the extraction.

Figure 8.3.4: After Multiple Object Extraction

This test has shown that it is possible to extract a series of caked 3D printed objects from aged powder, using a one-shot 3D printed gripping mechanism, and that this can be done automatically using a robot arm, based on the known locations of the objects within the powder.

Chapter 9

Strain Array Sensor

Although it has been shown that caked objects can be reliably extracted from aged PA12 powder, knowledge about the interaction between the objects and the gripper is currently very limited during the grasp. The strain gauge mounted to the compliant element has been effective at determining the force being applied or the apparent width of the object being grasped, and although slip can be inferred by a reduction in this strain as powder falls from between the gripper tips and the object, it is not possible to measure the amount of slip, the slip direction, the object mass, or if any external forces are being applied. It is also possible that objects could slip without causing a reduction in strain, if instead of powder falling, there is too little grasping force to overcome the friction between the gripper tips and the object, due to the robot arm acceleration being too high, the object too heavy, or an external force/collision. In these cases, the current strain sensing setup would not be able to detect the slip occurring.

In many complex gripping applications, some form of tactile sensor is used to provide a richer understanding of the interaction between the gripper and object. These are often able to measure shear forces applied to the tip of the gripper, which can also help to detect things like slip. However, as shown in the literature review, these are often complex to manufacture, with many individual non-3D printable parts. The geometry of the tactile sensors can also be large and rely on a relatively big deformation of the sensor, which is in conflict with the relatively rigid toothed tips of the gripper which has been shown to be suited for reducing slip when an object is covered in powder.

In a similar way to many existing tactile sensors which usually feature an array of individual sensing elements, a strain gauge on each tooth of the gripper could allow more information about the grasp to be determined.

9.1 Initial Prototypes

9.1.1 Non-Gripper Sensor

Figure 9.1.1 shows an array of 9 tabs sticking out from a flat face, each with a strain gauge adhered to one of the sides. In a similar way to the tactile sensors described in Section 2.6.3, these individual tabs (or sensor elements) can be compared and an overall sensor output can be determined.

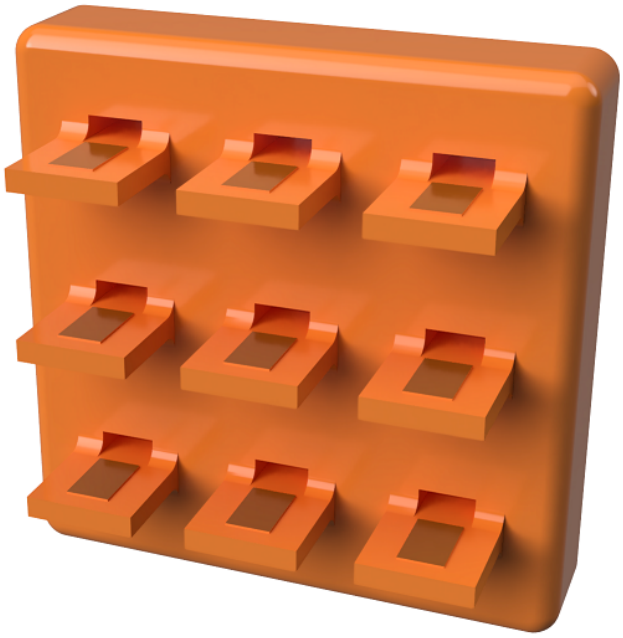

Figure 9.1.1: Strain Gauge Tab Array

In the most simple cases, where there is a constant force applied to all tabs in the same direction (Figure 9.1.2a), this would indicate that there is a force being applied directly across the sensor. Figure 9.1.2b shows a slightly more complex

loading scenario where the force directions are opposite on each side. This would indicate that the object is rotating around the centre of the sensor. As the loading cases increase in complexity, the overall output will be less easy to determine, but similar methods to those used by TacTip (Section 2.6.3) or other tactile sensors may be appropriate to use in order to classify the interaction.

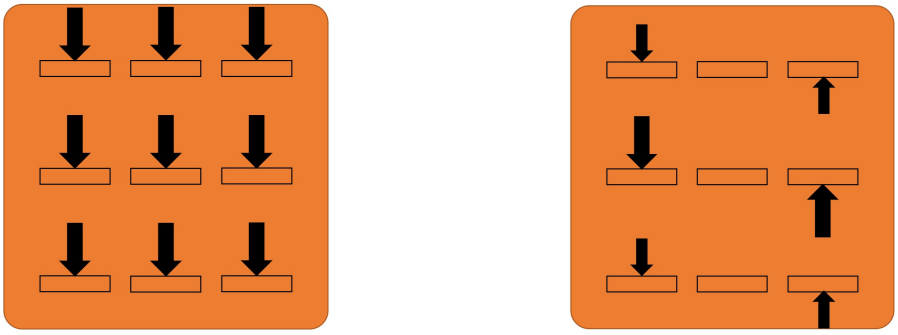

(a) Translation (b) Rotation

Figure 9.1.2: Strain Array Example Forces

Each stressed strain gauge will be configured in a quarter-bridge configuration, alongside an unstressed strain gauge for temperature compensation, and two resistors of a similar resistance to the strain gauges. Each of these bridge circuits will be connected to a HX711 amplifier board, which will measure the strain output and send the signal back to an Arduino for further processing and recording, in a similar way to the individual strain gauge on the compliant gripper element. As HP have demonstrated 3D printed conductive traces using the MJF process, in the future the strain gauges, and wires to connect them to the HX711/Arduino, could be embedded in the gripper as part of the 3D printing process.

A prototype sensor base will be 3D printed with a mount to attach it to the side of the existing robot arm test rig (Figure 9.1.3). The robot arm can then be used to apply repeatable loads onto the sensor, and the outputs can be recorded for analysis.

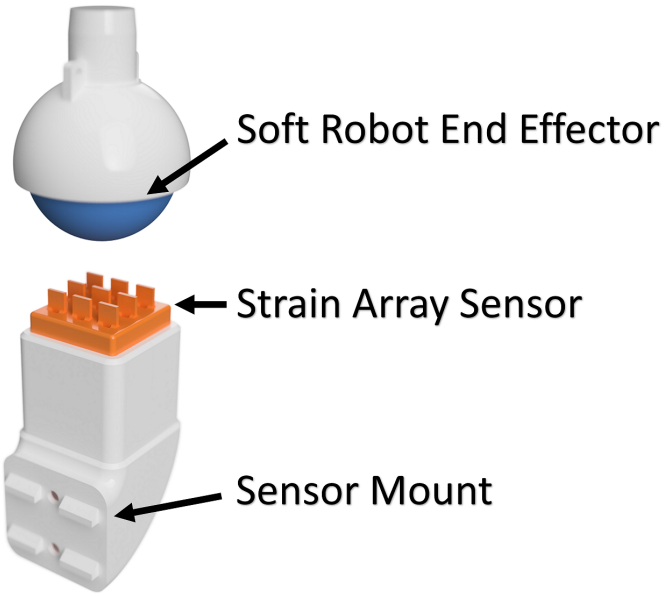

Figure 9.1.3: Strain Array Sensor CAD

An initial prototype sensor was made and is shown in Figure 9.1.4. It can be seen in this image that the middle tab is missing. It was broken during an initial strength test, which showed each tab could handle approximately 3 kg of load. The main sensor array plate 3D printed in orange is attached to a white 3D printed housing which contains the unstressed gauges, resistors, and HX711 modules (Figure 9.1.5). The power and data wires can be seen at the back of this housing, which can be routed to a nearby Arduino for data processing.

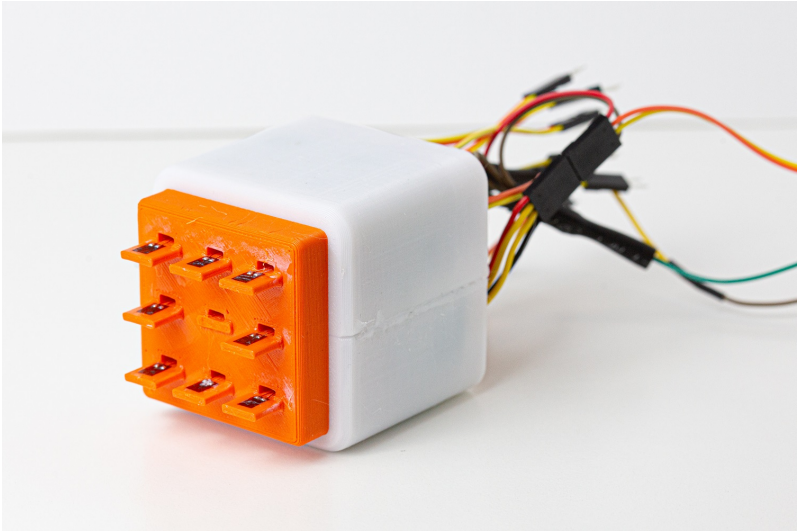

Figure 9.1.4: Strain Array Sensor

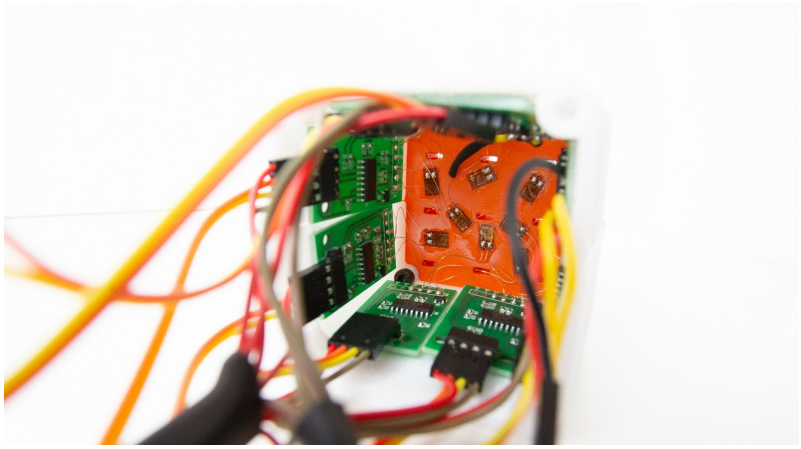

Figure 9.1.5: Strain Array Sensor Inside

For initial testing of the strain array sensor, it was mounted in a fixed position on the side of the existing test rig, next to the robot arm. A soft foam ball was then mounted to the end of the UR5 to provide repeatable input movements across the sensor. Table 9.1 shows the order of movements for this test. The first of these will be a translation test (similar to Figure 9.1.2a), and the second will be a rotation test (similar to Figure 9.1.2b).

Step	**Movement**
1	Lower Object
2	Translate Forwards
3	Translate Backwards
4	Raise Object
5	Lower Object
6	Rotate Clockwise
7	Rotate Anti-Clockwise
8	Raise Object

Table 9.1: Strain Array Test Movement

For this initial test, only the first 5 strain elements were functional, which were arranged as shown in Figure 9.1.6.

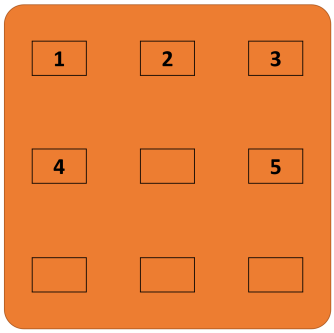

Figure 9.1.6: Strain Array Output Numbering

Figure 9.1.7 shows the output from the strain array sensor. An error in the setup resulted in gauge 4 not being able to output negative strain values.

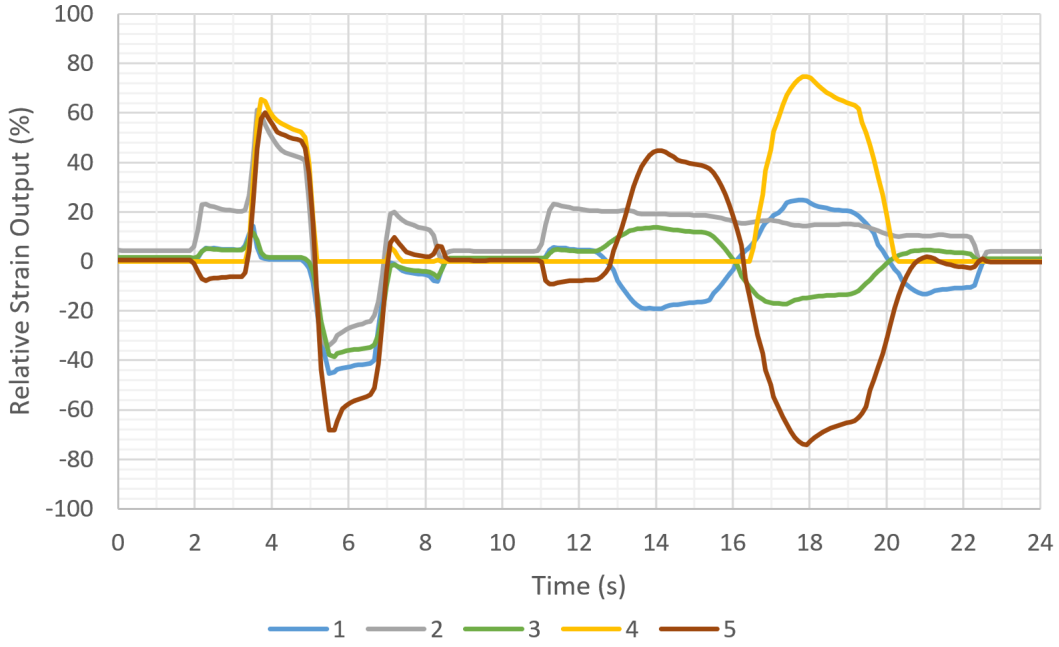

Figure 9.1.7: Strain Array Output

It can be seen that as the object comes into contact with the sensor there is some amount of strain output on a few of the tabs (at around 2-3 seconds). The direction and magnitude of this initial output could be used to show where the object is located across the array. In this case the output from tabs 1,2,3 are positive, tab 4 is zero and tab 5 is negative. This suggests that the initial object contact pushed in somewhere between the first and second row of tabs.

On the translational movements (3-7 seconds) it can be seen that all of the individual strain outputs trend in the same direction as expected. On the rotational movements (13-20 seconds) the individual strain outputs do not all trend in the same direction. Tab 2 stays relatively consistent across the rotations, indicating it is close to the centre of rotation. The outputs from tabs 1 and 4 trend in the same direction, and tabs 3 and 5 trend in the opposite direction. This is also expected and close to what was shown in Figure 9.1.2.

This initial testing shows that an array of strain gauges mounted to tabs can show how an object it is making contact with is translating or rotating. However the array is much larger than what would fit on the tips of the existing gripper mechanism. A revised design which shrinks the array and moves all of the HX711 modules away from the sensor is needed.

9.1.2 Single Column Gripper Sensor

For an initial test of this sensor setup on a gripper, a single column array will be used, formed of three tabs on each side of the gripper, aligned vertically (Figure 9.1.8). This setup should allow vertical force or movement to be measured, but not rotational force or torque. If successful, this design can be expanded to allow for a more complex array.

Figure 9.1.8: Single Axis Gripper Sensor Setup

Figure 9.1.9 shows a 3D printed gripper where two of the tabs contain strain gauges. These strain gauges are then paired with an identical gauge mounted in a relatively unstressed location and orientation to help provide temperature compensation. Each pair of gauges is connected to a dedicated HX711 module. As objects are grasped and moved, the output from each HX711 module is processed by an Arduino microcontroller and recorded on a connected computer.

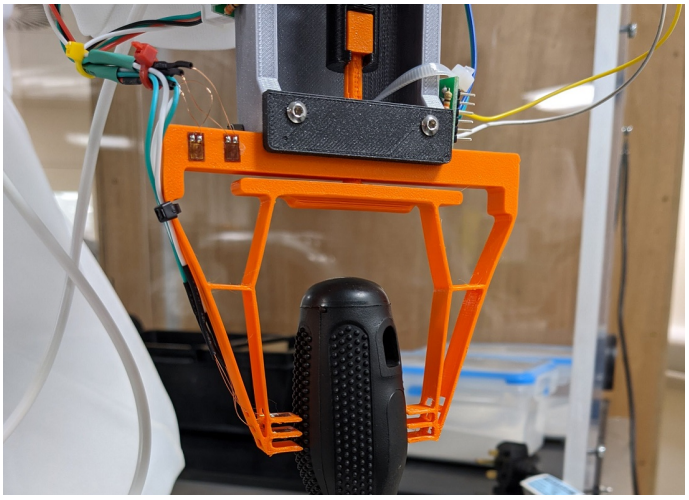

Figure 9.1.9: Single Axis Gripper Sensor Testing

Figure 9.1.10 shows the strain output from two gauges as an already gripped object is lifted. This change in strain is due to the reaction force from the acceleration and deceleration of the robot arm during a vertical movement. The only difference between the two tests was an addition of more mass to the object, which results in a higher force being applied to the tabs with the same acceleration. A similar result occurs when the same mass object is moved with a higher acceleration, as $F = ma$.

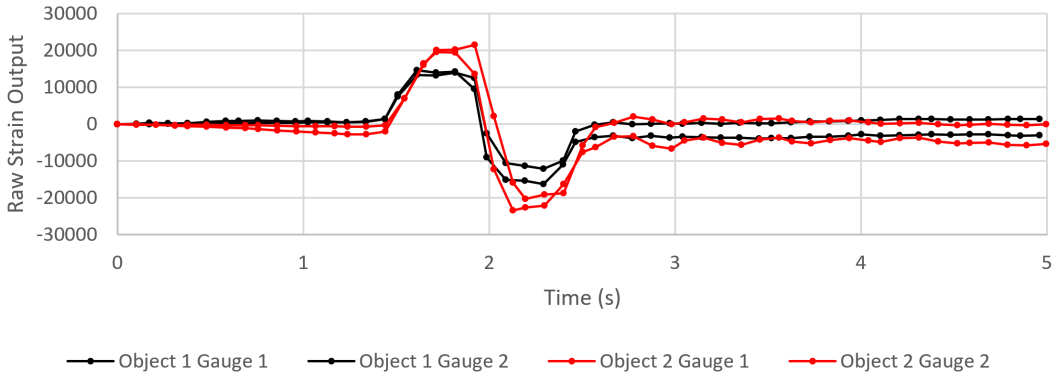

Figure 9.1.10: Single Axis Strain Output Comparison

During initial testing it was noticed that as the tabs are all perpendicular to the gripping direction, they are compressed with a normal force directly through the tab when gripping objects with relatively parallel sides. Currently this makes it difficult to know if the tab is being flexed or compressed. Adding a strain gauge to the other side of each tab would allow this normal force to be measured independently to the perpendicular force, as both gauges in each pair would strain in the same direction during compression, but in opposite directions during bending.

9.1.3 Two Column Gripper Sensor

Figure 9.1.11 shows a revised gripper with two columns of teeth. The additional column should mean that a torque or rotation of the object being gripped can be found, as well as the overall mass or acceleration.

The output from a series of forces and torques applied to an object in the grasp of the two column strain array is shown in Figure 9.1.12. The first (5s to 8s) is a vertical

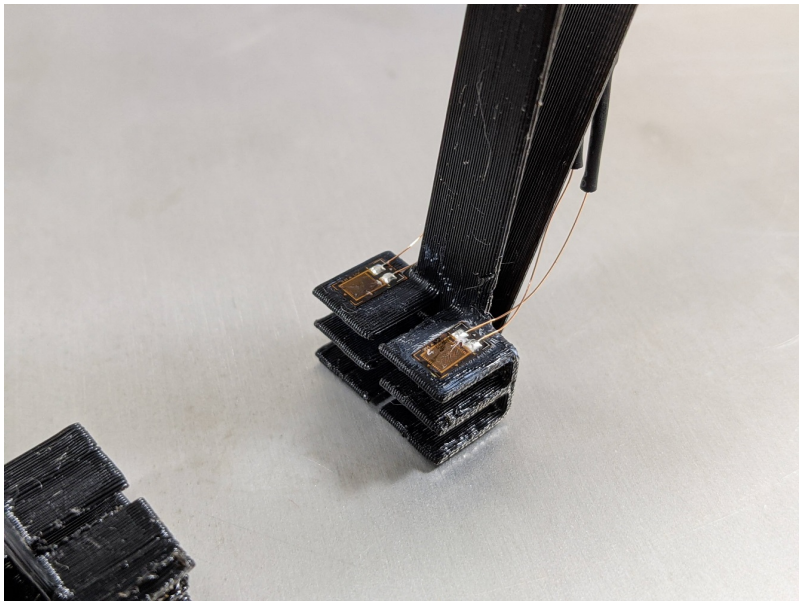

Figure 9.1.11: Two Column Strain Array Sensor

force pulling down on the array, as would be present when lifting an object. It can be seen that both strain gauges are flexing in the same direction by approximately an equal amount, and so the output is very similar. The next applied force (11s to 14s) is again vertical, but pushing up on the strain array. It can be seen that both strain gauge outputs again move together, but in the opposite direction to before, as expected. If a torque or rotation is applied to the object being grasped, rather than a vertical load, the two strain gauges flex in opposite directions. This can be seen starting at 16s for a clockwise rotation and at 21s for an anti-clockwise rotation, as the output from each strain gauges oppose each other.

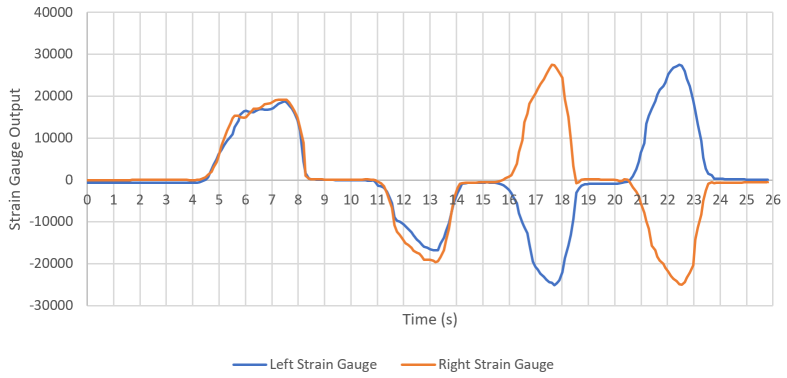

Figure 9.1.12: Two Column Strain Array Output

This shows that the toothed geometry which was added to the compliant gripper mechanism, to improve grasping performance for objects covered in powder, can also be used as a tactile sensor array if stain gauges are added to determine the tooth flex.

9.2 Slip Detection

Being able to detect that an object has slipped or is slipping from the grasp is a useful feature for any automated gripping process. Although the toothed gripper with vibration reduces or eliminates the slip that occurs due to unfused powder between the tips and the object, other factors could still cause the object to slip or move in the grasp. Being able to detect this slip and either prevent it or at least flag an alert for manual inspection, could prevent further errors in the process, especially for subsequent steps such as automated post-processing or assembly.

9.2.1 Static Grip Test Stand

Figure 9.2.1 shows a static grip test stand for carrying out tests which do not require the full motion of a robotic arm, or any powder to be present[1]. It features an identical actuator, gripping mount, and control electronics (Figure 9.2.2) as that shown previously, minus the components for communication with the UR5 arm, and the twisting mechanism. This allows the same code and grippers to be used on this static test stand and on the robot arm.

[1]Required due to lab access restrictions during COVID-19

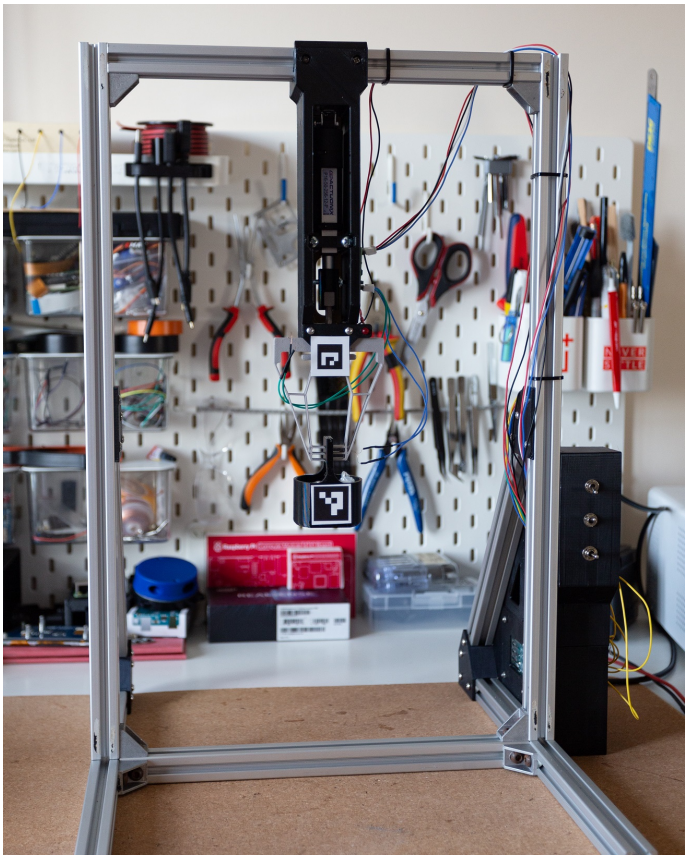

Figure 9.2.1: Static Grip Test Stand

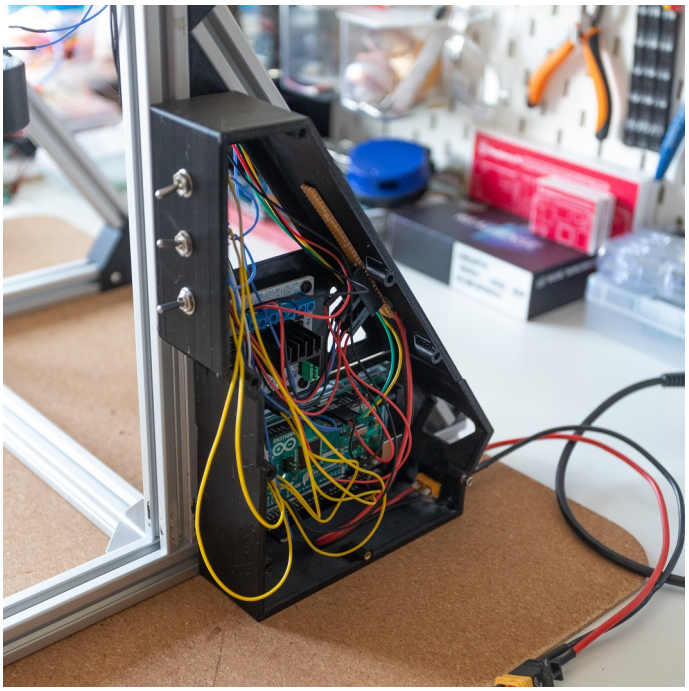

Figure 9.2.2: Control Box

Two additions to this static setup are an LED near the base of the gripper, and tracking markers on the gripper mount and on the object to be gripped (Figure 9.2.3). These markers allow a camera to be used to help understand what is happening during slip, even if a visual system such as this would likely not be suitable for use with powder present. The LED can be used to help sync the video frames with the gripper data after the test, or as a slip detection indicator for the recorded video. It can also be seen that the object being grasped has been designed to allow objects to be placed inside, to vary the weight.

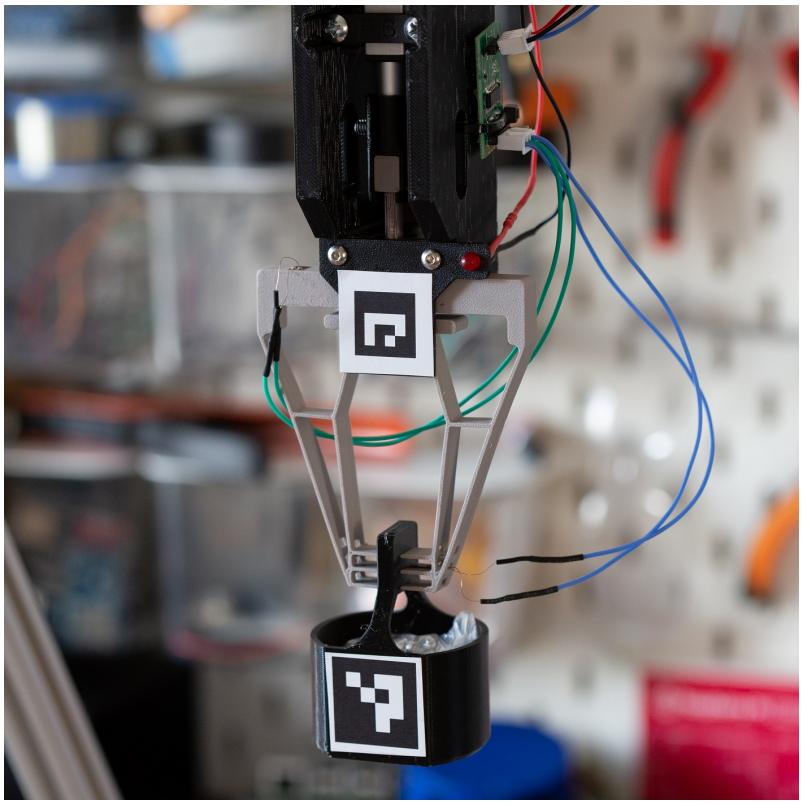

Figure 9.2.3: Gripper and Object Close Up

9.2.2 Object Tracking

To help in the analysis of the strain data, an object tracking system was developed to measure the relative movement of the object as it slips. This system does not interface with any part of the gripper control system, it is purely a method of capturing more data to help understand what the gripper/strain gauges are measuring.

ArUco markers are placed on the object and the fixed actuator/gripper mount. These markers are detected using OpenCV, which gives the pixel co-ordinates of the four corners of each marker. The pixel distance between the two marker centre co-ordinates is then found, calculated from the intersection of two lines from diagonally opposite corners. Figure 9.2.4 shows the detection of the two markers, with a red line indicating the distance between the two centres. This distance should remain fixed whilst the grasp is stable, and then start to increase as the object begins to slip. This can then be related to the output measured by the strain gauges applied to the tabs on the gripper tips.

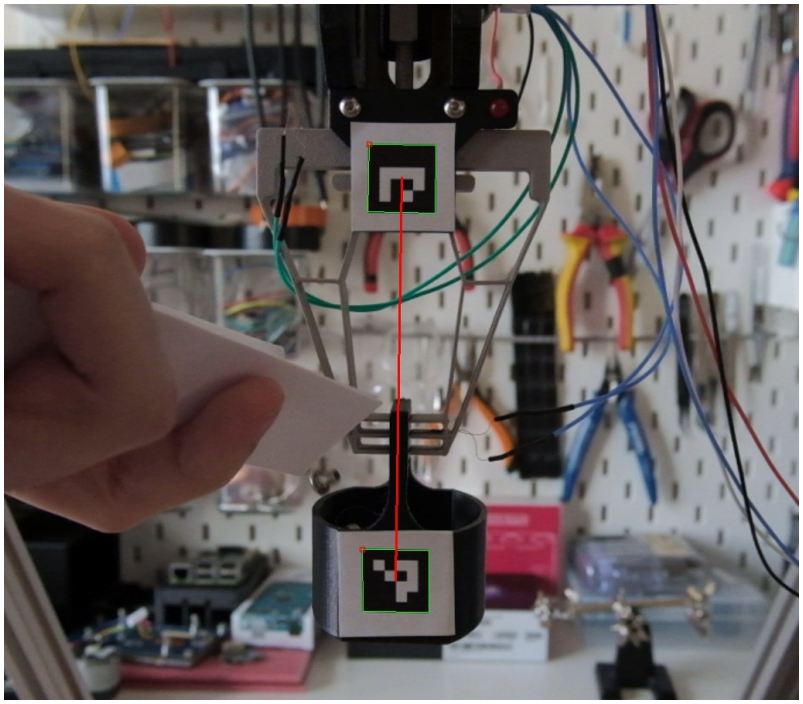

Figure 9.2.4: Object Tracking Markers

To initiate a slip event whilst the gripper is fixed in place and an object is already grasped, two different methods were tested:

- Decreasing the gripping force.
- Increasing the object weight.

These two methods also seem to be the most frequently used in the existing literature to initiate slip. Adding an external force or load to the object could also be used to

initiate slip whilst the gripper is fixed, but this would have the same overall reaction on the gripper as just increasing the object weight. An external load could also be a suitable method to test rotational slip, however increasing the object weight off-centre would also still work.

9.2.3 Decreasing the Gripping Force

In this test, an object was placed into the grip and the actuator position was moved slowly to reduce the contact force until it was low enough for the object to slip. Figure 9.2.5 shows that the strain output from the gauge mounted to one of the gripper teeth changes in steps throughout the test, indicating that the strain in that location is at least partly dependant on the contact force. The stepped reduction in strain is due to how the actuator is controlled, as this correlates to the minimum resolution of its built-in potentiometer for closed loop position control. At around 26 seconds, there is a much larger step change in the strain, and a sharp rise in the object displacement from the visual tracking. This larger drop in strain is due to the force being applied to the gripper tooth reducing to zero as there is no longer an object in the grip to cause it to flex or compress. Although the drop in strain during the slip is much larger than the individual drops as the gripper is opened, this seems to be the only indication in the strain data that shows a slip has taken place. As this method relies on the decreasing gripping force to initiate the slip, it is difficult to completely isolate the strain change due to slip and due to the actuator movement. This means that detecting a slip as the actuator is opening or closing would not be easy. From the visually tracked object displacement, it also seems as if the large drop in strain occurs at the same time as the object falls from the gripper. This results in what could be a suitable detection method, but not necessarily one which would be able to correct for any slip before the object has fallen.

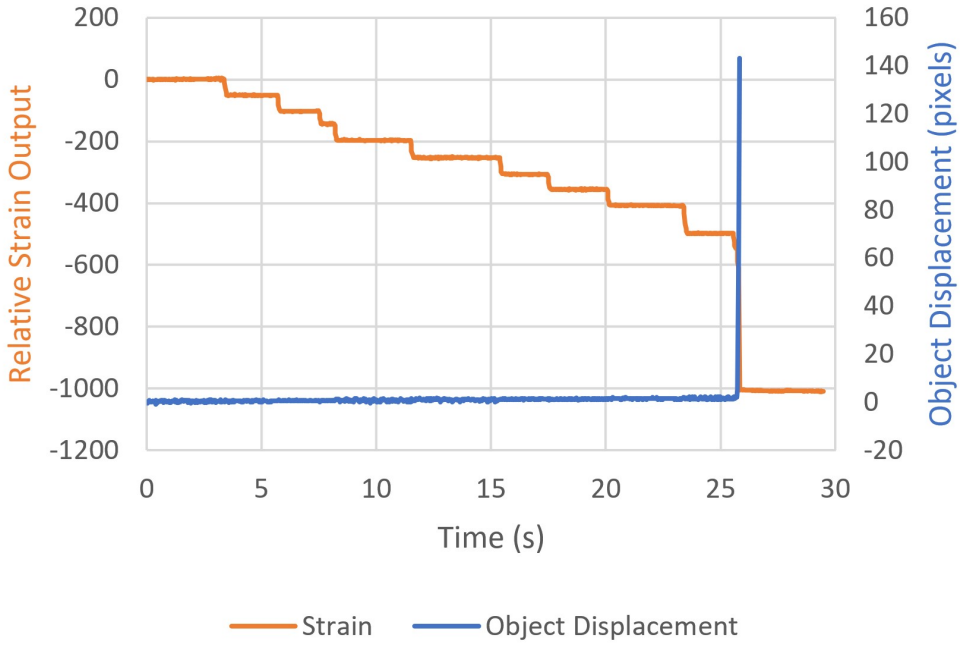

Figure 9.2.5: Decreasing Grip Force Strain and Object Displacement vs Time

Figure 9.2.6 shows the target and actual actuator position over time, compared to the strain data. It can be seen that the resolution of the actuator's onboard position sensor is quite low for the range that this test is conducted over. As this position sensor is used for closed-loop control of the actuator position, it causes a slight error between the actual and desired position throughout the test. Although this is not ideal, the strain follows the actual position much more closely, indicating a good relationship between the force being applied to the object, and the input position of the actuator and gripping mechanism.

As the object mass is also relatively low, reducing the gripping force until it slips means that the slip occurs when there is already a low amount of strain experienced by the strain sensor, making it harder to detect the slip when it occurs.

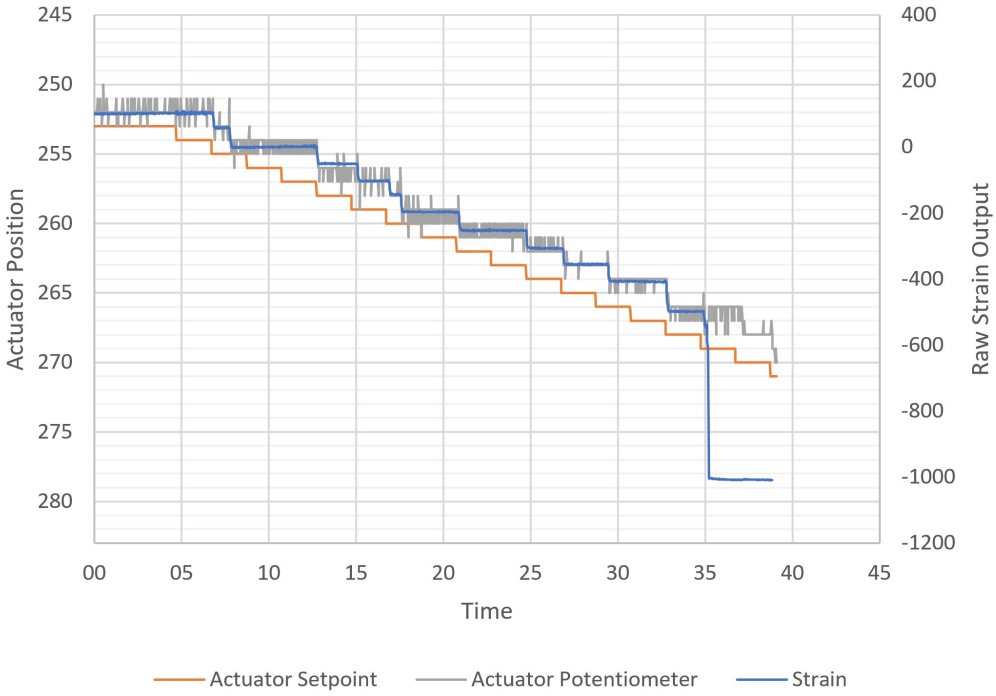

Figure 9.2.6: Decreasing Grip Force Actuator Position and Strain vs Time

9.2.4 Increasing the Object Weight

Another way to initiate slip using a static gripper is to increase the mass of the object, which could be more representative of how slip could be caused in real applications, as the resultant force applied to the gripper digits would be similar if instead of an increase in mass, there was a change in the robot's velocity whilst moving an object.

In this test, small 0.3g nuts were gradually poured into the object 'basket', causing its weight to increase. At some point this causes the object to become too heavy, and it slips from the gripper. Figure 9.2.7 shows the strain and object displacement during this test. It can be seen that the strain gradually increases as the teeth flex more due to the increasing weight. Just after 10 seconds, the strain begins to change more erratically, followed by a sharp reduction. Looking at the object displacement from the visual tracking, it can be seen that the onset of the more erratic strain data coincided with the object beginning to move, or slip, but whilst it was still within the grasp. At some point, the object then completely falls from the gripper causing

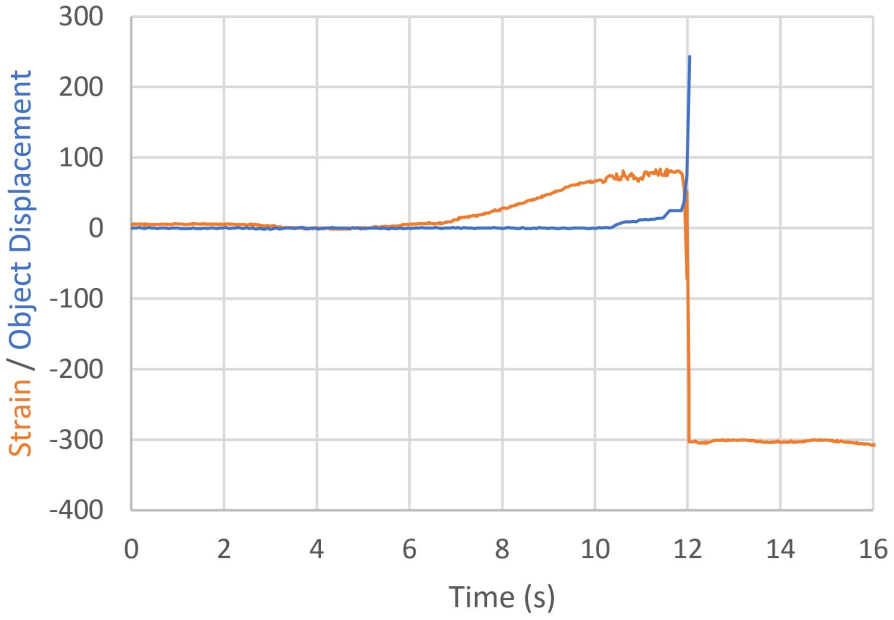

Figure 9.2.7: Increasing Object Weight Strain and Object Displacement vs Time

the teeth to rapidly return to their unstressed position, which results in the sharp drop in strain.

Based on this knowledge of erratic changes in strain indicating a slip is occurring, a slip indicator was added to the gripper control system. When the latest measured strain is outside of a specified range from a running average, the LED is set to light up. This specified range was set to be wide enough that the gradual increase in strain from the weight increase does not cause a false positive and light up the LED. Although this method does mean that object slip can be successfully detected before the object has fully fallen (Figure 9.2.8), it would also be triggered by a sharp increase in strain caused by a robot quickly lifting an object, or a quick change in movement, even if slip does not actually occur in either case.

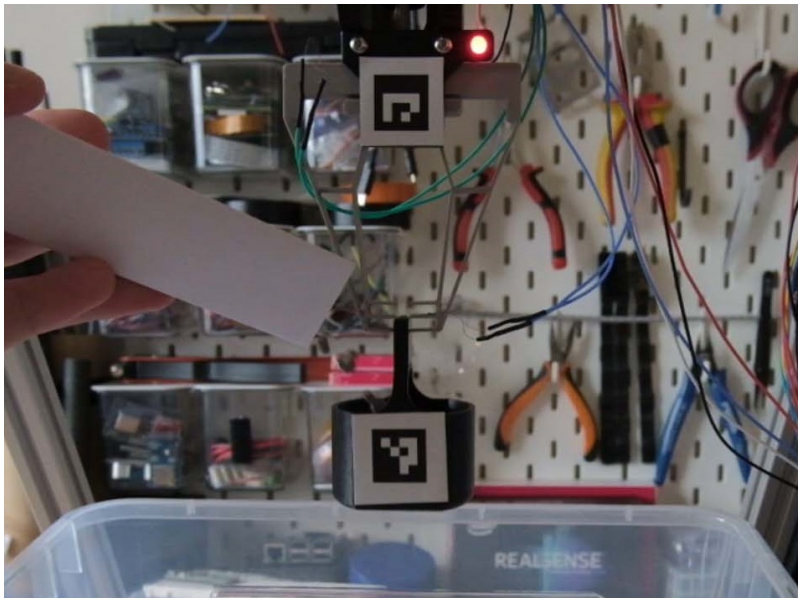

Figure 9.2.8: Slip Detection Indicated Before Object has Left Gripper

Figure 9.2.9 shows the rate of change of strain vs time and object displacement vs time. This also shows an erratic behaviour in the rate of change of strain, just as the object begins to slip, followed by a large spike as the object falls from the gripper. The rate of change of strain, (or even the second derivative) could also be used as an indication of slip instead of just the change in strain, to increase detection reliability.

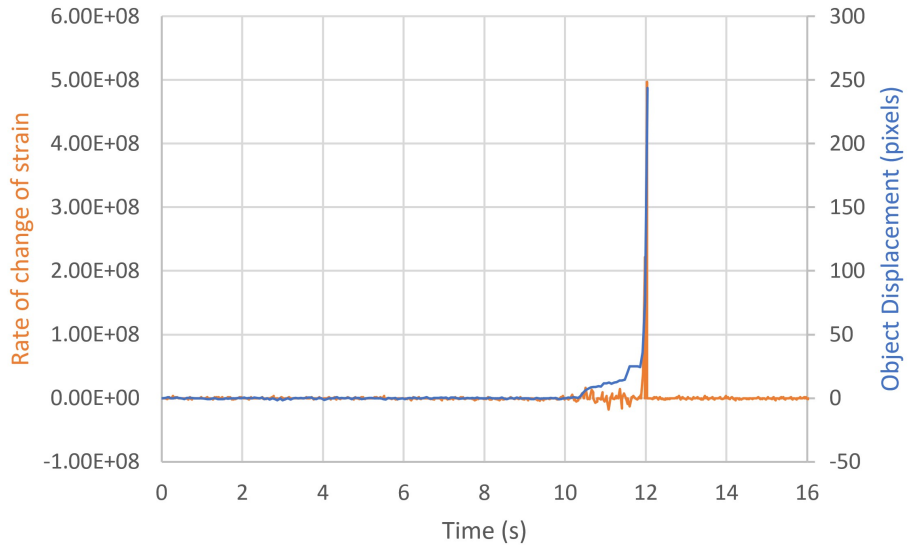

Figure 9.2.9: Strain Rate of Change and Object Displacement vs Time

9.2.5 Comparison with Existing Methods/Sensors

James *et al.* (2018) showed a method of detecting slip using the TacTip sensor, based on the vector field of pin velocities. To initiate slip, a TacTip sensor mounted to the end of a UR5 robot arm was used to push against and lift up an object mounted to a low friction linear rail. The robot arm then slowly moved away, reducing the contact force until the object began to slip. In a similar way to the strain array, the weight of an object causes some amount of downward flex/stretch in the TacTip surface, which then returns back to an unstressed state once an object has slipped/fallen. Figures 9.2.10 and 9.2.11 show the vector field of pin velocities during a slip, and the displacement and velocity in the vertical axis during a slip. It can be seen that the sharp change in pin displacement and corresponding spike in pin velocity, are similar to the sharp change in strain and spike in rate of change of strain shown in the strain array slip tests. As this test initiated slip by gradually reducing the gripping force, a steady change in the pin positions can be seen leading up to the rapid slip onset. This is similar to the steady decrease in strain in the decreasing contact force strain array data, but the difference here is that as all of the pins are attached to the same surface which deforms, some will decrease and some will increase steadily as the applied force is decreased, depending on where the pin is located on the TacTip array.

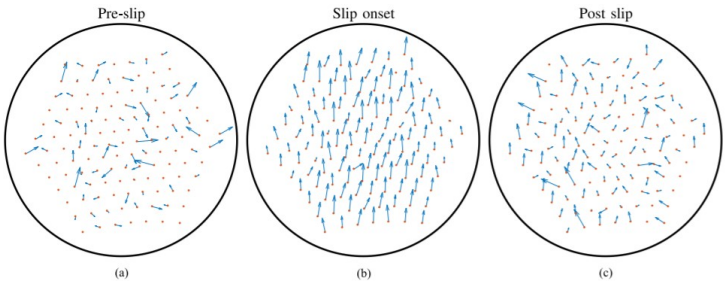

Figure 9.2.10: James *et al.* (2018) TacTip Vector Field of Pin Velocities

"Velocity was chosen because a change in velocity will always be present when an object starts to slip and it is easily inferred from the pin positions." (James *et al.*, 2018). Whilst it is true that a change is velocity will be present when slip starts, a

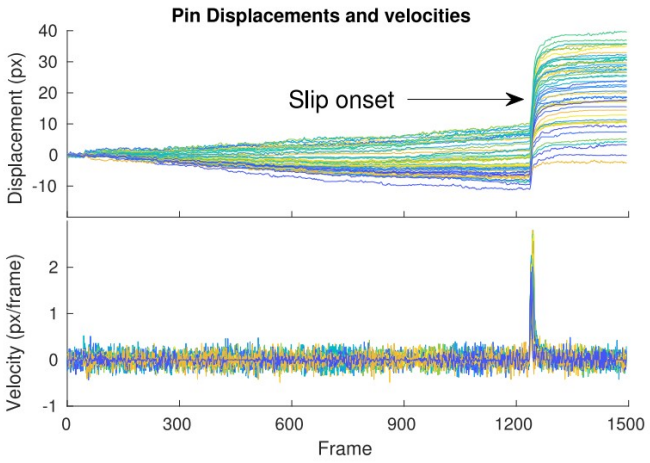

Figure 9.2.11: James *et al.* (2018) TacTip Pin Displacements and Velocities

change in pin velocity will also be present when the robot arm changes direction or accelerates in any way. The authors do note that their method may be susceptible to false positives when lifting an object, but do not show any vector fields or pin displacement results for lifting an object for comparison.

In theory, any planned or measured movement or acceleration from the robot arm could also be fed into the classifier to help it distinguish between planned and unplanned pin velocity changes, reducing false positives. Currently, the results and limitations shown in this paper seem very similar to the ones those shown for the strain sensor array - albeit with the addition of a robust classifier and the ability to move the robot arm back to 'catch' the object. Due to the speed of the actuator currently used for the 3D printed compliant gripper, it is not able to catch the object once it has begun to slip, even if the slip is detectable before the object has fully left the grasp.

Kawamura *et al.* (2013) describes a tactile sensor based on Carbon Micro-Coil (CMC) touch sensors and force sensors. Slip was initiated by a reduction in gripping force, which could then be increased once slip was detected to prevent the object from completely falling. It also isn't clear if this system could tell the difference between actual slip and just a fast movement or immediately after lifting an object, as all testing was done by slowly decreasing the force applied to an already gripped

object in a static gripper.

Veiga *et al.* (2015) used a supervised learning method to classify the current grip state of either slip or non-slip, as well as a prediction of if slip is going to occur. A BioTac sensor was used, which contains an array of pressure sensors across the fingertip, along with pressure transducers, and a set of heaters and thermistors to measure temperature and temperature flow. Data from these sensors was recorded during stable and unstable grasps where slip is occurring. Again, each test begins with an object already grasped, and the gripping force reduced until the object slips. The data was then manually labelled based on if the object was visually slipping using a video which was captured during the test. It is also not known how well this method would perform when classifying slip vs non-slip whist moving or lifting an object.

Although detecting slip is helpful, if it occurs the object is now likely in an unknown pose in the gripper. Without the ability to accurately measure the slip amount and correct for it, or determine the new object pose, clearly the best solution is to try and ensure slip does not happen. Extracting 3D printed objects from unfused powder with a 3D printed gripper is a rare application where although the objects to be gripped may vary widely, they all share the same co-efficient of friction - assuming the gripper can penetrate the powder consistently. If the co-efficient of friction between an MJF gripper and an MJF object is known, then a theoretical minimum gripping force could be calculated based on the known mass of the object before it is gripped and the added mass of any unfused powder stuck to or on top of the part, plus a safety factor. Slip detection and correction could then be used more as a way of tracking possible errors in an automated gripping process, rather than an active part of the process to constantly measure and correct for.

Chapter 10

Conclusions

This thesis looks at the challenges of extracting 3D printed objects from unfused PA12 powder using a robotic gripping system, and how a one-shot 3D printed compliant gripper mechanism can be used to effectively carry out this task, with strain based sensors being used to assess grip performance.

The literature review found that there was limited research that had been conducted on the interaction between solid objects surrounded by powder, and none on gripping and extracting objects buried in powder. A review of end-effector types and sensors showed that a compliant impactive type gripper using strain gauges would be the most suited for 3D printing using MJF and for operation around and within unfused powder.

FEA simulations were used to aid in the development of a compliant gripping mechanism, and a visual tracking tool was created to validate the simulations were representative of the 3D printed gripper. Commercial strain gauges were shown to work well at measuring how the compliant elements were flexing during the gripping process.

Initial tests extracting a cleaned 3D printed object from virgin PA12 powder showed that although it was possible, unfused powder would clump between the gripper and the object, causing its perceived width to be larger than in reality. The powder also caused instability and slip when the object was lifted and moved, resulting in a change in the pose of the object, and an increased risk of being dropped.

Modifying the tip geometry of the gripper to feature toothed sections allowed it to pass through more of the powder, reducing the prolonged slip during extraction to a single sharp slip event. Although this does not completely solve the problem, it does mean that as soon as the object is lifted, the tips moved through effectively all of the unfused powder, making the remainder of the gripping process stable. Adding some localised vibration to the tips of the gripper as it initially closes removes the initial clump of powder, and combining this with the toothed geometry results in the sensor showing an almost identical output to that when no powder is present. Quantitative object slip results match well with the strain data, showing a substantial amount of slip present when attempting to extract an object from powder using a gripper with standard flat tips, compared to minimal slip when no powder is present. A reduction in slip was shown using the toothed gripper or local vibration, and a combination of both resulted in the amount of slip being identical to that of when no powder is present.

Aged powder which has already been through the MJF process was shown to have a small but measurable effect on the grasping process, with a reduction in flowability causing less powder to fall from between the gripper tips and the object. Caked objects which had not been cleaned or post-processed in any way showed a significant increase in the level of strain when attempting to extract them from powder. This is due to the additional powder which is already clumped to the side of the objects which does not easily flow away like the loose powder. There is also a noticeable variability between the amount of caked powder present on the objects, causing substantial variability between each test. More testing should be conducted to gather reliable data on the effectiveness of different gripper tip geometries and grasping techniques for extracting caked objects from aged powder, as due to the resource intensive nature of these tests, not enough repeats could be carried out to gather consistent results. Even with these non-ideal behaviours, especially from the sensor perspective, 3D printed objects still caked in powder can be reliably extracted from aged powder automatically, individually, and in a known pose.

To provide more detailed information about the grasp, a sensor based on an array of strain gauges mounted on the toothed geometry of the gripper was created, which is able to determine the object mass, or the forces being applied to it. It was also shown that object slip can be determined before the object has fallen from the gripper using the same sensor. The output from this tactile sensor array, and its limitations, were shown to be similar to that of other tactile sensors in the literature, albeit without a robust classifier for high-level outputs.

This research has shown that it is possible to extract individual 3D printed objects from PA12 powder in a known pose, using a compliant gripping mechanism that is 3D printed in one-shot. The gripper is able to be accurately simulated before it is created, making it easily tailorable to other object geometries that need extracting. Strain based sensors mounted to the mechanism are also able to successfully gather rich information about the performance of the grasp, and are a realistic step away from being 3D printed in one-shot as part of the mechanism.

10.1 Limitations

Although the final gripper features commercial strain gauges and a small vibration motor (both of which are not 3D printed) these are not strictly necessary for successful extraction of printed parts, but they do improve the stability of the grasp, and provide useful information during the gripping process.

Existing literature has shown that strain gauges are already 3D printable, however their performance is not yet at the same level as commercial gauges, and they require a more complex 3D printing process to create. Motors have been shown to be at least partially 3D printable, and other methods of localised vibration could also be trialled that do not require assembly with the 3D printed gripper.

In this research, only PA12 powder was tested for surrounding and manufacturing the test objects, as that is the most common material used in the MJF pro-

cess. Other materials are available for the MJF process such as thermoplastic polyurethane (TPU), polypropylene (PP), and metal powder for the HP Metal Jet process. Each of these other materials may behave slightly differently compared to PA12, and so might require slight changes to the geometry and technique shown in this thesis.

Although some tests were carried out where a series of objects were extracted from powder in succession, these were all relatively far from each other, and all were at the same depth in the powder. It is not known if there is any depth dependant effect to the amount of clumping that occurs whilst gripping objects, or how pulling them from the powder may cause others surrounding more closely to move. As the current technique requires the object location to be known, if they move once the printing process has finished, this automated gripping process is not able to extract them, as the current sensors are intended for assessing the performance of the grasp, and not for searching for the objects within loose powder.

All of the objects extracted and gripped featured two parallel faces that were rigid in relation to each other. Although the explicit compliant gripper has some ability to grip a range of object widths and shapes, it is expected that if the object geometry was substantially different from this, then the current design would not be as effective at grasping it. However in these cases, adding a small gripping surface to each part would allow for more reliable grasping. Manufacturing aids such as "sinter boxes" which are already used to protect small or delicate parts could also be modified to including a gripping surface. The underactuated gripper was shown to be able to grasp a wide range of objects, but its performance was worse when extracting objects from powder, and it was not able to keep them in a known pose.

10.2 Future Work

Expanding the testing that has been shown in this thesis to include other powder and object materials could highlight adjustments that need to be made to the gripper

geometry or technique, or it could show that the ones shown here are applicable across a wide range of materials.

Following the experimental test results shown in this thesis on interacting and grasping solid objects surrounded by PA12 powder, it may be possible to develop computer simulation models of the same problem, using the results shown here as validation.

Although this thesis is a good step towards being able to automatically extract 3D printed objects from the MJF build unit, more testing would be required to understand the effect of stacked objects, and how extracting one object affects others located close to it. Extracting multiple objects was shown to be possible, but the minimum distance between parts or the movement of nearby parts was not determined. For a complete build unit, this gripping process would need to be combined with a method of extracting the unfused powder as well as extracting the printed parts, as the current solution is not intended to reach deep into the powder.

Unlike the concentrated compliant grippers which failed almost instantly due to high stress, the concentrated compliant grippers have shown good continued performance over time, with no noticeable reduction in strength or visible wear after 10s or 100s of grasps. However, the exact fatigue life of the gripper and the effect the powder has on wear at the contact area, is not yet known.

Testing with prototype 3D printed strain gauges would show how close the performance is to the current commercial gauges. This would allow the grippers to be printed in one-shot with the sensors already embedded, rather than requiring them to be placed after printing. Further testing with a larger vibration motor attached to the actuator instead of the gripper tip could remove the need for it to be assembled to each gripper, or other sources of vibration that are already 3D printable could be investigated. Being able to use the gripper without cleaning the caked unfused powder from it would also save time and cost above it being one-shot 3D printed. Although the gripper has been shown to work in the presence of unfused powder, further testing would need to be done to assess how the caked powder on the gripper would affect its operation.

Although the strain array sensor was able to detect slip and measure an applied shear force or torque, more work needs to be done to develop a robust classifier for the sensor, in order to use it as part of an automated closed loop gripping process, rather than just for error indication. By placing a strain gauge on each of the teeth, object slip would result in the top teeth loosing contact before any of the others. This means that it could be possible to detect if the object is slipping during the initial lifting phase, which the current method or many in the existing literature do not show. This technique of looking for the loss of contact of sensors on the boundary would in theory also work for other systems which measure force/contact/pressure across an array of discrete sensors. However, on many sensors such as TacTip and BioTac, although they are a made up of an array of individual pins or sensor elements, they are all mounted to the same deforming surface, meaning it could be harder to detect loss of contact at the edges without more complex classification methods. Once tested in more depth to gain a better understanding of the tactile sensor array outputs in relation to the magnitude and direction of object slip, future testing within powder can be done to assess its effectiveness in gaining a better understanding the interaction between the gripper, powder, and object, and potentially the shape and properties of the object itself.

Appendix A

Automated Extraction of 3D Printed Parts[1]

A.1 Introduction

As 3D printing moves from being used almost exclusively for one off prototype parts to now larger quantities of production ready parts, the desire to further automate the process increases. In the majority of 3D printing processes, the printed parts are extracted from the 3D printer by hand, before the manual removal of any support structure or excess material.

In many production lines, individual manufacturing processes such as injection moulding are fully automated, from the injection of the raw material, to the extraction of the part by a robot or similar system. Many of these large mass production scale systems can justify automation as many thousands of identical parts are being produced. This is a problem for 3D printing, as the benefits lay mostly in creating unique or small runs of parts, making automation more challenging.

For individual users or low volume cases such as a university, full automation of a 3D printing process including the extraction of the parts from the printers is difficult

[1]This appendix was submitted as part of the Advanced Specialist Text Study Module UFMFJG-15-M, submitted January 2020. It was written before the HP Automatic Unpacking Station was announced, which is able to separate printed parts from unfused powder, but using a method that causes the part pose to become unknown and could damage delicate parts.

to justify, as the person removing the part is often the end user (i.e. student or technician). But when the volume of parts increases, labour costs and the time wasted as the printer sits idle waiting for a finished part to be removed, have a large potential to save production costs and improve lead times (Schwartz and Friefield, 2017).

This report will focus on specialist texts which describe methods of extracting printed parts from a 3D printer. It will begin with a general 3D printing process overview, followed by a series of automation examples, ranging from research papers to blog posts. The technical automation methods will be compared, as well as the how the information is presented in each text.

My PhD focuses on creating a 3D printed gripper with embedded sensors, designed at least in part to allow the extraction of objects from a 3D printer. This means that although many of the specific methods and solutions shown in this report are not directly relevant to my PhD research, they work towards the same goal, and share many of the same requirements and limitations.

A.2 3D Printing Process Overview

The focus of this report is on the higher level process overview, so the individual working principle of each 3D printing process is not as important. 3D printing is not a continuous process - each printer has a finite print volume, and each printed part must be removed before a new one can be created. Below is an overview of the steps for most 3D printing processes.

1. Loading the raw material (e.g. powder, filament, resin). This is usually a manual step, but it is often not required before every print.

2. Sending the part file/g-code to printer. For low-cost hobbyist printers this needs to be done with a memory card, but often printers are now network connected making automation of this step relatively simple.

3. Printing the part. This step is entirely controlled by the machine itself.

4. Removing the part from the printer. This is usually done by the machine operator.

5. Further processing (removing excess material/supports, or shipping/assembly). This is usually either done by the machine operator or end user.

3D printing is currently used for creating a wide range of parts, at various production scales. For some production volumes, automation may be far more suitable than at others.

In low volume production such as a hobbyist with a 3D printer, or a small lab/workshop, 3D printers often sit idle until they are needed. The end user for parts printed on these machines is usually the same person who is using the printer or collecting the parts. This means they will remove the part, carry out any finishing tasks such as excess material removal, and use the part for whatever its intended purpose is. As there is often not a rush for the printers in these cases, and the part variety is high, there is little need to automate the removal of parts.

As the production volume increases automation starts to become appealing, and some methods of removing parts from the printer have been developed. Often there is still a high part variety and finishing that is happening, so the main focus is part extraction, in order for the machine to continue and start the next job. This reduces the time the machine sits idle.

In high volume manufacturing, automation can be a way to save time and cost. High volume 3D printing is currently used in many applications where there is a high part variety, such as by SmileDirectClub (Hartzell and Moore, 2019) who print dental molds. As each of these molds are unique, creating an automation system to handle them is complex. Many modern mass production processes are completely autonomous, and currently a 3D printer still needs some manual intervention to remove parts or excess material/support structure. Some examples have been shown on how various steps of a 3D printing process can be automated (such as part

removal) but few examples of a completely automated production system have been shown.

A.3 Literature/Examples

Existing solutions for removing printed parts from 3D printers can be split into two types. The first type utilises a common base or build plate which can be manipulated, removing the part from the printer and enabling it to continue with the next job. The second type aims to directly remove the printed part, without needing to replace or re-build a common build plate.

A.3.1 Build Plate Removal

Maurer (2014)

Maurer (2014) aimed to reduce the time a 3D printer spends idle in between prints, before the finished part is manually removed and the next job can start. This idle time can be quite substantial, especially if a print finishes during the night. The concept was to use a desktop robot arm to load and unload jobs from the printer, enabling it to continue printing, even when a person is not present. To do this, a suction cup end effector was used to remove the glass print bed with the part attached, and replace it with a clean one.

This technique meets the original goal of being able to start a new print job by removing the previous one, but it still requires a person to manually remove parts from the build plate, and replenish the stack of clean plates. It is a good step towards automating the system, but it is not a complete solution.

This article was posted on a personal blog and features lots of technical details about the system, from the individual components which were used, to the problems that were faced in the development process.

Figure A.3.1: Maurer (2014) Build Plate Replacement

Voodoo Manufacturing (2017)

Voodoo Manufacturing is a 3D printing service which caters for jobs up to 10,000 units (Voodoo Manufacturing, 2017). The company has a goal for a future with short lead times, fast cycle times, customisable products, and production runs that can start small and scale instantly. They highlighted that the majority of worldwide production is greater than 10,000 units, which makes it difficult to cost-compete with injection molding processes. According to Voodoo Manufacturing, the current main costs are material, machines, and labour. Raw material costs are difficult to control, and machine costs are likely to stay the same if better performance is desired. This leaves labour as a key place to save costs. When looking at 'Overall Equipment Effectiveness' which is a measure of how well a machine is being utilised, it was found that each machine was only in use around 40% of the time. This is due to the fact that when a print finishes, the print must be manually removed or 'harvested' before a new print can start.

This lead Voodoo manufacturing to develop a solution to automatically remove finished prints from each machine, allowing it to start the next job more quickly. This is especially effective during the night, when prints finish but nobody is around to harvest them. The problem statement and solution are similar to that of Maurer (2014), but with Voodoo Manufacturing taking a more 'professional' approach as a commercial company, rather than as an individual.

Figure A.3.2: Voodoo Manufacturing (2017) Print Harvesting

Figure A.3.2 shows the prototype print harvesting station. A set of 3D printers are mounted in a series of server racks, each reachable by the robot arm. When a printer has finished a job, the arm can reach in and remove the build plate with the print attached, and place it on the rack in the bottom right of the image. The robot can then place an empty build plate (far right of the image) into the printer so the next part can be started. The finished prints can then be removed from the build plates manually.

Voodoo Manufacturing says that for a set of 9 printers, the output was increased 3x, mostly due to the fact that harvesting can happen at any time of the day instead of only during the 8 hour working shift. This results in each employee being able to oversee 400 printers, up from 40. It was highlighted that automating the print harvesting reduces the time which employees spend on trivial repeatable tasks, so they can spend more time on abstract ever-changing problems, and it allows Voodoo Manufacturing to keep operating in the USA as the lower labour costs elsewhere are less of a factor in cost saving.

The Voodoo Manufacturing article was posted to an online publishing platform which is mostly used as a blog post host by individuals, professionals, and publications. Unlike a journal paper or thesis, the article lacks a lot of technical detail,

giving a higher level overview of the system, with a focus on how it can affect their operations and place within the manufacturing market. They are not trying to sell the automation technology, and it is unknown how (or if) these cost reductions will be directly passed on to the 3D print service's customers. It seems that the article is mostly just an interesting insight into their operations as a company.

Brockmeier (2000)

An automated loading and unloading system was developed by Brockmeier (2000) for an industrial 3D printer, and detailed in a masters thesis. The objective was to develop a system to minimise the non-productive time between print jobs. The solution, named Continuous Layer Manufacturing (CLM), consists of a rolling table placed in front of the printer, with a mechanism to open the door, remove the build plate with the printed part, and replace it with an empty one. An illustration of the system is shown in Figure A.3.3.

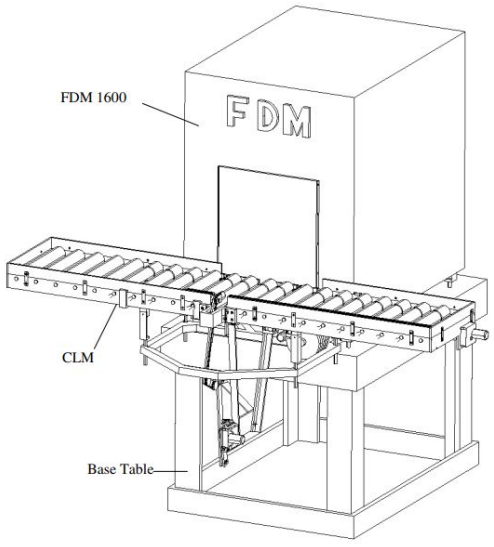

Figure A.3.3: Automatic Loading and Unloading System. Image used with permission from Brockmeier (2000).

The thesis contains good technical information on how the system was designed and manufactured, down to how each mechanism functioned, including what torques and forces were required at each linkage. The overall cost of the system was calculated,

and comparisons were made between buying a second printer versus the time savings of using the CLM solution (8 weeks down to 3.5 weeks for a particular set of prints). A test plan was also detailed, showing the reliability of the system, the mean time between failures, the mean time to repair, and the cause of each failure. This is something that is not shown in other texts.

Formlabs (2017)

Formlabs (2017) have shown a Form Cell system which aims to take their Form 2 desktop SLA (stereolithography) printer to an industrial production scale by parallelising and automating tasks such as removing printed parts. This system uses a robot gripper mounted to a gantry, which can move the build platforms and place them on a rolling rack (Figure A.3.4). Similar to the solutions shown above, the Form Cell is aimed at removing and replacing build platforms, which enables the printer to be used more, but the parts still require manual removal from the platform.

Figure A.3.4: Formlabs (2017) Form Cell

Since this is a solution that Formlabs is selling/configuring for customers, there is little technical information given about how the system is designed, or any numbers on how well it performs. The only link to more information is a sales contact form. Similarly, a press release by Kögler *et al.* (2018) describes a 'NextGenAM' manufacturing line for a powder based 3D printing system, claiming the benefits of a solution along with a series of marketing videos, with little accompanying technical

information.

A.3.2 Direct Part Removal

MatterHackers and Anderson (2015)

MatterHackers and Anderson (2015) created an automatic print ejector aimed at removing finished objects from a 3D printer "in the most amusing Rube Goldebergish way possible". The solution was to create a scissor mechanism to eject the prints with a boxing glove. Although there is no real justification for the project (in terms of saving time/cost), and the solution is clearly supposed to be more humorous than serious, there is still a high amount of technical detail present in the text. Figure A.3.5 shows the print ejector next to a 3D printer with a finished part, ready to be removed.

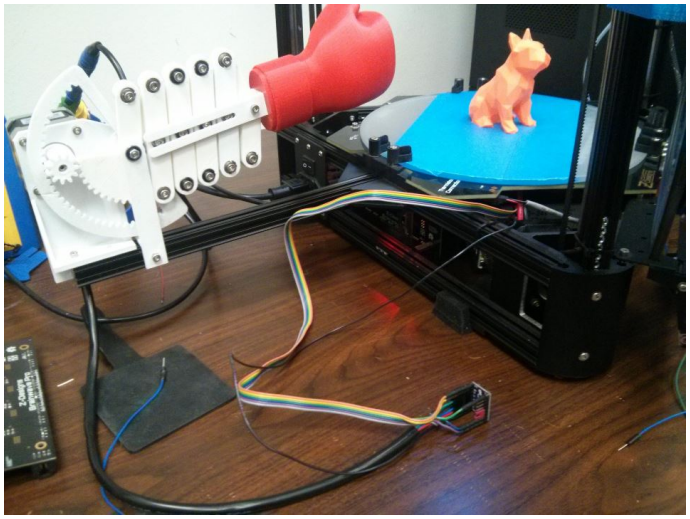

Figure A.3.5: Automatic Print Ejector (MatterHackers and Anderson, 2015) Photo courtesy of MatterHackers, Inc.

This project was posted to Hackaday.io, a project hosting site and social network where users can document hardware and software development projects for others to view and interact with. The article contains a high level of detail on how the solution was developed, such as the mechanical mechanisms like gears and bearings, the 3D print settings for parts, the electronics which were used, and how it integrates

with the 3D printer's firmware. The author has also detailed the development of the solution, with justifications for design decisions. There is also an openness to the text, where any problems with the design are clearly highlighted. As the solution is not intended to be used in a serious production scenario, there is little information on what shape/size/strength parts can be removed successfully. If the part is too small it may be damaged, too big and it could cause damage to the printer or removal system.

Alongside the text is a parts list and a link to download the 3D printable files and software source code. The article is written in a way to provide all of the necessary resources for others to replicate the solution, and freely build upon it.

Aroca *et al.* (2017)

A more serious method of removing parts from the build plate of a 3D printer was shown in a research paper by Aroca *et al.* (2017). A two degree of freedom robot manipulator was used to swipe across the build plate, pushing the part into a tray. One of the system goals was to further automate the 3D printing process, reducing the need for human operators, and enabling the process to be more cost-effective for higher volume manufacturing. Similar to MatterHackers and Anderson (2015), the concept attempts to remove parts from the printer directly, instead of removing and replacing the build plate.

It was found that to make the solution remove parts effectively, a specific adhesive needed to be used on the print surface to ensure the printed parts would stick at print temperatures (>100°C), but release easily once the printing had finished and the build plate had cooled (<40°C). As the adhesion between the part and build plate varies by the individual materials, surface finishes, temperature and any adhesive, this specific method only works when printing in ABS polymer. As the robot arm is unable to apply this adhesive to the build plate, this step still needs to be done manually before every print. Figure A.3.6 shows the manipulator and 3D printer. Although this paper is only a couple of years old, recent advancements in

FFF/FDM 3D printing have meant that new build plates have been created which allow parts to break free once it cools to room temperature. This would allow such an extraction method to be more viable, as the adhesive application process is not necessary.

Figure A.3.6: Aroca *et al.* (2017) Print Removal Robot Arm

The paper describes two patches of PVA (shown in blue) attached to the manipulator which were "soft enough to sweep the build plate without causing any damage to it but, at the same time, hard enough to remove all the parts on the build plate". It was also mentioned that several parts ranging from small to almost the size of the build plate were tested and successfully removed. These statements lead the reader to believe that the solution is completely effective at removing parts, however attached videos show small pieces of material still adhered to the build plate, which would require manual removal. This issue may be solvable through more accurate positioning of the manipulator, but the author does not highlight this as a problem with the solution anywhere within the text.

A computer vision system was created to identify and locate the 3D printer extruder, allowing the system to identify when the print had finished. The research paper contained lots of technical information about the removal solution and how the system integrated with the 3D printer and computer vision system, but unlike the MatterHackers and Anderson (2015) article, there were no external links to source code, 3D printable files or a list of parts.

A similar study was shown by Pena Doll (2014), which used a blade to swipe across the bed instead of a robot arm. This allowed other materials such as PLA to be

successfully removed, however it was found that careful attention must be taken to print parameters such as temperature, or the part could not be removed.

Bredt (2007)

A patent by Bredt (2007) details an invention relating to methods and apparatus for removing printed parts from a powder-based 3D printer. The main method involves a series of pistons which either push the part up through the un-fused powder, or hold the part as the build unit base drops. Figure A.3.7 shows two illustrations from the patent, with the pistons (34a and 34b) holding the 3D printed part (9), whilst the build unit base (27) drops, revealing the part from the un-fused powder (40).

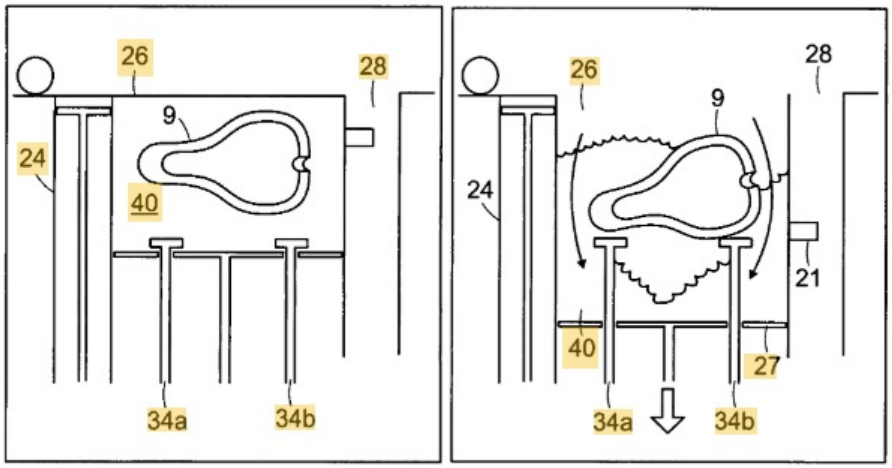

Figure A.3.7: Bredt (2007) Part Removal Method (Images Public Domain)

The patent contains a large amount of detail, with a series of illustrations containing alternative apparatus to displace the printed part, or to change the build chamber boundary to expose it. Although the patent title and abstract outline an invention for removing finished parts from a 3D printer, the methods described within the patent seem to result in the part being exposed from within the un-fused powder, but not necessarily removed from it. This solution would still require further manual manipulation to remove the part so the next print can begin. No real example of this solution has been found to be currently in use.

A.4 Text Comparison

From the texts studied, the main aim for automated part extraction was to improve the yield for a 3D printer, by decreasing the time between individual prints. Some of the texts directly mention the cost saving this would provide as the main aim, with others implying this through savings in time. The two exceptions to this aim were the Bredt (2007) patent, which cited human safety and machine reliability as the reason for automation, and the solution by MatterHackers and Anderson (2015) which was more of a humorous solution with no direct aim to save time or cost.

One thing that stands out across the texts is that there seems to be no correlation between the level of technical depth or information contained in the text, and how professional or 'serious' the solution is. The humorous solution by MatterHackers and Anderson (2015) contained more technical information about how the system was designed and developed than almost any other text. The texts containing the least technical depth are those which are trying to sell the developed solution directly to manufacturing partners, such as the solution by Formlabs (2017), and Kögler *et al.* (2018). In these texts the capability and purpose of the solution is clear, but there is little technical information or details on limitations. Blog posts, research articles and thesis papers all show a large amount of technical information, as developing the solutions is often the main reason for the text to exist. The exception to this is the patent by Bredt (2007) from Z Corporation (a company involved in the creation of 3D printing solutions, ultimately acquired by 3D Systems Inc (2019)), which provided a large amount of technical depth as required by the patent application, but no clear examples or proof of the solution in use. Voodoo Manufacturing (2017) strikes a balance with the level of technical depth provided, as they are not directly marketing the solution for sale, but they still have competitors within the 3D print service industry who may copy their solution if too much information is shared.

This difference continues through to the titles for each text and the use of the word 'automation'. Although all of these texts involve some form of automation, some

are slightly misleading in the way that the solution is automating only part of the process, but almost being described as a complete automation solution.

A.5 Conclusion

These texts show a wide range of solutions for part extraction, as well as a large variety of styles and content, depending on the reason for publication and the intended reader. This is relevant for my PhD, which contains research on extracting 3D printed parts from un-fused powder, as it can help me understand what each text style is supposed to achieve, and what content should be included, or is often forgotten, in each type of text.

One thing that is noted from these texts, is that the their end goal is just to extract the parts, where for a 'complete' automation solution, it would be desirable for the system to further manipulate the parts. In a fully autonomous production line, the extracted parts would often need to be added to some kind of larger assembly, however this is not considered in most texts. Many also gloss over the fact that many 3D printed parts need support structure or excess material to be removed. For these solutions, even if part extraction is automated, this process would still need to be done manually.

Bibliography

3D Hubs (2020a). *How to design parts for FDM 3D Printing*. URL: https://www.3dhubs.com/knowledge-base/how-design-parts-fdm-3d-printing/ (visited on 02/10/2020).

– (2020b). *What is 3D printing? The definitive guide*. URL: https://www.3dhubs.com/guides/3d-printing/ (visited on 06/14/2020).

3D Systems Inc (2019). *3D Printers, 3D Scanning, Software, Manufacturing and Healthcare Services — 3D Systems*. URL: https://www.3dsystems.com/ (visited on 11/27/2019).

Abbot, D. W., Kallon, D. V., Anghel, C., and Dube, P. (2019) Finite element analysis of 3D printed model via compression tests. In: *Procedia Manufacturing*. Jan. 2019. Elsevier B.V. Pp. 164–173.

Adam Bilodeau, R., White, E. L., and Kramer, R. K. (2015) Monolithic fabrication of sensors and actuators in a soft robotic gripper. In: *IEEE International Conference on Intelligent Robots and Systems*. Hamburg, Germany, 2015. IEEE. Pp. 2324–2329.

Albert, I., Sample, J. G., Morss, A. J., Rajagopalan, S., Barabási, A.-L., and Schiffer, P. (2001) Granular drag on a discrete object: Shape effects on jamming. *Physical Review E*. 64 (6), p. 061303. URL: https://link.aps.org/doi/10.1103/PhysRevE.64.061303. DOI: 10.1103/PhysRevE.64.061303.

ANSYS Inc (2019). *ANSYS*. URL: https://www.ansys.com.

Arduino (2019). *Arduino*. URL: https://www.arduino.cc/.

Aroca, R. V., Ventura, C. E., De Mello, I., and Pazelli, T. F. (2017) Sequential additive manufacturing: Automatic manipulation of 3D printed parts. *Rapid Prototyping Journal*. 23 (4), pp. 653–659. URL: www.emeraldinsight.com/1355-2546.htm. DOI: 10.1108/RPJ-02-2016-0029.

Askari, H. and Kamrin, K. (2016) Intrusion rheology in grains and other flowable materials. *Nature Materials*. 15 (12), pp. 1274–1279. URL: http://www.nature.com/articles/nmat4727. DOI: 10.1038/nmat4727.

Bajd, T., Mihelj, M., Lenarcic, J., Stanovnik, A., and Munih, M. (2010) *Robotics*. Springer Netherlands.

Berger, U. (2012) Rapid Manufacturing of Mechatronic Components - Applications of Stereolithography. *Mecatronics-REM 2012*. Pp. 128–134.

Bigneat Ltd (2020). *Ductless Fume Cabinet — Chemcap Clearview*. URL: https://bigneat.com/product/ductless-fume-cabinet/ (visited on 06/12/2020).

Birglen, L., Laliberté, T., and Gosselin, C. (2008) *Underactuated Robotic Hands*. Springer-Verlag Berlin Heidelberg.

Blanes, C., Mellado, M., and Beltran, P. (2014) Novel Additive Manufacturing Pneumatic Actuators and Mechanisms for Food Handling Grippers. *Actuators*. 3 (3), pp. 205–225. URL: http://www.mdpi.com/2076-0825/3/3/205. DOI: 10.3390/act3030205.

Bredt, J. (2007). *Apparatus and Methods for Removing Printed Articles from a 3-D Printer*.

Brockmeier, Ø. (2000) *Automated Loading and Unloading of the Stratasys FDM 1600 Rapid Prototyping System*. MA thesis.

Calì, J., Calian, D. A., Amati, C., Kleinberger, R., Steed, A., Kautz, J., and Weyrich, T. (2012) 3D-printing of non-assembly, articulated models. *ACM Transactions on*

Graphics. 31 (6), pp. 1–8. URL: http://dl.acm.org/citation.cfm?doid=2366145.2366149%20https://dl.acm.org/doi/10.1145/2366145.2366149. DOI: 10.1145/2366145.2366149.

Casiraghi, C., Macucci, M., Parvez, K., Worsley, R., Shin, Y., Bronte, F., Borri, C., Paggi, M., and Fiori, G. (2018) Inkjet printed 2D-crystal based strain gauges on paper. *Carbon*. 129 pp. 462–467. URL: https://doi.org/10.1016/j.carbon.2017.12.030. DOI: 10.1016/j.carbon.2017.12.030.

Chen, S. and Wang, M. Y. (2007) Designing Distributed Compliant Mechanisms With Characteristic Stiffness. In: *ASME 2007 International Design Engineering Technical Conferences & Computers and Information in Engineering Conference*. Las Vegas, Nevada, 2007. ASME.

Chitta, S., Sturm, J., Piccoli, M., and Burgard, W. (2011) Tactile sensing for mobile manipulation. *IEEE Transactions on Robotics*. 27 (3), pp. 558–568. DOI: 10.1109/TRO.2011.2134130.

Conway, C. D. (1995) *Analytical Analysis of Tip Travel in a Bourdon Tube*. PhD thesis, Naval Postgraduate School. Monterey, California.

Crooks, W., Vukasin, G., O'Sullivan, M., Messner, W., and Rogers, C. (2016) Fin Ray® Effect Inspired Soft Robotic Gripper: From the RoboSoft Grand Challenge toward Optimization. *Frontiers in Robotics and AI*. 3 (November), pp. 1–9. URL: http://journal.frontiersin.org/article/10.3389/frobt.2016.00070/full. DOI: 10.3389/frobt.2016.00070.

Cuellar, J. S., Smit, G., Plettenburg, D., and Zadpoor, A. (2018) Additive manufacturing of non-assembly mechanisms. *Additive Manufacturing*. 21 (May 2017), pp. 150–158. URL: https://doi.org/10.1016/j.addma.2018.02.004%20https://www.sciencedirect.com/science/article/pii/S2214860417302130. DOI: 10.1016/j.addma.2018.02.004.

Davies, S. (2019). *HP on HP: How the internal use of 3D printing is shaking up one of the world's biggest plastic supply chains - TCT Magazine*. URL: https://www.tctmagazine.com/3d-printing-news/hp-on-hp-3d-printing-shaking-up-plastic-supply-chain/ (visited on 07/24/2019).

Deckard, C., Beaman, J. J., and Darrah, J. F. (1989). *Method and Apparatus for Producing Parts by Selective Sintering*. URL: https://patents.google.com/patent/US4863538%20https://docs.google.com/viewer?url=patentimages.storage.googleapis.com/pdfs/US5155324.pdf.

Dijkshoorn, A., Werkman, P., Welleweerd, M., Wolterink, G., Eijking, B., Delamare, J., Sanders, R., and Krijnen, G. J. (2018) Embedded sensing: Integrating sensors in 3-D printed structures. *Journal of Sensors and Sensor Systems*. 7 (1), pp. 169–181. URL: https://www.j-sens-sens-syst.net/7/169/2018/. DOI: 10.5194/jsss-7-169-2018.

Dunst, P., Bornmann, P., Hemsel, T., and Sextro, W. (2018) Vibration-assisted handling of dry fine powders. *Actuators*. 7 (2), p. 18. URL: http://www.mdpi.com/2076-0825/7/2/18. DOI: 10.3390/act7020018.

Edwards, K. (1996) Mechanisms & mechanical devices sourcebook. *Materials & Design*. 17 (4), p. 230. URL: https://linkinghub.elsevier.com/retrieve/pii/S0261306997889443. DOI: 10.1016/S0261-3069(97)88944-3.

Eijking, B., Sanders, R., and Krijnen, G. (2017) Development of whisker inspired 3D multi-material printed flexible tactile sensors. *Proceedings of IEEE Sensors*. 2017-Decem pp. 1–3. DOI: 10.1109/ICSENS.2017.8233952.

Ellery, A. (2018) Universal construction based on 3D printing electric motors: Steps towards self-replicating robots to transform space exploration. In: *Proceedings - 2017 IEEE 5th International Symposium on Robotics and Intelligent Sensors, IRIS 2017*. Ottawa, ON, Canada, Oct. 2018. IEEE. Pp. 81–85.

Espalin, D., Muse, D. W., MacDonald, E., and Wicker, R. B. (2014) 3D Printing multifunctionality: Structures with electronics. *International Journal of Advanced Manufacturing Technology*. 72 (5-8), pp. 963–978. URL: http://link.springer.com/10.1007/s00170-014-5717-7. DOI: 10.1007/s00170-014-5717-7.

Fantoni, G., Capiferri, S., and Tilli, J. (2014) Method for supporting the selection of robot grippers. In: *Procedia CIRP*. Jan. 2014. Elsevier. Pp. 330–335.

Fantoni, G., Santochi, M., Dini, G., Tracht, K., Scholz-Reiter, B., Fleischer, J., Kristoffer Lien, T., Seliger, G., Reinhart, G., Franke, J., Nørgaard Hansen, H., and Verl, A. (2014) Grasping devices and methods in automated production processes. *CIRP Annals - Manufacturing Technology*. 63 (2), pp. 679–701. URL: http://dx.doi.org/10.1016/j.cirp.2014.05.006. DOI: 10.1016/j.cirp.2014.05.006.

Festo AG & Co. KG (2020). *Electric Parallel Grippers EHPS*. URL: https://www.festo.com/cat/en-gb%7B%5C_%7Dgb/products%7B%5C_%7DEHPS (visited on 01/25/2021).

Formlabs (2017). *Form Cell: Automated 3D Printing Solutions — Formlabs — Formlabs*. URL: https://formlabs.com/uk/3d-printers/form-cell/ (visited on 01/25/2019).

– (2020). *The Ultimate Guide to Stereolithography (SLA) 3D Printing*. URL: https://formlabs.com/blog/ultimate-guide-to-stereolithography-sla-3d-printing/%7B%5C#%7Dsla-systems (visited on 06/14/2020).

Galati, M., Calignano, F., Defanti, S., and Denti, L. (2020) Disclosing the build-up mechanisms of multi jet fusion: Experimental insight into the characteristics of starting materials and finished parts. *Journal of Manufacturing Processes*. 57 (July), pp. 244–253. URL: https://doi.org/10.1016/j.jmapro.2020.06.029. DOI: 10.1016/j.jmapro.2020.06.029.

Garrido-Jurado, S., Muñoz-Salinas, R., Madrid-Cuevas, F. J., and Marín-Jiménez, M. J. (2014) Automatic generation and detection of highly reliable fiducial markers under occlusion. *Pattern Recognition*. 47 (6), pp. 2280–2292. DOI: 10.1016/j.patcog.2014.01.005.

Gooding, J. and Fields, T. (2017) 3D Printed Strain Gauge Geometry and Orientation for Embedded Sensing. *58th AIAA/ASCE/AHS/ASC Structures, Structural Dynamics, and Materials Conference*. URL: http://arc.aiaa.org/doi/10.2514/6.2017-0350. DOI: 10.2514/6.2017-0350.

Grzesiak, A., Becker, R., and Verl, A. (2011) The Bionic Handling Assistant: A success story of additive manufacturing. *Assembly Automation*. 31 (4), pp. 329–333. DOI: 10.1108/01445151111172907.

Gupta, A., Arora, S., and Westcott, J. (2017) *Industrial Automation and Robotics*. Mercury Learning and Information.

Hartzell, N. and Moore, C. (2019). *HP and Smile Direct Club Collaborate on Largest Multi Jet Fusion 3D Production Factory in the U.S.* URL: https://press.ext.hp.com/us/en/press-releases/2019/hp-and-smile-direct-club-collaborate-on-largest--multi-jet-fusion-3d-production-factory-in-the-us.html (visited on 06/07/2019).

HP (2018). *How to complement CNC production with HP Multi Jet Fusion 3D printing*.

HP Development Company L.P. (2019) HP Jet Fusion 4200 3D Printing Solution User Guide. URL: http://h20195.www2.hp.com/v2/GetDocument.aspx?docname=4AA6-4892ESE.

Hughes, A. (2013) *Electric Motors and Drives*. 4th. Newnes.

Hull, C. (1986). *Apparatus for production of three dimensional objects by Stereolithography*. URL: https://patents.google.com/patent/US4575330A/en.

Hussain, I., Iqbal, Z., Malvezzi, M., Seneviratne, L., Gan, D., and Prattichizzo, D. (2018) Modeling and Prototyping of a Soft Prosthetic Hand Exploiting Joint Compliance and Modularity. *2018 IEEE International Conference on Robotics and Biomimetics, ROBIO 2018*. 3 (4), pp. 65–70. DOI: 10.1109/ROBIO.2018.8665231.

IAM 3D Hub (2018). *MJF_pneumatic_IAM3DHUB*.

Ida, N. (2014) *Sensors, actuators, and their interfaces: A multidisciplinary introduction*. Institution of Engineering and Technology.

James, J. W., Pestell, N., and Lepora, N. F. (2018) Slip Detection With a Biomimetic Tactile Sensor. *IEEE Robotics and Automation Letters*. 3 (4), pp. 3340–3346. URL: https://ieeexplore.ieee.org/document/8403292/. DOI: 10.1109/LRA.2018.2852797.

Jimenez, M. C. and Fishel, J. A. (2014) Evaluation of force, vibration and thermal tactile feedback in prosthetic limbs. *IEEE Haptics Symposium, HAPTICS*. Pp. 437–441. DOI: 10.1109/HAPTICS.2014.6775495.

Joris (2008). *FDM and 3D printing support material explained*. URL: https://www.shapeways.com/blog/archives/89-fdm-and-3d-printing-support-material-explained.html (visited on 06/14/2020).

Kang, W., Feng, Y., Liu, C., and Blumenfeld, R. (2018) Archimedes' law explains penetration of solids into granular media. *Nature Communications*. 9 (1), p. 1101. URL: http://www.nature.com/articles/s41467-018-03344-3. DOI: 10.1038/s41467-018-03344-3.

Katsuragi, H. and Durian, D. J. (2007) Unified force law for granular impact cratering. *Nature Physics*. 3 (6), pp. 420–423. DOI: 10.1038/nphys583.

Kawamura, T., Inaguma, N., Nejigane, K., Tani, K., and Yamada, H. (2013) Measurement of slip, force and deformation using hybrid tactile sensor system for robot

hand gripping an object. *International Journal of Advanced Robotic Systems*. 10. URL: www.intechopen.com. DOI: 10.5772/55476.

Keil, S. (2017) *Technology and Practical Use of Strain Gages With Particular Consideration of Stress Analysis Using Strain Gages*. Berlin, Germany: Wilhelm Ernst & Sohn.

Kögler, S., Sedlmayr, C. J., Grebner, M., and Sagel, B. (2018). *NextGenAM-pilot project for automated metallic 3D printing proves a complete success*. Tech. rep.

Kollmann, T. H. and Tomas, J. (2002) Effect of applied vibration on silo hopper design. *Particulate Science and Technology*. 20 (1), pp. 15–31. DOI: 10.1080/02726350215332.

Kwok, S. W., Goh, K. H. H., Tan, Z. D., Tan, S. T. M., Tjiu, W. W., Soh, J. Y., Ng, Z. J. G., Chan, Y. Z., Hui, H. K., and Goh, K. E. J. (2017) Electrically conductive filament for 3D-printed circuits and sensors. *Applied Materials Today*. 9 pp. 167–175. URL: https://www.sciencedirect.com/science/article/pii/S235294071730152X. DOI: 10.1016/j.apmt.2017.07.001.

Leigh, S. J., Bradley, R. J., Purssell, C. P., Billson, D. R., and Hutchins, D. A. (2012) A Simple, Low-Cost Conductive Composite Material for 3D Printing of Electronic Sensors. *PLoS ONE*. 7 (11), e49365. URL: http://dx.plos.org/10.1371/journal.pone.0049365. DOI: 10.1371/journal.pone.0049365.

Levenhagen, N. P. and Dadmun, M. D. (2018) Interlayer diffusion of surface segregating additives to improve the isotropy of fused deposition modeling products. *Polymer*. 152 pp. 35–41. URL: https://doi.org/10.1016/j.polymer.2018.01.031. DOI: 10.1016/j.polymer.2018.01.031.

Lopes, A. J., MacDonald, E., and Wicker, R. B. (2012) Integrating stereolithography and direct print technologies for 3D structural electronics fabrication. *Rapid*

Prototyping Journal. 18 (2), pp. 129–143. URL: http://www.emeraldinsight.com/doi/10.1108/13552541211212113. DOI: 10.1108/13552541211212113.

Mahmoodi, F. (2012) *Compression Mechanics of Powders and Granular Materials Probed by Force Distributions and a Micromechanically Based Compaction Equation*. PhD Dissertation, Uppsala.

MakeSEA (2017). *Brushless Motor - makeSEA*. URL: https://www.makesea.com/web/claimer/brushless-motor (visited on 07/16/2018).

Manufactur3D (2018). *A Comprehensive List of All 3D Printing Technologies*. URL: https://manufactur3dmag.com/comprehensive-list-all-3d-printing-technologies/ (visited on 06/14/2020).

Matsusaka, S., Yamamoto, K., and Masuda, H. (1996) Micro-feeding of a fine powder using a vibrating capillary tube. *Advanced Powder Technology*. 7 (2), pp. 141–151. DOI: 10.1016/S0921-8831(08)60509-9.

MatterHackers and Anderson, T. (2015). *Automatic Print Ejector — Hackaday.io*. URL: https://hackaday.io/project/5023-automatic-print-ejector (visited on 10/30/2019).

Maurer, F. (2014). *Steps towards home manufacturing with robotics and 3D printing — cuddleburrito*. URL: http://www.cuddleburrito.com/blog/2014/5/31/valuing-yourself-offloading-manufacturing-to-3d-printing-robotics-to-concentrate-on-what-matters (visited on 10/22/2019).

Molitch-Hou, M. (2016). *The Future of HP's Multi Jet Fusion 3D Printing*. URL: https://www.engineering.com/3DPrinting/3DPrintingArticles/ArticleID/12298/The-Future-of-HPs-Multi-Jet-Fusion-3D-Printing.aspx (visited on 02/22/2019).

– (2017). *HP Opens 3D Open Materials and Applications Lab for 3D Printing*. URL: https://www.engineering.com/3DPrinting/3DPrintingArticles/

ArticleID/14527/HP-Opens-3D-Open-Materials-and-Applications-Lab-for-3D-Printing.aspx (visited on 02/22/2019).

Monkman, G. J., Hesse, S., Steinmann, R., and Schunk, H. (2007) *Robot Grippers*. Weinheim: Wiley-VCH.

Montambault, S. and Gosselin, C. M. (2001) Analysis of underactuated mechanical grippers. *Journal of Mechanical Design, Transactions of the ASME*. 123 (3), pp. 367–374. DOI: 10.1115/1.1374198.

Muth, J. T., Vogt, D. M., Truby, R. L., Mengüç, Y., Kolesky, D. B., Wood, R. J., and Lewis, J. A. (2014) Embedded 3D Printing of Strain Sensors within Highly Stretchable Elastomers. *Advanced Materials*. 26 (36), pp. 6307–6312. URL: http://doi.wiley.com/10.1002/adma.201400334. DOI: 10.1002/adma.201400334.

Omega Engineering Inc. (2018). *Strain Gages*. URL: https://www.omega.com/en-us/resources/strain-gages (visited on 05/13/2019).

Open Bionics (2019). *Hero Arm - User Guide*. URL: https://openbionics.com/hero-arm-user-guide/ (visited on 01/27/2020).

OpenCV Team (2021). *OpenCV*. URL: https://opencv.org/ (visited on 02/15/2021).

Ozawa, R., Hashirii, K., and Kobayashi, H. (2009) Design and control of underactuated tendon-driven mechanisms. *Proceedings - IEEE International Conference on Robotics and Automation*. Pp. 1522–1527. DOI: 10.1109/ROBOT.2009.5152222.

Pena Doll, M. (2014) *Part Removal of 3D Printed Parts*. BSc, Massachusetts Institute of Technology.

Peters, J. F., Muthuswamy, M., Wibowo, J., and Tordesillas, A. (2005) Characterization of force chains in granular material. *Physical Review E*. 72 (4), p. 041307. URL: https://link.aps.org/doi/10.1103/PhysRevE.72.041307. DOI: 10.1103/PhysRevE.72.041307.

Platt, C. (2012) *Encyclopedia of Electronic Components*. Brian Jeps. Sebastopol, CA: Maker Media, Inc.

Prusa Research (2019). *Original Prusa i3 MK3S - Prusa3D - 3D Printers from Josef Prusa*. URL: https://www.prusa3d.com/original-prusa-i3-mk3/ (visited on 02/11/2020).

Saggio, G., Riillo, F., Sbernini, L., and Quitadamo, L. R. (2015) Resistive flex sensors: A survey. *Smart Materials and Structures*. 25 (1), p. 013001. URL: http://stacks.iop.org/0964-1726/25/i=1/a=013001. DOI: 10.1088/0964-1726/25/1/013001.

Schotborgh, W. O., Kokkeler, F. G. M., Tragter, H., and Van Houten, F. J. A. M. (2005) Dimensionless design graphs for flexure elements and a comparison between three flexure elements. *Precision Engineering*. 29 (1), pp. 41–47. DOI: 10.1016/j.precisioneng.2004.04.003.

SCHUNK GmBh (2020). *SVH 5-Finger Hand*. URL: https://schunk.com/gb%7B%5C_%7Den/gripping-systems/highlights/svh/ (visited on 05/15/2020).

Schwartz, J. and Friefield, M. (2017). *How We're Building a Robotic 3D Printing Factory*. URL: https://medium.com/voodoo-manufacturing/announcing-project-skywalker-bf9efa99a677 (visited on 08/19/2019).

Scott Crump, S. (Oct. 1992). *Apparatus and Method for Creating Three-Dimensional Objects*. URL: https://patents.google.com/patent/US5121329A/en.

Sillani, F., Kleijnen, R. G., Vetterli, M., Schmid, M., and Wegener, K. (2019) Selective laser sintering and multi jet fusion: Process-induced modification of the raw materials and analyses of parts performance. *Additive Manufacturing*. 27 (January), pp. 32–41. URL: https://doi.org/10.1016/j.addma.2019.02.004. DOI: 10.1016/j.addma.2019.02.004.

Singamneni, S., Diegel, O., Huang, B., Gibson, I., and Chowdhury, R. (2010) Curved Layer Fused Deposition Modeling. *Journal for New Generation Sciences*. 8 (2), pp. 95–107.

Spectra Symbol Corp. (2019). *Resistive Flex Sensors — Spectra Symbol Flex Sensors*. URL: https://www.spectrasymbol.com/product/flex-sensors/ (visited on 04/24/2019).

The British Standards Institution (2002). *BS EN ISO 14539:2001 Manipulating industrial robots. Object handling with grasp-type grippers. Vocabulary and presentation of characteristics*. URL: https://shop.bsigroup.com/ProductDetail?pid=000000000019976173.

Thornton, C. (1997) Force transmission in granular media. *KONA Powder and Particle Journal*. 15 (May), pp. 81–90. DOI: 10.14356/kona.1997012.

Uddin, M. S., Sidek, M. F., Faizal, M. A., Ghomashchi, R., and Pramanik, A. (2017) Evaluating Mechanical Properties and Failure Mechanisms of Fused Deposition Modeling Acrylonitrile Butadiene Styrene Parts. *Journal of Manufacturing Science and Engineering, Transactions of the ASME*. 139 (8). URL: https://asmedigitalcollection.asme.org/manufacturingscience/article-pdf/139/8/081018/6273715/manu%7B%5C_%7D139%7B%5C_%7D08%7B%5C_%7D081018.pdf. DOI: 10.1115/1.4036713.

Uemura, M., Mitabe, Y., and Kawamura, S. (2019) Simultaneous gravity and gripping force compensation mechanism for lightweight hand-arm robot with low-reduction reducer. *Robotica*. 37 (6), pp. 1090–1103. DOI: 10.1017/s0263574718001479.

Ultimaker (2017). *Open Bionics: 3D printed prosthetic limbs*. URL: https://ultimaker.com/learn/open-bionics-3d-printed-prosthetic-limbs (visited on 02/11/2020).

Universal Robots (2019). *Collaborative robotic automation — Cobots from Universal Robots*. URL: https://www.universal-robots.com/ (visited on 01/29/2019).

Veiga, F., Hoof, H. van, Peters, J., and Hermans, T. (2015) Stabilizing novel objects by learning to predict tactile slip. In: *2015 IEEE/RSJ International Conference on Intelligent Robots and Systems (IROS)*. Sept. 2015. IEEE. Pp. 5065–5072.

Volkmann, W. (2016). *3D printing will transform manufacturing as AWS transformed software services*. URL: https://developers.hp.com/hp-3d-printing/blog/3d-printing-will-transform-manufacturing-aws-transformed-software-services (visited on 02/22/2019).

Voodoo Manufacturing (2017). *Press_Photo_2*. URL: https://voodoomfg.com/press.

Walker, I. R. (2011) *Reliability in scientific research: Improving the dependability of measurements, calculations, equipment and software*. Cambridge University Press.

Ward-Cherrier, B., Pestell, N., Cramphorn, L., Winstone, B., Giannaccini, M. E., Rossiter, J., and Lepora, N. F. (2018) The TacTip Family: Soft Optical Tactile Sensors with 3D-Printed Biomimetic Morphologies. *Soft Robotics*. 5 (2), pp. 216–227. URL: www.optoforce.com%20https://www.liebertpub.com/doi/10.1089/soro.2017.0052. DOI: 10.1089/soro.2017.0052.

Wenbin, H., Tsui, L. Y., and Haiqing, G. (2005) A study of the staircase effect induced by material shrinkage in rapid prototyping. *Rapid Prototyping Journal*. 11 (2), pp. 82–89. DOI: 10.1108/13552540510589449.

Wilson, J. S. (2005) *Sensor Technology Handbook*. Elsevier Inc.

Wu, H., Pritchet, D., Wolff, S., Cao, J., Ehmann, K., and Zou, P. (2020) A VIBRATION-ASSISTED POWDER DELIVERY SYSTEM FOR ADDITIVE MANUFACTURING - An experimental investigation -. *Additive Manufacturing*. 34 p. 101170. DOI: 10.1016/j.addma.2020.101170.

Wu, L. C., Carbone, G., and Ceccarelli, M. (2009) Designing an underactuated mechanism for a 1 active DOF finger operation. *Mechanism and Machine Theory*. 44 (2), pp. 336–348. DOI: 10.1016/j.mechmachtheory.2008.03.011.

Wu, Q., Wang, X., Chen, B., Wu, H., and Shao, Z. (2017) Development and hybrid force/position control of a compliant rescue manipulator. *Mechatronics*. 46 pp. 143–153. URL: https://www.sciencedirect.com/science/article/pii/S095741581730106X%20http://dx.doi.org/10.1016/j.mechatronics.2017.08.003. DOI: 10.1016/j.mechatronics.2017.08.003.